SHEET PILE WALL DESIGN AND PERFORMANCE IN PEAT

Research Report
Prepared for

Geosciences Testing & Research, Inc. (GTR)
N. Chelmsford, Massachusetts

By

Samuel G. Paikowsky, Principal Investigator
Yong Tan, Graduate Research Assistant

Geotechnical Engineering Research Laboratory
Department of Civil & Environmental Engineering
University of Massachusetts Lowell
Lowell, Massachusetts 01854 USA

July 2005

ACKNOWLEDGMENTS

This research has been supported by Geosciences Testing and Research Inc. (GTR) of North Chelmsford, Massachusetts through P.A. Landers and Northeast Pile Driving (contractors) in a contract with the Massachusetts Highway Department (MHD).

The collaboration and assistance of Mssrs. Nabil Hourani and Peter Connors of the geotechnical section at the MHD are greatly appreciated. Mr. Peter Connors and Professor Heather J. Miller of UMass Dartmouth are also acknowledged for their contribution in reviewing the doctorate thesis of Mr. Yong, which serves also as this report.

The assistance of Mr. Gary Howe, laboratory director of the Civil & Environmental Engineering Department is greatly appreciated. So are appreciated Mr. Les Chernauskas of GTR for his sheet pile design and Mssrs. Leo Hart and Josh Adams of GTR for their assistance with field data acquisition. The collaboration of Mr. Pierre Gouvin of RocTest in developing the instruments to the specific needs are acknowledged. Mr. Larry Rolwes conducted the instrumentation and sheet pile stiffness analyses. Professor Sam Frydman of the Israel Institute of Technology had conducted the original PLAXIS FEM analyses for the Rt. 44 site, which were helpful in our initial stages of analysis. The craftsmanship of Mr. Mike Helfriech and his workers of H&H Machine shop is appreciated. Mr. Ken Soltz of Tekscan is acknowledged for his help obtaining the tactile single cell as part of an NSF project carried out by the first author. The peat parameters tested by Mr. Assem Elsayed and presented in the first report (Paikowsky and Elsayed, “The Characteristics and Engineering Properties of Peat in Bogs”) were extensively used in this research.

The field work was carried out by Northeast Pile Driving. The help of P.A. Landers and the assistance obtained from Mr. Glen Stewart is appreciated. The collaboration of WPC and Mr. Edward Hajduk is acknowledged. Ms. Mary Canniff is appreciated for her help in putting this manuscript together.

ABSTRACT

As part of a highway relocation project (RT44) in Carver Massachusetts, long sheet pile walls were installed in Cranbury bogs and ponds in order to mitigate environmental concerns. The subsurface consisting of deep peat deposits challenges the current understanding of the pressures developing on sheet piles and the parameters used for its design. A large instrumentation program has been conducted over a period of 2.5 years, measuring the peat pressure developing along the sheet pile walls during construction and service. This project includes (i) original wall design and associated assumptions, (ii) a detailed field and laboratory study investigating the vertical and lateral properties of the peat, (iii) the instrumentation of the walls using inclinometers and vibrating wire total pressure cells along with a new thin film tactile pressure sensors, (iv) the measurements of the pressures and deflections developing along the wall and independent surveying over various stages of construction including excavation, fill, deep dynamic compaction (DDC) and MSE wall construction, (v) the modeling of the wall-soil interaction during the aforementioned stages using the FEM code PLAXIS, (vi) comparisons between the modeling results and measured values at the different stages, and (vii) the development of recommended parameters for future design of walls in peat.

TABLE OF CONTENTS

LIST OF TABLES

TABLE

LIST OF FIGURES

FIGURE

CHAPTER 1
INTRODUCTION

1.1 RESEARCH OVERVIEW

Parts of US Route 44 relocation project carried out by the Massachusetts Highway Department (MHD) spans through cranberry bogs and ponds areas with deep peat deposits. As a result, a large number of embankments were required to be built, entailing the excavation of all the peat soils at the embankments' location and its replacement with adequate borrow materials. During the peat excavation, steel sheet pile walls were installed in the pond and bog areas as a temporary retaining structure and for the support of the Mechanically Stabilized Earth (MSE) retaining walls. A typical cross-section is shown in figure 1.1.

Peat is regarded as one of the worst foundation soils, because it is extremely compressible and has low strength, which challenges the current sheet pile design state of the art. Very limited data are available regarding the passive earth pressures resistance supporting cantilever sheet pile walls in soft soils, especially in peat, where none has been reported to be measured.

An instrumentation program was developed in order to investigate; (i) the passive earth pressure and peat-structure interaction, and (ii) sheet pile walls performance in peat during different construction stages, including deep dynamic compaction (DDC). Five stations located in peat deposits were chosen for monitoring with instrumentation that included pressure cells, piezometers, and inclinometers measuring total passive pressures on the retaining side, and wall deflections, respectively. Prior to the instrumentation installation, most of the peat at the embankments locations had been completely excavated and replaced with adequate granular fills.

Earth pressure calculations in sheet pile design are commonly based on the classical soil pressure theories; while, the actual earth pressure distributions acting on sheet pile walls are not very well understood. Field measured data are helpful to verify and when needed, to modify the current design criteria. Finite element method (FEM) was employed to model the cantilever sheet pile wall performance in the peat and the field measurements were used for comparison with the FEM calculation results. Recommended parameters for earth pressure design are suggested.

1.2 PURPOSE

The objectives of this research are: (1) to study the soil-structure interaction in peat during different construction stages via laboratory tests, field measurements and finite element method (FEM) analysis, and (2) to develop design parameters for future sheet pile wall design in peat deposits.

1.3 METHOD OF APPROACH

The following steps were taken to attain the above objectives:

1. Obtain undisturbed peat samples at the instrumentation site and conduct laboratory tests including consolidation test, triaxial tests and direct shear tests to

evaluate the peat characteristic and engineering properties. This stage was presented by Elsayed (2003) and provided to the MHD in the form of a report.

2. Obtain backfill samples at the site and perform laboratory tests including sieve analysis, triaxial tests and direct shear tests to evaluate its characteristic and engineering properties. Piezocone tests (PCPT) were employed before and after deep dynamic compaction (DDC) tests to verify the effect of the DDC on the properties of the backfills.
3. Calibrate the total pressure and single load cells in the laboratory.
4. Measure and record the total lateral earth pressures and water pressures developing against the retaining side of the sheet pile walls during all stages of construction since the installation of the instrumentation.
5. Measure and record the sheet pile wall displacement during all stages of construction since the installation of the instrumentation in the field.
6. Compare the field measurements with pressures predicted by classical theories.
7. Employ Finite Element Method (FEM) to model the sheet pile wall performance in Peat and compare the FEM results with those measured in the field.
8. Recommend earth pressure calculation parameters for sheet pile wall design in Peat.

1.4 MANUSCRIPT LAYOUT

The following is a brief description of the content of each chapter.

Chapter 2 presents a background. The aim of the chapter is to introduce the subject matter and all relevant information which is used in this research study. A literature survey of earth pressure measurements is first provided. Sheet piles are briefly introduced, followed by instrumented sheet piles, vibrating wire technology, tactile sensor technology, deflection and inclination measurement system, standard penetration test (SPT), piezocone penetration test (PCPT), deep dynamic compaction (DDC) test, and finite element method (FEM).

Chapter 3 describes the project and the site conditions. It introduces the Route 44 relocation project, original site subsurface conditions, geotechnical analysis and construction recommendations, peat and backfill characteristics and engineering parameters.

Chapter 4 presents the sheet pile instrumentation design. It introduces the location of the instrumented sections, instrumentation design and the subsurface conditions at the instrumentation locations.

Chapter 5 introduces the vibrating wire total pressure cells (TPC). It presents the TPC design, calibration system and procedures as well as calibration results.

Chapter 6 describes the thin film total pressure sensors. It presents TekScan sensor design, the TekScan calibration system and procedure as well as calibration results.

Chapter 7 introduces the construction and installation of the instrumented sheet piles at the site. Procedures of instrumentation installation in the machine shop, on site sheet pile installation, and initial readings at the completion of the installation.

Chapter 8 presents total lateral earth pressure and sheet pile deflection monitoring results. The long-term field total lateral earth pressure and sheet pile deflection monitoring results are presented.

Chapter 9 presents the FEM modeling of the soil-sheet pile wall interaction. Different types of soil and structure models for modeling soil-structure interaction are introduced along with

parameters for modeling the construction stages and the final earth pressures and wall deflections.

Chapter 10 presents a comparison between the FEM modeling results and field measurements.

Chapter 11 provides recommended parameters for future design. The suggested design parameters include peat engineering parameters, the lateral earth pressure coefficient for supporting Carver peat and the required wall rotation to reach fully passive states of stress in the peat.

Chapter 12 discusses the conclusions of the present research and recommendations for future work.

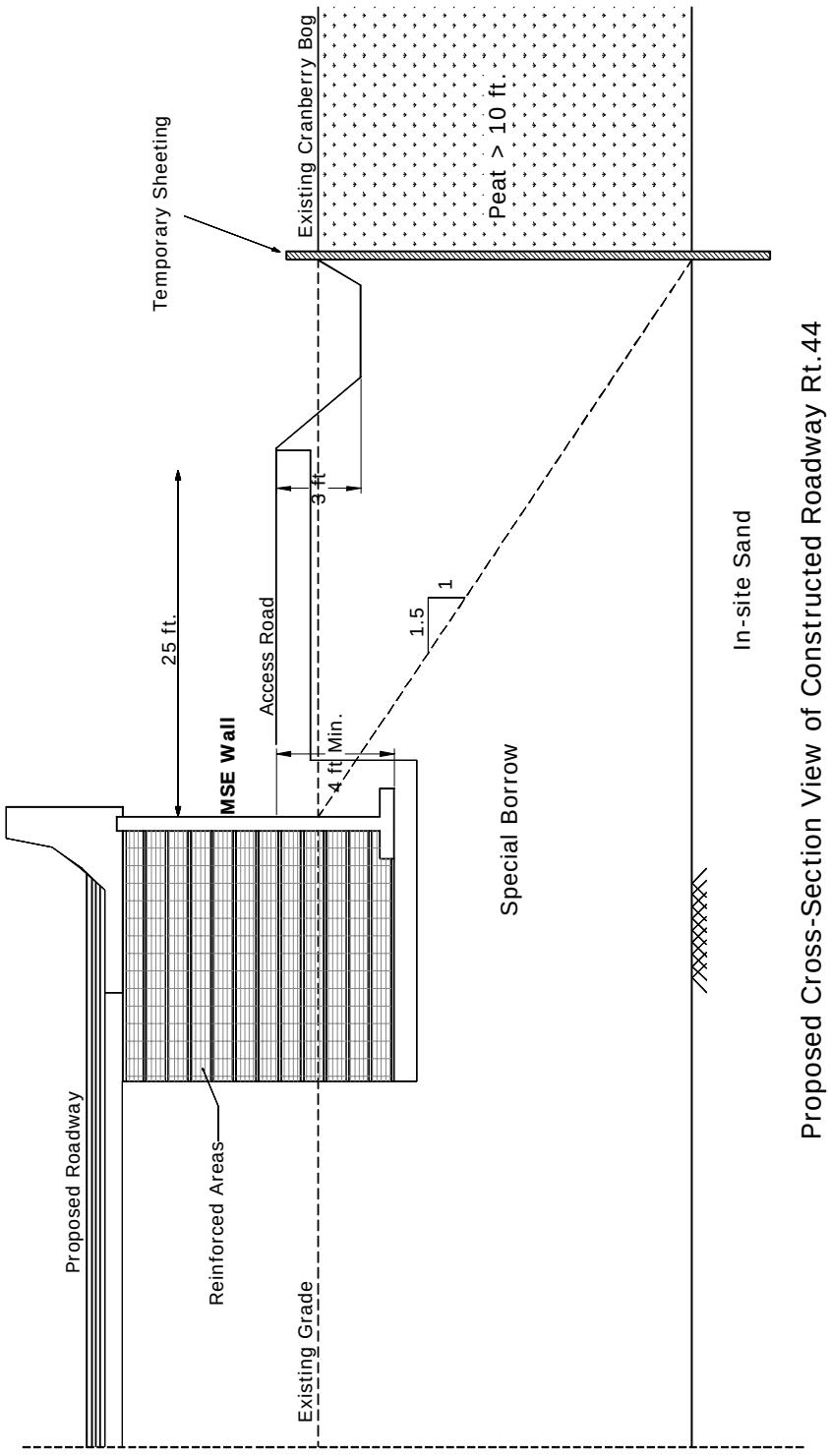

Figure 1.1 Cross-section view of roadway at US Rt.44

CHAPTER 2
BACKGROUND

2.1 OVERVIEW

This chapter provides the background for the different topics researched in this manuscript. A literature survey of earth pressure theories and measurements is first introduced. Sheet piles are briefly reviewed followed by previous research on instrumented sheet piles and instrumentation, namely vibrating wire technology, tactile sensor technology, and the inclinometer software GTILT system for deformation monitoring. In situ testing are presented, standard penetration test (SPT) and piezocone penetration test (PCPT), as well as soil improvement technology deep dynamic compaction test (DDC). A review of the basic principles of the Finite Element Method (FEM) is provided with some details about the finite element code PLAXIS. Detailed review of the PLAXIS modeling is provided in Appendix A.

2.2 LITERATURE REVIEW OF EARTH PRESSURES AGAINST RETAINING STRUCTURES

2.2.1 Overview of Earth Pressure Theories

Earth pressure has an important role in retaining wall design. Previous work including both theories and experiments had been conducted to study the earth pressures acting on retaining structures. Early lateral earth pressure theories include that of Couplet (1726), Coulomb (1776) and Rankine (1857). Earth pressure calculations for retaining structure designs are based primarily on the theories proposed by Coulomb (1776), Rankine (1857) and empirical earth pressure charts of Terzaghi and Peck (1967). Coulomb theory treats the pressure problems in terms of force, and Rankine theory treats the problems in terms of stress. Although the logarithmic spiral earth pressure theory developed by Terzaghi (1941) can provide more accurate estimation of earth pressure, it is much less widely used than the Coulomb and Rankine theories due to its complexity.

Both Coulomb and Rankine theories use limit equilibrium mechanics with many simplifying assumptions. According to both Coulomb and Rankine theories, the lateral earth pressure is equal to the vertical stress at one point multiplied by a lateral earth coefficient K, namely,

$$\sigma'_h = K \times \sigma'_v \tag{2.1}$$

The basic assumptions for the earth pressure theories proposed by Coulomb (1776) are:

(1) Soil is isotropic and homogeneous and has both internal friction and cohesion.
(2) The rupture surface is a plane surface and the backfill surface is horizontal.
(3) The friction resistance is distributed uniformly along the rupture surface and soil-to-soil friction coefficient is $f = \tan\phi$.
(4) The failure wedge is a rigid body undergoing translation.
(5) Friction forces are developed between the wall and the soil.
(6) Failure is a two-dimensional problem, namely a plane strain problem.
(7) The extreme values of force determined by Coulomb theory are expressed as:

$$P_{a(p)} = \frac{1}{2} K_{a(p)} \gamma H^2 \tag{2.2}$$

In which, P_a, P_p and K_a, K_p are active and passive forces and earth pressure coefficients, respectively.

Rankine (1857) considered soil in a state of plastic equilibrium and used essentially the same assumptions as Coulomb, except that he has assumed no wall friction or soil cohesion. According to Rankine theory, the active effective stress is expressed as:

$$\sigma'_a = \sigma'_0 \tan^2\left(45^0 - \frac{\phi'}{2}\right) - 2c' \tan\left(45^0 - \frac{\phi'}{2}\right) \tag{2.3}$$

And the passive effective stress as:

$$\sigma'_p = \sigma'_0 \tan^2\left(45^0 + \frac{\phi'}{2}\right) + 2c' \tan\left(45^0 + \frac{\phi'}{2}\right) \tag{2.4}$$

in which, ϕ' is effective friction angle and c' is effective cohesion.

Substantial research effort has been carried out to illustrate the inaccuracies associated with Coulomb's and Rankine's theories. These inaccuracies have been verified by experiments and in engineering practice. Terzaghi (1920) indicated that the fundamental error proposed by Coulomb was that Coulomb ignored the fact that the sand consists of grains, and he dealt with the sand as if it was homogeneous mass with certain mechanical properties. After conducting several large-scale retaining wall tests with dry sand backfill, Terzaghi (1934) determined that the unit weight of the backfill and the amount of wall movement greatly affect the lateral pressure on the retaining walls. He also determined that the soil friction angle and the wall friction vary during wall movement and that the resultant pressures acts at a point higher than the lower third point proposed by Coulomb. Terzaghi (1936) further pointed out that the faults and limitations of Coulomb and Rankine theories are in relation to the assumption of a hydrostatic pressure distribution. Packshaw (1946) indicated the error assumption of zero wall friction in Rankine theory and stated that most walls are not frictionless. Bowels (1996) stated that the principal deficiencies in the Coulomb's theory are in the assumption of an ideal soil and a plane rupture surface. Duncan and Mokwa (2001) pointed out that the main disadvantage of the Coulomb's theory stems from the fact that it is assumed that the passive pressure failure mechanism involves sliding along a plane surface. Duncan and Mokwa suggested that values of passive lateral earth pressure coefficient, K_P, estimated by Coulomb theory are too high when the value of interface friction angle δ is larger than 0.4ϕ.

Since the first major advancement made by Terzaghi (1932), research has been conducted in order to understand the nature of earth pressure and soil-structure interaction. The following sections summarize much of the research work done to examine and modify current retaining walls design based on the classical earth pressure theories.

2.2.2 Active Earth Pressure against Retaining Structures

After conducting several earth pressure tests on large-scale retaining wall models, Terzaghi (1932) concluded that "a small yield of structure will cause shear resistance to develop in a sand backfill. When sufficient movement has occurred, the developed shear

resistance reduces the earth pressure on the wall to the active state. The soil placed in front of the retaining wall undergoes compression as the retaining wall moves in the direction of the applied loading. The resisting soil pressure will increase and then exceed the value of the pressure at-rest. Ultimately, if the lateral movement is great enough, the full shear resistance of soils will be developed and soils will reach its passive state of stress. Deformation of soils excess of this condition will not significantly affect the magnitude of the resisting force. Fully developed passive earth pressure requires much more displacements than that is required to develop the active earth pressure for the same soils."

In 1936, Terzaghi's classical experiments established that the change in wall pressure from at-rest to active or passive state is a function of the wall movement. He suggested that "for compact cohesionless materials an average movement of 0.0005 times the wall height reduces the total horizontal pressure to the active value and the pressure distribution becomes hydrostatic if the top of the wall moves 0.005 times its height. For loose materials, the necessary movement is greater." Terzaghi and Peck (1967) prepared earth pressure charts by adding their experience. In these charts, soils are classified into 5 different types and the earth pressures are given for each of these soils. These charts are practical and easy to handle, and at present they are widely used in design.

Lambe and Whitman (1969) indicated that "if the thrust against a retaining wall were greater than the active it would not mean that the wall was potentially in trouble. On the contrary, it would mean that the soil underlying the wall is much stronger than it needs be." They further pointed out that long before a wall can fail, it must move enough to mobilize the shear strength of the soil and to drop the thrust to its active value. Each of the above researches indicated that soil pressures against retaining structures were related to wall movements.

Sims et al. (1970) reported investigation results concerning the lateral active earth pressure acting on a large retaining wall. The wall was instrumented with strain gages and pressure cells were installed in the backfill to measure vertical and horizontal earth pressures. The backfill was made up of hopper ash. Based on the measurements, Sims et al. observed that lateral earth pressure was greater than expected and the pressure distribution was different from that used in the design of the wall, which was based on the classical earth pressure theories.

Casagrande (1973) pointed out that due to gradual yielding of the retaining wall during backfilling, only those movements occurring after backfilling contribute to the development of the totally active case. Casagrande (1973) also measured essentially at rest earth pressure on the lower portion of retaining structures.

Coyle and Bartoskewitz (1970) began a five year study to measure the lateral earth pressure on full scale precast panel retaining walls and cantilever retaining walls supporting highway fill sand, and to compare the measured earth pressures with that computed by the Coulomb and Rankine theories. The positions of pressure cells are shown in figure 2.1. Lateral earth pressure measurements were carried out for 385 days after the start of backfilling as shown in figure 2.2. According to reported results of Coyle and Bartoskewitz (1974), the measured pressure on the upper portion of the retaining wall was in good agreement with the calculated pressure by Coulomb and Rankine theories for the full active case on the upper portion of the panel. The measured pressure on the lower portion of the wall was more than twice those predicted by Coulomb and Rankine theories as shown in figure 2.3. Measured movements in the lower elevations were so small as to be negligible

and it was postulated that at-rest earth pressures were acting on this wall and at-rest earth pressure were acting near the bottom of the retaining wall, which was also observed by Casagrande (1973). Coyle and Bartoskewitz also pointed out that pressure changes occurred as a result of temperature variations and construction equipment activity both during and after backfilling shown in figure 2.4. For the higher pressures measured on the lower portion of wall, Coyle and Bartoskewitz suggested that it was due to the little movements in the lower part of the wall. They also indicated that higher measured pressures in the lower part of the wall could be the dead zone phenomenon. According to Coyle and Bartoskewitz's explanation, "if a wall yields by tilting or sliding until the backfill starts to fail, one part of the backfill adjoining the wall, represented by triangular bed as shown in figure 2.5, remains undisturbed and acts as if it were part of the wall. When considering a cantilever retaining wall, the Rankine active earth pressure is assumed to act on a vertical plane through the heel. However, the self-weight of the dead zone may be adding some additional pressures to the back of the wall that is not taken into account when calculating the lateral earth pressure according to Coulomb's theory. The dead zone could be contributing to the higher pressures in the lower part of the wall."

After conducting the rigid model retaining tests with a soft clay backfill, Moore and Spencer (1972) indicated that "the lateral earth pressure and pore pressure decreased as the wall moved outward. The magnitude of these pressure variations was found to depend on the magnitude and types of wall displacement. When the wall movement was stopped the lateral pressure and pore pressure rapidly increased and exceeded the initial pre-movement values. Ultimately, the pore pressure and lateral pressure decreased to the same magnitudes that existed before the wall was moved as shown in figure 2.6, 2.7 and 2.8. By further tests, Moore and Spencer observed that the time required for the lateral active and pore pressures to increase back to the post-consolidation values following the cessation of wall movement decreased as the amount of wall movement decreased.

From the field measurements on rigid retaining walls during and after fill placing, Jones (1973) concluded that the measured pressure exceeded the usual computed values and the distribution of pressure was differed from that assumed in design using classical earth pressure theories.

Fukuoka et al. (1977) reported measurement results of lateral active earth pressure against a large scale model steel cantilever retaining wall, 5 m height backfilled with cohesive soils, with and without 3m of surcharge respectively. From Fukuoka et al. reported result, it can be observed that the lateral active earth pressure increased with backfilling. After completion of backfilling, the lateral active earth pressure at different depth became constant as shown in figure 2.9 and 2.10. Fukuoka et al. observed that the increment of measured earth pressure due to surcharge load in the experiment was not as large as that predicted by Terzaghi-Peck theory. Fukuoka et al. further pointed out that this was due to the wall friction along the vertical side of the wall, which was developed by the relative settlement between the retaining wall and the backfill materials behind it.

Sherif et al. (1982) conducted unique shaking table experiments of rigid retaining walls backfilled with Ottawa sand to determine at-rest and active state and dynamic stress generated by granular soils against rigid retaining walls. They compared the experimental data with Coulomb's earth pressure calculation results. Sherif et al. pointed out that "active stress developed when the friction angle (δ) between the backfill soils and wall reached its maximum value. The backfill soils entered the active state at much lower wall displacement

levels than generally believed. The average wall translation, S, necessary for the development of active case (at $\tan\delta_{max}$) can be expressed as a function of the internal friction angle, ϕ of granular soils (in degree) and wall height, H:

$$S = H \cdot (7.0 - 0.13\phi) \cdot 10^{-4} \qquad (2.5)$$

The coefficient of active lateral earth pressure (when the active state is defined at peak $\tan\delta$) are higher on the average by about 30% than the active lateral earth pressure coefficient values given by the Coulomb solution. When the coefficient of lateral earth pressure is defined at wall displacement, S, equaling 1/1000 of the height, H, of the retaining wall, the experimental values and the Coulomb solution are almost the same."

Sherif et al. (1982) also investigated the coefficient of active earth pressure, K_A and found out that active earth pressure was mobilized and affected when the wall under consideration was rotated about its toe. Based on the experimental results, Sherif et al. observed that there was an initial abrupt drop in the horizontal stress values up to a certain wall rotation level and the rate of stress reductions decrease with further rotation and eventually a state of stress is reached whereby no reduction in stress values is observed with further wall rotation as shown in figure 2.11. The horizontal deformation necessary to mobilize the active state of stress at each transducer level is almost the same. The horizontal displacement necessary to mobilize the active state of stress was independent of soil angle of internal friction or density. Sherif et al. also observed that: (1) the at-rest stress distribution behind rigid walls and active stress distribution behind the rigid walls rotating at their bases are linear and that compaction or overstressing of the backfill sand increases the magnitude of the at-rest stresses behind the rigid walls. (2) The Jacky equation ($K_0 = 1 - \sin\phi'$) describing the at-rest pressure distribution behind a rigid wall is only applicable if the soil is deposited at its loosest state.

Fang and Ishibashi (1986), modeled rigid retaining wall tests with Ottawa sand backfill. The test results indicated that the distribution of active earth pressure against retaining wall rotating about its top is nonlinear, and the stress at the top of the rotating wall increased beyond the active conditions due to soil arching and the magnitude of the arching stress increased with increasing density of soil as shown in figure 2.12. Fang and Ishibashi (1986) suggested that for retaining wall rotating about its top, the arching zone extended downward from the top of the backfill to a depth ranging from one third to one fourth the height of the wall. For translational wall movement, the lateral earth pressures measured at various depths decreases rapidly with wall movement until the active state was reached. After that, the lateral earth pressure did not change with further wall translation movements as shown in figure 2.13. According to Fang and Ishibashi's, for the wall rotating about base, the lateral pressure at the upper elevations decreased very quickly, however, the lateral stress near the base of the wall decreased very slowly with wall rotation as shown in figure 2.14.

Tedd and Charles (1981, 1983) measured both the active and passive earth pressures on both sides of braced embedded retaining wall in over-consolidated clay at bell common tunnel construction in London. It was observed that the push-in action of the tunnel initially generated high pressures that dissipated within a few days. Carder and Symons (1989) reported similar results in a field study measuring earth and water pressures on a cantilever diaphragm wall in over-consolidated clay at bell common tunnel construction. Figure 2.15 to 2.19 present the measured earth and pore pressures reported by Carder and Symons. After

pile formation on site, the pore pressure readings and spade pressure readings kept constant with time, and after active state was reached there was no further pressure changes with wall displacements. This was also noticed by many researchers, such as Sherif et al.(1982) and Fang and Ishibashi (1986). Tedd and Charles (1981, 1983) additionally found that a minimum period of 1.5 months was necessary for all readings to reach final equilibrium for London clay, and the magnitude of the over-read pressure was estimated to be equivalent to approximately half the un-drained shear strength in stiff clay. Tedd et al. (1984) observed that both during and after construction, a significant reduction in horizontal active total stresses occurred during the process of the installation of the secant bored wall in London clay. A similar phenomenon was also observed by Gunn and Clayton (1992) in bell common tunnel construction in London. According to Tedd et al. (1984) and Symons and Tedd (1989), total lateral earth pressure on both sides of a retaining wall and water pressures close to a retaining wall showed no significant changes over a 43-month period of observation as shown in figure 2.20 and 2.21.

Symons et al. (1992) presented the measurements of total lateral earth pressure developing along the embedded retaining wall constructed in London Clay and compared it with the limiting active and passive values used in assessing wall stability. According to Symons' report, the measured active earth pressures were about twice the calculated maximum active earth pressure values as shown in figure 2.22. Table 2.1 summarizes the many researches on active earth pressure against retaining wall.

2.2.3 Passive Earth Pressure against Retaining Structures

Compared to active earth pressure problems, passive earth pressure problems receive relatively little attention. Passive earth pressure plays a very important role in soil-structure interaction, as it resists movement of structures and provides a stabilizing force for retaining structures. Maximum passive earth pressures can be calculated using Rankine, Coulomb and Log Spiral earth pressure theories. However, each of these theories has limitations and none provides information on the relationship between the resistance and wall movements (Duncan and Mokwa, 2001). Many studies indicated that the magnitude of the passive earth pressure is closely related to the magnitude of the structures' movements, the direction in which the structure moves, strength and stiffness of the soils that resist the structure movements, friction or adhesion on the interface between the structure and the soils in contact, and the shape of the structure.

Most publications about the subject of passive earth pressures are theoretical only. Based on the frictional resistance alone (friction angle, ϕ), many researchers had developed passive pressure coefficients, e.g., Coulomb (1776), Rankine (1857), Caquot and Kerisel (1948), Brinch-Hansen (1953), Sokolovski (1955), Janbu (1957), Sokolovski (1960), Terzaghi and Peck (1967). Morgenstern and Eisenstein (1970) compared the passive earth pressure coefficient K_P calculated with theories proposed by the above researchers and concluded that Coulomb's theory overestimated passive resistance, and noticeable differences exist between these theories. All above theories are theoretical solutions and depend on the assumption that the deformation prior to failure may be neglected. At failure, yield occurs simultaneously throughout the mass at a constant yield stress (Rowe and Peaker, 1965), which lack experimental and field measurements verification.

The first advanced known measurements of horizontal passive earth pressure appeared to be those of Terzaghi (1920) using a two-inch high wall. Passive earth pressure coefficients were observed to be greater than 10 for dense sand after smaller wall movements, and well in the excess of the value of two (2.0) for loose sand at a wall movement equal to 15% of its height. Based on experiments, Terzaghi had noticed that the translational movement of a retaining wall greatly influences the horizontal passive earth pressure against the wall.

Franzius (1924) built a single wall 1 m wide and 0.6 m high to determine the effects of wall friction on passive resistance. From the tests results, he concluded that the observed values were at least twice the values computed on the assumption of zero wall friction.

Streck (1950) summarized his continuation of Fanzius' work with a single wall 2m×2m where the side wall friction was reported to be reduced to 10% of the passive pressure via an interface made of paper and grease. At failure, the passive pressure coefficients were stated to be about twice of the Rankine values based on the angle of repose. These values were less than those derived from the Mohr-Circle analysis using the measured wall friction angle, δ_m.

Brinch-Hansen (1953) studied the rupture planes under different types of wall movements in a small scale model with a wall 15cm×15cm. He indicated differences in the shape and size of the rupture wedges under different wall displacements and with different wall frictions.

Tschebotarioff and Johnson (1953) used a single wall, 10 ft wide and 2 ft high, to investigate the effect of a rigid horizontal boundary at the level of the base of the wall and the effects of wall rotation. Five tests were made on walls with movements approximated to a translation and where the sand extended well below the wall. They developed curves of K_P under different wall friction angles, δ at failure.

In order to examine the validity of their assumptions, Rowe and Peaker (1965) directly measured the passive earth pressure on a vertical wall moved by translation against a horizontal fill of dry sand. The test apparatus was erected within part of a bin 14ft×9ft in a new 60-ton sand flume. The wall contact with the sand is 6 ft wide and 1.5 ft high and consisted of three separate sections each 2 ft wide. The central sections housed three columns of six earth pressure cells. This elaborate equipment allowed a control of the wall direction and of the consequent rate of mobilization of wall friction. From the tests results, Rowe observed that the distribution of pressure on the translating wall was essentially linear in all the tests at each stage of deformation up to failure.

Rowe and Peaker (1965) also discovered that the angle of wall friction, δ, changed in relation to the rate of wall displacement. The rate of displacement depends on the instantaneous direction of the wall movement from the horizontal and the volume change rate of the sand behind the wall at each stage of the tests as shown in figure 2.23 and 2.24. Rowe and Peaker's test results show that the passive earth pressure coefficient K_P, the soil friction angle ϕ and the wall friction angle δ, increased initially with the increase of the wall's translational movements and kept constant after they reached peak values as shown in figure 2.25. This fact was later observed also by Narain and Nandakkumaran (1969), Sherif et al. (1982, 1984), Fang et al. (1994, 1997, 2001). Rowe and Peaker (1965) pointed out that neglecting the influence of the displacement on the soil's friction angle ϕ and wall friction δ would lead to errors in the use of all existing earth pressure theories. The tests also discovered that for loose sand, the observations were in a good agreement with that predicted

by theories only after large wall displacements to be unacceptable in practice. For dense sand, progressive failure of elements in the mass lead to average maximum Coulomb values of ϕ' that are smaller than those predicted by the plane strain compression tests.

D'Appolonia and D'Appolonia (1967) reported that if the backfill was loose, the passive earth pressure obtained experimentally compared well with those obtained from Coulomb theory as observed by Rowe and Peaker (1965); if the backfill was dense, the Coulomb solution was approximately 100% higher than the experimental results.

Researchers such as Narain and Nandakkumaran (1969), Fang et al. (1994), Broms and Ingleson (1971) had noticed that in addition to wall translation, wall rotation also induces passive earth pressure. Narain and Nandakkumaran (1969) carried out series of tests with both loose and dense sand to study the passive earth pressure acting on a rigid retaining wall under three different wall movements (figure 2.26): translation and rotations about its top or toe. From the test results shown in figures 2.27 and 2.28, Narain and Nandakkumaran discovered that:

(1) For translation, pressures distribution along the wall height was linear. A different wall movement, the pressures at different depths increased with the increase in wall displacements and the maximum pressure at all depths were reached simultaneously. Passive earth pressure coefficient increased directly with wall movements till a maximum value was reached. Similar results were reported by Rowe and Peaker (1965), and Fang et al. (2001). Fang et al. (1994, 2001) indicated that Rankine theory underestimated the passive thrust, while Coulomb theory overestimated the passive pressure, and experimental values were in good agreement with Terzaghi's prediction based on the general wedge theory as shown in figure 2.29. According to Narain and Nandakkumaran (1969), the maximum passive earth pressure occurred at a wall displacement accounting to 8.6% and 6.4% of the wall's height, when translating in loose and dense sands respectively. Fang et al. (1994, 2001) reported that as the wall movement exceeded 12% of the wall height, the passive earth pressure would reach the maximum constant value, regardless of the initial density of the backfill as shown in figure 2.30.

(2) For rotation about its top. The displacement of the wall required to cause the maximum coefficient of passive earth pressure equaled to 6.6% and 3.3% of the wall height for loose and dense sand respectively. According to Fang et al. (1994) observations as shown in figure 2.31 and 2.32, pressure measured near the lower edge of the wall increased rapidly with wall rotation before reaching an ultimate value. The pressure near the top did not however change so significantly. There were some differences between the displacement models proposed by Narain and Nandakkumaran (1969) and those proposed by Fang et al. (1994).

(3) For rotation about its toe. The maximum values of pressures were not reached simultaneously at all points. Similar results had been observed by Sherif et al. (1982) for active earth pressure modeling along the walls. The pressure distribution on the wall was far from being triangular and approximated a parabola. Similar observations were reported by Fang et al. (1994) as shown in figure 2.33 and 2.34. According to Narain and Nandakkumaran (1969), The coefficient of passive earth pressure increased approximately linearly with the wall movement and the maximum values were reached at a wall displacement (at mid-height of the wall) corresponding to 10% of the height of the wall for loose sand and 7.5% of the height of the wall for dense sand. According to Fang et al. (1994), an ultimate value for passive earth pressure coefficient K_P did not exist. Fang et al. (1994)

discovered that soil pressures measured near the top increased with the increasing of wall movement, while the change of stress detected near the wall base was quite small, and the stress monitored near mid-height of the wall rose continuously with increasing wall movement. The wall movement models set up by Narain and Nandakkumaran (1969) were the same as those shown in figure 2.35.

Broms and Ingleson (1971) and later Ingold (1979a) had observed that a small rotation of the wall of 0.01 rad (0.57°), was sufficient to generate a full passive pressure in front of a wall with dense fill. According to the South African Code (1972), a rotation of up to 0.05 rad (2.86°) is required to fully mobilize passive thrust for very stiff clays.

Much of the research work about passive earth pressure acting on a retaining structure had been conducted in the laboratory. Clayton and Milititsky (1983) conducted a field experiment on a small diameter bored pile in London clay and observed that there were few changes in the measured total passive stresses over a period of 150 days. Tedd et al. (1984) reported the measurements of earth pressure acting on the cantilever diaphragm wall in over-consolidated clay. They pointed out that the clay in the supporting side had reached the passive state during construction and the measured passive earth pressure and pore pressure did not show significant changes during the observation period.

Carder and Symons (1989) reported the field measurements of passive earth pressure acting on a retaining wall (diaphragm wall) during the Bell common tunnel construction in London clay and discovered that full passive earth pressure remained after the excavation was completed at the front of the wall. Table 2.2 summaries the research studies conducted on the passive earth pressure against retaining walls.

2.2.4 Compaction-Induced Earth Pressure against Retaining Structures

Compaction-induced earth pressure and deformation of structures are a serious concern in the design and analysis of retaining structures. Duncan and Seed (1986) observed the following: “Today, despite progress made in understanding the phenomenon of compaction-induced stresses, it remains true that compaction of soils induces soil stresses that not yet amenable to accurate and reliable analysis with existing theories and procedures.”

During his large scale model tests, in 1932 Terzaghi observed that compaction on backfill sand, significantly affected lateral earth pressures acting against structures and resulting wall deflections. Terzaghi (1934) repeated the biscuit bin experiment of Darwin (1883) on a grander scale and discovered that the pressures exerted by loose fill were smaller than for compacted materials. Since that, several researchers had investigated the effects of compaction using different compaction methods on the backfill behind a rigid wall to determine the extent to which the compactions could influence the earth pressure acting on the wall. All relevant work indicated that compaction of the backfill behind a rigid retaining wall causes lateral earth pressures that exceed those predicted by the classical earth pressure theories.

During the laboratory tests on modeling retaining walls, Rowe (1954) had observed that the soil was preconsolidated, leaving a high residual lateral pressures; “The horizontal stress does not return to its original value since if $\Delta\sigma'_v$ is caused by compaction, there will be lateral strains induced that are largely plastic and therefore unrecoverable.” Whiffin (1954) indicated that the vertical earth pressures increased with the increase of the degree of

compaction and the maximum vertical earth pressure was about twice that of a static roller with the same weight.

Sowers et al. (1957) pointed out that the lateral earth pressure developed by soil compaction and remained after compaction completion, could be a critical factor in the deflection of the structure, as it could produce excessive deflections. Sowers et al. conducted laboratory and field tests investigating the compaction induced earth pressure against retaining structures, using a 4 in. diameter cylinder filled with sand and clay respectively. Sowers et al. observed that pressure for the compacted sand or clay greatly exceeded those for loosely un-compacted sand or clay dumped against retaining structures and also exceeded at rest pressure as shown in figure 2.38. For rigid non-yielding retaining structures, the residual pressures in the sand did not change appreciably with time after the compaction work was completed. The residual pressures in clay decreased about 30% in the first 24 hours but had experienced little change thereafter. Sowers et al. additionally indicated that if the structure deformed under the action of lateral earth pressure, the residual lateral pressure would be reduced.

Forssblad (1963) measured earth pressure distribution under different types of vibratory compactors. He found out that when the relative density of the sand was high, the measured vertical earth pressure distribution at different depths below the ground surface was close to the results calculated using the Boussinesq stress equation. For loose sand, the measured vertical earth pressure increase was lower than that calculated by Boussinesq equation, in good agreement with that reported by Whiffin (1954).

Davies and Stephens (1966) investigated a model cubic container with the dimensions 24in×24in×24in, filled with cohesionless soils under various degree of compaction. They found out that compaction increased the magnitude of the lateral pressures exerted on the walls of the container and this increase was the greatest towards the top of the container, accompanied by additional lateral deflection of the sides of container.

Terzaghi and Peck (1967) observed that for rigid structures, the magnitude of the earth pressure depends to a large extent on the methods of placing the fill. D'Appolonoa et al. (1969) conducted a field test program of sand compaction with vibratory rollers. It was observed that a large horizontal stress was built up as the result of several successive passes of the roller. At a given depth, the lateral earth pressure coefficient K_0 was larger when measured perpendicular to the roller path than parallel to the path as shown in figure 2.39. However, when rolled in an orthogonal crisscross pattern, K_0 was isotropic with a value between the extremes of the unidirectional rolling.

Broms (1971) proposed that above a certain critical depth, the residual lateral earth pressure is greater than the at rest pressure (after the compaction pressure was removed), while below the critical depth, the residual lateral earth pressure is equal to the at-rest pressure as shown in figure 2.40. Youd (1972) studied the compaction behavior of Ottawa sand in response to repeated cycles of simple shear and concluded that shear strain was the primary factor causing compaction of granular materials. Casaggrande (1973) cited the results of field measurements that revealed that even light compaction could result in the development of greater than active earth pressure. Based on field measurements of earth pressures against motorway retaining walls and bridge abutments during and after fill placing, Jones (1973) concluded that the measured pressure exceeded the usual computed values and that the distribution of pressures differed from the one assumed in design. Aggour and Brown (1974) numerically analyzed the effects of compaction on various levels of

backfill behind a retaining wall. Aggour and Brown (1974) indicated that the resulting wall deflections and earth pressure magnitudes and distribution against the wall, considerably modified the “at-rest” pressures and were of practical significance as shown figure 2.41.

Matsuo et al. (1976) observed considerable increase in both the measured vertical and horizontal pressures, throughout the entire depth of a dry sand deposit upon the completion of the compaction. There was no sudden drop in the vertical pressures compared to their normal overburden values upon the removal of the compaction device; rather, the decrease in the vertical pressures commenced after the completion of the compaction and continued over a specific period of time. They further pointed out that decrease in vertical pressure with time may take a few hours and could extend up to 72 hours. This period mainly depended on the level to which the vertical pressure had increased above the normal overburden values. According to Matsuo et al. (1976), the vertical pressures in the deeper depths in the denser sand remained appreciably above the normal overburden pressure values long after the compaction completed so that further decrease in the stresses ceased. In case of horizontal pressures, the decrease of the measured pressure with time (maximum of 72 hours) was not significant.

Fukuoka et al. (1977) reported measurements of lateral active earth pressure against a large scale 6m height cantilever retaining wall, subjected to variable degrees of compaction of sandy backfill materials. Fukuoka et al. observed that earth pressure in loose sand was large and reacted very sensitively to the surcharge load. The poorly compacted backfill mass easily followed the movement of the wall, making it difficult to reduce the earth pressure. The degree of the backfill compaction had a remarkable influence on the magnitude and distribution of the earth pressure. In the case of well compacted backfill soils, active earth pressure was clearly observed with gradual movement of the wall. However, for loose sand, the initial earth pressures were maintained in spite of wall movement as shown in figure 2.42. Fukuoka et al. further indicated that the size of sliding soil mass was much smaller than in Coulomb’s theory, because a well compacted backfill had the ability to self support itself. In the case of well compacted sand, the earth pressure distribution was trapezoidal, completely different from the hydrostatic distribution. It was additionally pointed out that the earth pressure increase developed as a result of the compaction tended to remain constant as shown figure 2.43. A reduction in earth pressure with time after the compaction was observed in a well-compacted backfill. Whereas, for loose sand, a tendency of increasing earth pressure was observed for loosely compacted backfill.

Ingold (1979b) reported about the performance of a long reinforced concrete cantilever retaining wall during backfilling. Fill sand was placed in front of and behind the wall to minimize bending moments and any risk of sliding due to unequal filling. Compaction was done by four passes of a Stothert and Pitt 54T vibrating smooth-wheeled towed roller with the filled placed in 1.3 ft thick layers. Ingold (1979b) observed that several cracks were found in the front face of wall, and no further widening of the cracks took place after the discovery of the failure. The wall movement did not increase once the compaction was completed. The distribution and magnitude of the lateral earth pressures behind the retaining structures were found to be different from those predicted by the classical earth pressure theories as shown in figure 2.44.

Coyle and Bartoskewitz conducted a five-year study starting at 1970 at Texas A&M University, to measure field lateral earth pressure on full scale cantilever retaining walls with strip footing. According to their report Coyle and Bartoskewitz (1981), the lateral pressure

remained at a high level immediately adjacent to the structures. According to their explanation, during the process of compaction, soils moved downward against the structures, developing friction. When the compaction pressure was released, the upward movement was restrained by the friction, and full expansion could not take place, therefore the lateral earth pressure remained at a high level.

Carder et al. (1977, 1980) performed a series of tests to measure the compaction-induced earth pressure with full scale rollers at the Transportation and Road Research Laboratory in England and reported the result of the measurements of compaction-induced lateral earth pressure behind the retaining walls. In 1977, Carder et al. performed an experiment in which sand was compacted behind a mass retaining wall using a vibratory roller. Carder et al. (1977) indicated that the horizontal earth pressures induced by the compaction of the sand did not change appreciably with time unless the wall moved towards or away from the backfill. Carder et al. (1980) conducted a test in which a silty clay backfill behind the same retaining wall was compacted by a static roller. They observed that in a clay backfill, the high horizontal earth pressure induced by compaction tended to decrease over time to normal at-rest values, as shown in figures 2.45and 2.46. The pressure exerted on the experimental retaining wall decreased to at-rest values within a period about four months after the backfill was compacted behind the wall as shown in figure 2.47. Carder et al. pointed out that the decrease in the measured pressures could be attributed to changes in pore pressures within the fill as within four months, all positive pore pressures had dissipated, and negative pore pressure existed through the depth of the fill. Carder et al. further pointed out that the stress decrease was also possible due to deviatoric stress relaxation caused by creep effects in soils. Clayton et al. (1991) performed different scale model laboratory tests to investigate the pressure exerted on retaining wall backfilled with compacted clay. Based on the test results shown in figure 2.48, they suggested that for a clay backfill, subsequent swelling of the fill may lead to further increase in lateral pressure after the end of construction.

Duncan and Seed (1986) developed analytical model and procedures for the evaluation of peak and residual compaction-induced lateral earth pressures. The pressures related either to the free field or adjacent to vertical, non-deflecting soil structure interfaces. The analytical results were compared with full-scale measurements in order to examine the analytical models. Duncan and Seed (1986) presented a finite element analysis of compaction-induced pressures based on a hysteretic model for residual soil stress induced by multiple cycles of loading and unloading. Duncan et al. (1991) further indicated that the residual horizontal earth pressures in a compacted soil mass could be considerably larger than the horizontal pressures in an un-compacted mass. The residual pressures were highest in cases where equipment was operated close to a non-yielding structure. When heavy equipment exerting intense pressure was used, the residual horizontal pressure could exceed the normal at-rest values to depths of 30 ft or even more. Table 2.3 summaries the researches on the compaction-induced earth pressure against a retaining wall.

2.2.5 Earth Pressure against Sheet Pile Walls

Substantial experimental research and field measurements were carried out regarding active, passive and compaction-induced pressures developing against rigid retaining walls. In contrast, relatively few experimental studies and field measurements were conducted for

earth pressures acting on sheet piles, especially in soft soils. Sheet piling is the most common type of flexible earth retaining systems used as waterfront structures. In contrast to the construction of other types of retaining walls, the building of sheet pile walls does not usually require dewatering of the site. Sheet piling is ideally suited to sites with high ground water tables or low bearing capacity soils. Many authors had developed theoretical solutions for cantilever sheet pile or anchored or propped sheet pile design, such as Blum (1931), Brinch Hansen (1953), Windles (1959), Weiβenbach (1969), Denatale and Ibarra-Encinas (1992), Hartmann-Linden (1997), and Kort (2002). The conventional method for analyzing cantilever sheet piling in homogeneous foundation soils is based on the assumption (Clayton and Milititsky, 1983) that the piling rotates about some pivot point, causing active state stress to develop in the back of the wall above the pivot point and in front of wall below the pivot point as shown in figure 2.49. The wall derives its stability from the passive pressures that develop in front of the wall above the pivot point and in back of the wall below the pivot point.

Only limited number of research studies has been conducted to examine the current sheet pile design procedures via field measurements. The following section presents studies that conducted field measurements monitoring the active earth pressures against the supporting side of a strutted sheet pile wall in excavation in cohesive soils.

DiBiagio (1977) reported the measured total lateral active earth pressure against a propped sheet pile wall during excavation. DiBiagio indicated that because of the corrugations in the wall, the cells must be placed either on the protruding or indented corrugations, as shown in figure 2.50. In this case, total pressure cells were placed at both the protruding and indented locations at the same depth in soft clay (figure 2.50). DiBiagio observed that measurements (at locations P_1 and P_2) were almost equal immediately after the sheet pile driving (at the same depth at different locations), but later, the measured total pressures (at the same depth) were different and changed with the excavation progress. DiBiagio pointed out that the different measured pressures P_1 and $P_{2,}$ presumably were due to sheet pile movements or clay consolidation or arching. DiBiagio (1977) suggested that a best estimate of the average total stress per unit length of the wall can be made by averaging P_1 and $P_{2,}$ but clearly this average may be significantly in error.

Stille (1979) measured anchor loads and deflection of anchored sheet pile wall during all excavation stages in clay. Stille observed that measured anchor loads were in good agreement with that calculated with new Swedish design rules. Stille indicated that the time-dependent properties of clay (the creep effect), must be considered to get a good agreement between the calculated and measured deflection. Tamano (1983) measured the lateral active earth pressure in the backfill behind a multi-tied anchored sheet pile wall in excavation. Tamano observed that the distribution of lateral earth pressure exerting on the anchored sheet pile wall was transformed by redistribution of earth pressure from triangular shape to trapezoidal distribution as the wall displace during excavation. Gigan (1984) measured the active soil pressure in a backfill behind an anchored wall with active tie-rods, as well as the sheet pile deformation in order to verify the validity of the most widely used calculation method.

Finno (1989) measured pore water pressure, sheet pile deformation, and strut loads in a 40 ft deep braced excavation in soft to medium stiff, saturated clays in Chicago. Finno observed that relatively high excess pore pressure developed during the sheet pile installation and strut loading; but these initial pore pressures dissipated rapidly as shown in figure 2.51.

Pore pressures due to excavation unloading were rather small. Little net change in pore pressure was observed at the end of construction. The maximum measured loads in each strut were approximately equal to the magnitudes specified by the design earth pressure envelop.

Kort and Van Tol (1999) conducted a full scale field test on two steel sheet pile walls in soft clay with one thin layer of peat (in Pernis, near Rotterdam) to model the braced excavation (shown in figure 2.52). The earth pressure and water pressure on the retained side and excavated side were measured. The earth pressure distribution at eight points on the retained side and four points on the excavated side did not show any significant changes during the various excavation stages. Kort et al. (2000) pointed out that the change of total pressure was due to the change of water pressure. Kort (2002) indicated that increase of lateral displacement and bending moment in the long-term was caused by a relatively small change in the earth pressure (shown in figure 2.53).

Endley et al. (2000) measured and analyzed the lateral earth pressure and deflection of an anchored sheet pile wall constructed as a dock. Endley et al. (2000) indicated that high lateral earth pressures resulted from the backfill construction methods, which in turn, produced large sheet pile deflection and stresses. Endley et al. proposed that "manufacturers' values of section modulus and moment of inertia are not correct for the Larssen section. Crimping (or even welding) the two sections do not alter the properties. The section modulus and inertia moment of the specified sheet pile sections should be independently verified. The values of section modulus and moment of inertia, in conjunction with lateral earth pressure, play an important role in wall deflection."

Peck (2002) reported the measurements of strut loads (shown in figure 2.54) based on field observations of open-cut in clay with propped-sheeting taken place during the construction of the Chicago subway. Peck indicated that the magnitude of the total lateral earth pressures was in satisfactory agreement with either the plane or general wedge theories for purely cohesive soils with no effective internal friction, but that the distribution of the pressure was non-hydrostatic.

To date, only several field measurements had been conducted to monitor the earth pressure against sheet piles. This work is summarized in table 2.4. However most of the studies are related to anchored or strutted sheet piles in excavation or do not include measurements of earth pressures directly in place, i.e. include measurements of strut or anchor loads. Even fewer studies are known to investigate the passive earth pressure against the supporting side of sheet piles. No studies had been found to directly measure the passive earth pressure against cantilever sheet pile wall, especially in a peat deposit, and also no recorded work is known to measure the compaction-induced passive earth pressure against a cantilever sheet pile wall in peat.

2.3 SHEET PILES

2.3.1 General

Sheet piles are widely used as retaining structures, especially in excavation projects. Sheet pile walls consist of continuously interlocked pile segments embedded into the soils to resist horizontal pressures. The sheet pile walls are constructed by driving the sheet piles into a slope or excavation. They are considered to be most economical where retention of higher earth pressures of soft soils is required.

Sheet piles have an important advantage in that they can be driven to depths below the excavation bottom and so provide a control to heaving in soft clays or piping in saturated sand. This is not possible to achieve with soldier pile and lagging support that is a more permeable structure. Sheet piles however are more costly and less adaptable to hard driving conditions, particularly where boulders or irregular rock surfaces occur.

Sheet piles are easily driven into clays, sand, and clay-sand mixture because of the comparatively small displacement of the soils required during driving. Sheet piles permit large movements in weak soils and also need effective dewatering on site because seepage often occurs through the interlocks, which is sufficient enough to cause consolidation of compressible materials such as organic soils and soft silty clays. For sandy soils raveling will not occur if the interlocks are tight, but driving sheet piles into loose sand can cause subsidence.

Sheet piles can function as temporary or permanent retaining structure and are often used in excavation projects. Temporary sheet piling structures are used to control or exclude earth or water, or both, and allow permanent work to be proceeded. Permanent sheet piling is commonly used as a retaining structure and at times is also used as part of the structure often for underground buildings.

Sheet piles are available as Z or U shaped profiles in a variety of sections and lengths. Classification of the sheet pile can be made based on the materials that the sheet pile was made up of, and its usages.

2.3.2 Sheet Pile Classification based on Materials

2.3.2.1 Background

Sheet pile walls are constructed from a variety of materials. The most common sheet piling are made of heavy-gauge steel, light-gauge steel, timber, concrete, light-gauge aluminum and other materials such as vinyl, polyvinyl, chloride and fiberglass. The designer must consider the possibility of material deterioration and its effect on the structure integrity of the system. Most permanent structures are constructed of steel or concrete. Concrete is cable of providing a long service life under normal circumstances but has relatively high initial costs when compared to steel sheet piling. They are more difficult to be installed than steel piling. Long-term observations indicate that steel sheet piling provides a long service life when properly designed.

2.3.2.2 Heavy-Gauge Steel

These piles consist of interlocking sheets manufactured by either a hot-rolled or cold-formed process and conformed to the requirements of the American Society for Testing and Materials (ASTM) Standards A 328 (ASTM 1989a), A 572 (ASTM1988), or A 690 (ASTM 1989b). Pilings conforming to A 328 are suitable for most installations. Steel sheet piles are available in a variety of standard cross sections. The Z type piling is a predominantly used in retaining and floodwall applications where bending strength governs the design. When interlock tension is the primary consideration for design, an arched or straight web piling should be used. Turns in wall alignment can be made with standard bent or fabricated corners. Typical configurations are shown in figure 2.55.

2.3.2.3 Light-Gauge Steel

Light gauge steel pilings are shallow depth sections. Cold formed to a constant thickness of less than 0.25 inch and manufactured in accordance to ASTM A 857 (1989c). Yield strength is dependent on the gauge thickness and varies between 25 and 36 kips per square inch (ksi). These sections have low modulus and very low moments of inertia in comparison to heavy gauge steel Z-sections. Specialized coatings such as hot dip galvanized, zinc plated, and aluminized steel are available for improved corrosion resistance. Light-gauge piling can be considered for temporary or minor structures. Light gauge steel can be considered for permanent constructions when accompanied by a detailed corrosion investigation. Field tests should minimally include PH and resistivity measurements. Figure 2.56 shows configuration of typical light gauge steel.

Advantages of steel sheet pile:

- Resistant to high driving stresses developed in hard or rocky soils;
- Relatively light weight and easy to handle;
- Can be used repeatedly;
- Long service life either above or below the water line with modest corrosion protection;
- Easy to increase pile length by welding or bolting;
- Joints are less likely to deform when wedged with soils and stones during driving.

Disadvantages of steel sheet pile:

- Corrosion of steel sheet pile is a consideration;
- Not aesthetically pleasing in high profile situation.

2.3.2.4 Timber

Timber sheet pile can be constructed of independent or tongue-and-groove interlocking wood sheets. This type of piling should be restricted to short to moderate wall heights (less than 9 feet) and used only for temporary structures. The most common types of timber sheet piles are wooden planks and Wakefield piles. Wakefield piles are constructed by nailing three planks together in an offset manner. Wooded pile walls may be considered permanent if the wall is permanent submerged underwater or if treated with preservatives. Figure 2.57 presents typical configuration of timber pile sections.

Advantage of timber sheet piles:

- Low cost;
- Readily available;
- Easy of handling.

Disadvantage of timber sheet pile:

- Difficult to install into dense or gravelly soils;
- Limited to short duration retaining walls at construction sights;
- Limited height of structures;
- Decay of structures may be hidden.

2.3.2.5 Concrete

These piles are precast sheets 6 to 12 inches deep, 30 to 48 inches wide, and provide with tongue and groove or grouted joints. The grouted type is cleaned and grouted after driving to provide a reasonably watertight wall. A bevel across the pile bottom, in the direction of pile progress, forces one pile against the other during installation. Concrete sheet piles are usually pre-stressed to facilitate handling and driving. Special corner and angle sections are typically made from reinforced concrete due to the limited number required. Concrete sheet piling can be advantageous for marine environments, streambeds with high abrasion, and where sheet pile must support significant axial load. Past experience indicates that this pile can induce settlement due to its own weight in soft ground materials. in this case the water-tightness of the wall will probably lost. Figure 2.58 presents typical concrete sections of concrete piles.

Advantage of concrete sheet pile:

- Rigid and incur larger earth pressure and greater bending stresses than a flexible wall;
- Longer service life than other walls;
- Good aesthetics;
- Advantageous in marine environments;
- Capable of supporting significant axial loads;
- Durable for use in streambeds with high abrasion.

Disadvantage of concrete sheet pile:

- Heavily and bulky and require larger equipment to deliver, handle and drive;
- Higher material cost;
- Large displacement piles and consideration must be given to adjacent structures;
- May cause settlement in soft soils;
- Require grouting and water stops to make watertight.

2.3.2.6 Light-Gauge Aluminum

Aluminum sheet piling is available as interlocking corrugated sheets, 20 to 4 inches deep, 0.10 to 0.188 inch thick and made from aluminum alloy 5052 or 6061. These sections have a relatively low-section modulus and moment of inertia necessitating tiebacks for most situations. A z-type section is also available in a depth of 6 inches and a thickness of up to 0.25 inches. Aluminum sections should be considered for shoreline erosion projects and low bulkheads exposed to salt or brackish water when embedment will be in free-draining granular materials. Figure 2.59 presents typical sections of light-gauge aluminum sheet piles.

2.3.2.7 Other Materials

Piling made from special materials such as vinyl, polyvinyl chloride, and fiberglass is also available. These pilings have low structural capacities and are normally used in tieback situations. Available lengths of piling are short when compared to other materials. Material properties must be obtained from the manufacturer and must be carefully evaluate by the designer for each application.

2.3.3 Sheet Pile Classification based on Wall Type

2.3.3.1 Background

Based on the supported type for the sheet piles, it can be classified as cantilever wall, anchored wall and propped wall. The selection of the wall type should be based on the function of the wall, the characteristics of the soils, and the proximity of the wall to existing structures.

2.3.3.2 Cantilever Walls

Cantilever walls are commonly used as floodwall or as earth retaining walls with low wall heights (10 to 15 feet or less), because of the large earth pressures and deflections that may be developed. However even this may be excessive where soft or loose soils occur in front of the wall. Stiffer cantilever walls, of concrete or steel including diaphragm walls and heavy composite walls, may be satisfactory to heights of 12 m providing the ground is string enough. Because cantilever walls derive their support solely from passive pressure exerted on the embedded portion of the pile, the required penetration is high. It is not advisable to use cantilever walls when foundation is with the active area, because the deflection at the head of the wall is high, which will cause damage. One advantage of cantilever wall is that it can be pulled out and reused. Figure 2.60 shows typical configuration of cantilever wall.

2.3.3.3 Anchored Wall

An anchored wall is defined as a sheet pile wall that derives its support from a combination of interaction with surrounding soil and one (or more) mechanical device that inhibit motion at an isolated point. An anchored wall is required when the height of the wall exceeds the height suitable for cantilever wall or when lateral deflection of the wall is a consideration. The proximity of the anchored wall to the existing structures is governed by the horizontal distance required for the installation of the anchor.

Following the installation of steel sheet piles a small excavation is made along the wall and the first row of anchors is installed. The trench is only made wide enough for the anchor installation machine and the excavation-anchor sequence is repeated until the bottom is reached. Well-constructed anchor walls undergo less lateral deflection than braced walls and so provide a better control of back slope subsidence. Anchor installation only requires a small excavation to allow equipment access. However for braced wall installation there is often a requirement to excavate below the level of support.

Anchored walls are always pre-stressed which essentially removes the slack from the system. The anchors will maintain their load throughout the excavation sequence unless creep occurs. The anchors also place the entire soil mass between the anchors and the wall in compression, thus creating a very large gravity wall. There are three causes of loss of subsidence for anchor systems:

- Caving of the anchor holes prior to grouting
- Flow of cohesion less material into the excavation through wall openings made for anchor installation

- Possible downward movement of the wall due to the vertical component of the anchor forces.

Figure 2.61 explains general procedures for anchor installation for support of the sheet pile or concrete diaphragm wall.

1) Trench excavated after wall installed;
2) First anchor row installed;
3) Trench excavated for next anchor row and excavation lowered.

Figure 2.62 shows one typical configuration of the anchored wall.

2.3.3.4 Propped (Braced) walls

Propped walls may have one of more levels of support in the upper part of the wall. They can be designed to have fixed or free earth support at the bottom and derive their stability from the bracing. Braced walls are commonly used in confined excavations and cofferdams.

For propped walls in the free earth condition the penetration of the piles should be such that the passive pressure in front of the piles will resist forward movement of the toes of the piles but will not prevent rotation. The piles are supported by ties at the top of the wall and the soil at the base of the wall.

In fixed earth conditions further penetration of the pile is required to ensure that not only the passive pressures in front of the wall resist forward movement but also that the rotation of the toe is restrained by the passive pressures. Figure 2.63 shows a typical configuration of a propped sheet pile wall using.

2.3.4 Failure Models of Sheet Pile Walls

There are mainly three types of failure models of sheet pile walls caused by loads exerted on the walls.

2.3.4.1 Deep-Seated Failure

A potential rotational failure of an entire soil mass containing an anchored or cantilever wall is illustrated in figure 2.64. This potential failure is independent of the structural characteristics of the wall and/or anchor. The adequacy of the system against this model of failure should be assessed through conventional analysis for slope stability (EM 1110-2-1902). This type of failure can not be remedied by increasing the depth of penetration nor by repositioning the anchor. The only recourse when this type of failure is anticipated is to change the geometry of the retained materials or improve the soil strengths.

2.3.4.2 Rotational failure due to inadequate pile penetration

Lateral soil and/or water pressures exerted on the wall tend to cause rigid body rotation of cantilever or anchored wall to failure as illustrated in figure 2.65. This type of failure is prevented by adequate penetration of piling in a cantilever wall or by a proper combination of penetration and anchor position of an anchored wall.

2.3.4.3 Other failure model

Failure of the system may be indicated by overstressing of the sheet piling and/or anchor components as illustrated in figure 2.66 and 2.67.

2.3.5 Steel Sheet Piles

2.3.5.1 Background

Steel sheet pile has the advantages of having relatively light weight, longer service life, lower costs compared to other type of sheet piles and a relatively high strength (in relation to weight). Steel sheet piles can also be often used. Z-shaped steel sheet piles were used in the cranberry bogs and other wetland areas of Route 44 at Carver MA.

According to ASTM A328/A328-03, there are mainly three types of steel sheet piles available in production: lightweight steel sheet pile, steel sheet pile, and steel pipe sheet pile. The steel pipe sheet piles are often used for permanent structures, while the lightweight steel sheet piles and steel sheet piles are used for both permanent and temporary structures. Of the lightweight steel sheet piles, the one most commonly used is the U-shaped design, which is available in two different cross sections when constructed to form a wall. One, in which the neutral axis of the wall becomes in line with the neutral axis of each sheet pile, and the other, in which the neutral axis of the wall becomes in line with the joint of the sheet pile. The steel sheet piles are manufactured by hot rolling of steel ingot, thus essentially different from the lightweight steel sheet piles that are manufactured by the cold rolling of steel sheets. The steel sheet piles are available in various designs, U-shaped, Z-shaped, H-shaped, and straight, which are used according to different application needs.

Hot Rolled (HR) indicates that the section shown is produced by the traditional steel hot-mill procedure. A semi-finished rough shape is reduced during a series of rolling stages to its final form. Metal thickness of flanges and webs may be varied and interlocks are shaped by the flow of hot metal.

Cold Forming (CF) describes a process whereby the desired sheet piling shape is obtained by passing a pre-finished sheet of steel through a series of rolls while in the cold state. While passing through these series of rolls, the interlock is also formed by bending the flange ends into a "hook and grip" type interlock. The section produced is of constant thickness.

2.3.5.2 Classification of Steel Sheet Piles according to Cross-Section Profiles

1. U-shaped steel sheet pile According to ASTM A328/A328-03, the U-shaped steel sheet piles feature the most available types. They also offer different effective widths, 400 mm, 500 mm, and 600 mm, as well as section modulus ranging from 529 cm^2/m to 3,820cm^2/m, thereby allowing optimum selection for required mechanical strengths. The joints are available in two types, Lackawanna and Larsen as shown in figure 2.68, though the production of Lackawanna type is discontinued at present. The U-shaped steel sheet piles feature the coincidence between the joint position and the neutral axis of wall in the wall application. In the curved application, a standard turning angle is six degrees in either side,

right and left, in relation to the neutral axis. U- shaped steel sheet piles are mainly used for intermediate to deep wall construction.

2. Z-shaped steel sheet pile The Z-shaped steel sheet piles feature joints located outside in the right and left when fit with each other. They are chiefly used for permanent structures. The section modulus ranges from 2,510cm^2/m to 4,550 cm^2/m. Z-shaped steel sheet piles are mainly used for intermediate to deep wall construction. Figure 2.69 presents the typical configuration of Z-shaped steel sheet pile sections.

3. Straight-web or flat type steel sheet pile The straight-web or flat type steel sheet piles feature very high mechanical strength of engaged joints, thus ideal-suited for cell structures. Figure 2.70 shows the typical configuration of straight or flat shaped steel sheet pile sections.

4. Arch shaped and lightweight gauge steel sheet pile Arch shaped and lightweight gauge steel sheet piles are mainly used for shallower wall construction. Figure 2.71 presents typical section configuration of arch shaped and lightweight gauge steel sheet pile.

5. Steel pipe sheet pile The steel pipe sheet piles are made from a single pipe with joints, and used for stand-alone permanent structures. The joints are available in three types, L-T, P-P, and P-T as shown in figure 2.72.

2.3.5.3 Classification of Steel Sheet Piles according to Applications

The steel sheet piles can be broadly divided into two categories, permanent and temporary structures. The detail classification is shown in figure 2.73.

2.3.5.4 Classification of Steel Sheet Pile Press Fit according to Structure Design

Steel sheet piles can be classified according to structure design as shown in figure 2.74. The steel sheet pile press-fit method offers the advantages listed below over the other methods.

1) Simplified work without the need for any large-scale equipment and facility for execution of work;
2) Rapid execution of work, contributing to considerably reduced construction period;
3) Selection of optimum cross section/length of steel sheet pile for different soil conditions contributing to reasonable and cost-effective planning;
4) Availability of lightweight walls, allowing advantageous earthquake-resistant design different from gravity-type structure.
5) Sheet pile with a capability of water drainage, prevent possible liquefaction caused by the earthquake in the vicinity of critical structure.

Recently developed construction machines allow pile installation even in sites where the driving method encounters difficulties in the upper section. This is done by adding shorter steel sheet piles in succession or in narrow roads or rivers where large scale machines fail to approach.

2.3.5.5 Classification of Interlocks

The main function of interlocks is to provide permanent connection of individual sheet piles in order to form a continuous, relatively water or earth-tight wall. The interlocks should permit reasonably free sliding to connect sheet piles during installation. The interlocks designed for tension applications should provide guaranteed minimum pull strength and allow some minimum swing between interlocks in order to form a circle. Various types of interlocks are depicted in figure 2.75.

2.4 INSTRUMENTED SHEET PILES

The instrumentation program includes five stations instrumented with total pressure cells (vibrating wire total pressure cells and tactile single load cells) and deflection monitoring system. As a first stage, the soil profiles were identified based on boring logs, sounding and SPT data. The instrumentation in each station was determined such that the instruments would be located in areas with deep peat layers. Secondly, the instrumentation specifications were determined based on considerations such as purpose, range, expected accuracy, cost etc. In summary, 30 vibrating wire total pressure cells along with 24 simple single load cells and inclinometer systems were chosen to be installed at five separate stations located in the areas with deep peat deposits. The instrumentation layout for each station was then designed as to the exact location of each cell on the instrumented sheet pile. The details of the instrumentation design are presented in chapter 4. The instruments were calibrated in the laboratory and calibration factors were determined before they were installed on the sheet piles. Following the calibration of all the pressure cells, they were transported to the machine shop for installation. Details of the instrumentation installation on the steel sheet piles are provided in chapter 4 and the field installation of the instrumented sheeting is described in chapter 7.

2.5 VIBRATING WIRE TECHNOLOGY

The TPC pressure cell consists of two steel discs welded around their periphery and then recessed on both sides to provide a central flexible pad. Both sides of the cell are active that gives more reliance on measurements at the inner face. A short length of thick wall steel tubing is welded into the edge of the pressure cell and communicates with a cylinder house containing a pressure transducer. During construction, the cell is first put under vacuum to remove any air, and deaerated oil is injected into the cell under pressure to force the plates apart separating them by a thin fluid film. The fluid also fills the steel tubing and cavity in the cylindrical housing containing the pressure transducer. Variations in fluid pressure resulting from changes of load acting on the cell are sensed by the pressure transducer. The TPC, equipped with vibrating wire pressure transducers, are fitted with a watertight cable to allow remote reading of the pressure changes.

The TPC exploits the dependency of a vibrating wire's resonant frequency on its tension to measure applied loads. Through mechanical means the applied load is transmitted to the wire causing a change in its resonant frequency from which the value of the applied load is measured by the MB-6T readout. The vibrating wire transducer pressure cells are monitored manually or automatically using the MB-6T readout unit or the SENSLOG data

acquisition system. In the model IRC-41A cable, the red and black wires are for the pressure transducer, and the green and white wires are connected to the thermistor. The MB-6T/6TL linear or frequency readings including the pressure readings and temperature readings are converted to pressure using the equations provided by TPC manuals.

Vibrating wire sensors are well known for their long-term stability. The advantage of vibrating wire sensors over more conventional types lies mainly in the sensor output, which is a frequency rather than a voltage. Frequencies can be transmitted over long (>2000m) cables without appreciable degradation of the signal caused by variations in cable resistance, which can arise from water penetration, temperature fluctuations, contact resistance, or leakage to ground.

2.6 TACTILE SENSORS TECHNOLOGY

Simple single tactile load cells were employed in the instrumentation project to measure the total horizontal pressure acting on the sheet piles in the peat. The cells are based on tactile sensor produced by Tekscan Corporation in Boston, MA and are developed specially for this project.

A tactile sensor consists of an array of pressure transducers, each of which produces a digital signal as the array is pressed and moved against the tissue. Just as an electronic camera digitizes the sense of sight, a tactile sensor digitizes the sense of touch. Tactile sensors are several times as sensitive as human touch and much more accurate and repeatable. Figure 2.76 presents an example of tactile images generated by measuring soil pressure against a wall as described by Paikowsky and Hajduk (1997).

2.7 DEFLECTIONS AND INCLINATION MEASUREMENT SYSTEM

2.7.1 General

The deflections measurement system consists of an inclinometer probe as part of a system, inclinometer casing, and data analysis and processing software. The various components are introduced below.

2.7.2 Inclinometer Casing

The function of the inclinometer casing is to control the orientation of the inclinometer probe. The casing sections are coupled and grouted inside the borehole, or fixed to the surface of piles or sheet piling. The casing and couplings have grooves spaced at ninety-degree intervals, which fit the wheels of the inclinometer probe, thus maintaining the orientation of the probe as it is traversed up and down the casing. The probe accurately measures the change in the angle of tilt, from the vertical, of each portion of the casing. These incremental changes are added together to give a vertical profile of the casing. Changes in the profiles become a measure of the stability of the structure. The inclinometer casing used is made by Geokon, which is manufactured from pultruded fiberglass, an ideal material, being very strong, lightweight and environment ally resistant. The pultrusion process guarantees there will be no spiraling of the grooves. Casing and couplers telescope snugly together. This has several advantages: the casing do not need specially machined or

molded ends and thus casing can be cut and joined together at any points along their length. Furthermore, connection can still be made even if the ends are damaged. A telescope joint can easily be made using an extra-long section of coupling, pop-rivets, to leave a space between the ends of the casings. Both casing and couplings have grooves so that the inclinometer probe can not lose its orientation as it passes through the telescoping coupling.

The casing and the coupling are pop-riveted together and the joints are waterproofed using caulk and tape. A bottom plug, pop-riveted and sealed, is used to cap the bottom of the casing and a top plug is used to cap the top of the casing. Lockable protective housings, made from galvanized steel pipe and cement-grouted in-place around the top of the casing, are recommended to help prevent damage and vandalism. Figure 2.77 presents the view of sections of inclinometer casing shown with standard length coupling. Figure 2.78 shows the configuration of the inclinometer casing and the telescope coupling.

2.7.3 Inclinometer System

2.7.3.1 General

The inclinometer system consists of inclinometer probe, cables, and readout box as shown in figure 2.79.

The inclinometer probe is designed for use with standard, grooved inclinometer casing. Spring-loaded wheels on the probe engage the grooves in the casing thus maintaining the probe in a known orientation.

While in use, the inclinometer probe (connected to cable) is lowered to the bottom of the casing and then is raised in increments equal to the wheel spacing. At each increment the probe is read by a readout box connected to the upper end of the cable as shown in figure 2.79. The readout device provides a measurement of the tilt of the casing to the vertical, at each depth increment. Repeat surveys of the casing reveal changes in these tilts, which can be analyzed to provide plots of lateral deflections of the casing, in orthogonal directions, at every depth increment.

2.7.3.2 Inclinometer Probe

The inclinometer probe itself (figure 2.80) is a cylindrical instrument typically about 800mm long and 25mm in diameter. Near each end it has a set of carefully machined spring-loaded wheels designed to center the probe in casing, while the wheels run in the grooves. Modern probes are biaxial, that is, the probe contains two accelerometers that measure the inclination of the probe axis with respect to the vertical. One accelerometer measures tilt in the plane of the inclinometer wheels, which track the longitudinal grooves of the casing. The other accelerometer measures tilt in the plane perpendicular to the wheels. Inclination measurements are converted to lateral deviations. Changes in lateral deviation, determined by comparing data from current and initial surveys, indicate the casing and hence the ground movements. Plotting the cumulative changes at each measurement interval yields a high resolution displacement profile. Displacement profiles are useful for determining the magnitude, depth, direction, and rate of ground movement. Figure 2.81 presents the view of inclinometer probe in casing.

2.7.3.3 Readout Box GK-603

The model GK-603 vibrating wire readout box (figure 2.82) is designed for use with all of Geokon's vibrating wire sensors. In use, the inclinometer probe is connected to the readout and lowered to the bottom of the hole. Readings are stored by pressing a button on the face panel (or the remote switch). An audible in the model GK-603 indicates the completion of the reading storages. When the survey is complete, the readings are saved in the solid state memory under an eight-character file name that can be transmitted to a host computer via RS-232 interface cable for archival purpose or further data reduction using spread sheets or GTILT software.

2.7.4 GTILT Software

GTILT is designed to handle the slope inclinometer data. A wide range of inclinometer probes, readouts, and loggers is supported, including equipment from other manufacturers.

GTILT is compatible with a wide range of inclinometer equipment; imports many types of inclinometer data files directly, and comes with conversion and/or downloading utilities for others.

Uses the same GTL data file format as GTILT for DOS. The file format is enhanced to include sketch objects to be included on graphs, but remains readable by the DOS versions of GTILT.

A plot of the current file is visible as soon as an inclinometer is loaded, and remains visible while GTILT is running. Plots of Cumulative Displacement, Incremental Displacement, and Absolute Position against Depth or Elevation, Plots Displacement, Shear Strain, Rate of Displacement, and Rate of Shear Strain against Time, all above plots are available in the inclinometer groove directions or at a skew angle. Ready access to all readings using a three-dimensional editor

Checksums can be viewed in histogram form, allowing an immediate quantitative assessment of the quality of each dataset. User-selectable plot colors reads files downloaded from a wide range of inclinometer loggers Supports probes of any base length plots in english or metric units, independent of probe type top-down plots can incorporate independent surveys of surface movement lines, polylines, and text can be drawn on the plots to show stratigraphy, piles, tunnels, excavations and so on, with user-definable point sizes and colors. Datasets can be marked for inclusion on all plots, on time plots only, or on no plots. For plots vs depth or elevation, individual dataset can also be toggled by clicking directly on the plot legend. Exports Windows Graphics Metafiles (WMF) for use with other applications. Scales can be modified by entering new ranges directly on plots. Downloadable free working model version is available.

2.8 STANDARD PENETRATION TEST (SPT)

The SPT is a well-established and unsophisticated soil field testing method, which was developed in the United States around 1925 and is widely used in geotechnical engineering. Relatively simple and inexpensive to perform, it is useful in determining certain properties of soils, particularly of cohesionless soils, for which undisturbed sample are not

easily obtained. The reliability of the method and the accuracy of the result depend largely on the experience and care of the engineer on site.

The SPT utilizes a split-spoon sampler. It is a 2-inch (51mm) O.D. 1⅜ inches (35mm) I.D. tube, 18 to 24 inches (457 to 610mm) long, which is split longitudinally down the middle. The split-spoon sampler is attached to the bottom of a drilling rod and driven into the soil with a drop hammer. Specifically, a 140 lb (623N) hammer falling 30 inches (762mmm) is used to drive the split-spoon sampler 18 inches (457mm) into the soils. As the sampler is driven the 18 inches (457mm) into the soil, the number of blows required to penetrate each of the three 6 inches (152mm) increments is recorded separately. The standard penetration resistance value (or N values) is the number of blows per foot (305mm). After blow counts have been obtained, the split-spoon sampler can be removed and opened (along the longitudinal split) to obtain a disturbed sample for subsequent examination and testing. SPT results (N values) are influenced by overburden pressure at locations where blow accounts are made. Several methods have been proposed to correct N-values to reflect the influence of the overburden pressure. In addition to the overburden pressure effects, SPT results (N-values) are also influenced by drill rod length, whether or not linear are present in the sampler, and borehole diameters.

Through empirical testing, corrections between (corrected) SPT N-values and several soil parameters have been established. These are particularly useful for cohesionless soils but are less reliable for cohesive soils. The Standard Penetration Test is mainly used to estimate the relative stiffness and strength (bearing capacity) of soils. Deformation characteristics of granular soils can be estimated from empirical correlations, like those provided by Peck et al. (1974). It is also possible to get from SPT some indications of the shear strength in cohesive soils. The SPT is used frequently for the evaluation of the liquefaction potential of water-saturated, loose sand and silts in seismic areas, see for example Seed and De Alba (1986). The configuration view of standard penetration test (SPT) is briefly shown in figure 2.83.

2.9 CONE PENETRATION TEST (CPT)

The CPT was invented and developed in Europe but has gained increasing importance in other parts of the world, especially in connection with soil compaction projects. It has the advantage of accomplishing subsurface exploration rapidly without taking soil samples. Different types of mechanical and electric cone penetrometers exist but the electric cone is most widely used. A steel rod with a conical tip (apex angle of 60° and a diameter of 35.7 mm) is pushed at a rate of 2 cm/s into the soil. The steel rod has the same diameter as the cone. The penetration resistance at the tip and along a section of the shaft (friction sleeve) is measured. The friction sleeve is located immediately above the cone and has a surface area of 150 cm^2. The electric CPT is provided with transducers to record the cone resistance and the local friction sleeve.

A CPT probe, equipped with a porewater pressure sensor is called CPTU. It is important to assure complete saturation of the filter ring of the porewater (piezo) element. Otherwise, the response of the piezo-transducer, which registers the variation of pore water pressure during penetration, will be slow and may give erroneous results. The CPTU offers the possibility to determine hydraulic soil properties (such as hydraulic conductivity - permeability) but is most widely used for identification of soil type and soil stratification. The CPT can also be equipped with other types of sensors, for example vibration sensors

(accelerometer or geophone) for determination of vibration acceleration or velocity. The "seismic cone" is not yet used on a routine basis but has, because of the relative simplicity of the test, potential for wider application especially on soil compaction projects.

The CPT measures the cone resistance q_c and the sleeve friction f_s from which the friction ratio, FR can be determined. FR is the ratio between the local sleeve friction and the cone resistance, expressed in percent (f_s/q_c). In spite of the limited accuracy of sleeve friction measurements, the valuable information, which can be obtained in connection with compaction projects, has not yet been fully appreciated. As will be discussed below, the sleeve friction measurement reflects the variation of lateral earth pressure in the ground, and can be used to investigate the effect of soil compaction on the state of stress.

One important objective of the CPT investigations in connection with soil compaction is to obtain information concerning soil stratification and variation in soil properties both in horizontal and vertical direction. The friction ratio is often used as an indicator of soil type (grain size) and can provide valuable information when evaluating alternative compaction methods.

Measurement of the excess pore water pressure with the CPTU can detect layers and seams of fine-grained material (silt and clay). It is also possible to obtain more detailed data information concerning soil permeability and thus soil stratification. The configuration view of cone penetration test (CPT) is present in figure 2.84.

2.10 DEEP DYNAMIC COMPACTION (DDC) TEST

2.10.1 Introduction

The following write up about deep dynamic compaction (DDC) is based on the book entitled "*Ground Treatment*" edited by Ye et al. (1992). Soil densification by dynamic compaction (DC), also called "heavy tampering", is a well-known ground improvement method. This method was "rediscovered" by Menard in 1969, who transformed the crude tamping method into a rational compaction procedure. This method is carried out essentially by repeatedly dropping a very heavy weight onto the soil surface from a relatively great height. The dropped weight may be an ordinary steel wrecking ball or be a mass especially designed for dynamic compaction. Typical weights range from 2 to 20 tons or higher, while dropping heights range from 20 to 100 feet. Commonly the heavier the weight and the greater the dropping weight, the greater the compactive effects will be. The impact of the tamper creates shock waves that can penetrate to a depth of 10 meters. In cohesionless soil these shock waves create liquefaction, immediately followed by compaction of the soil. In cohesive soil the shock wave creates excessive pore water pressure, followed by the consolidation of the soils. The imparted energy is transmitted from the ground surface to the deeper soil layers by propagating shear and compression wave types, which force the soil particles into a denser state. A crater is formed at the compact point that may be up to 2m deep. The craters are backfilled by end-dumping fill into the craters. Several phase or passes of tampering may be required across the site, depending on the level of the improvement required. On the first pass, the deepest layers are compacted. Subsequent passes compact successively shallower layers. Figure 2.85 introduces different compaction phases of the dynamic compaction. Following the completion of the high-energy tamping, a low-energy compaction is performed to compact the fill material in the craters and in the upper 5 feet of

the formation. The final compaction phase consists of dropping weight from height of 3 to 8m on close centers.

Dynamic compaction may be used for both cohesive and cohesionless soils. The most commonly treated soils are old fill or granular virgin soils including soil below the ground water table. For saturated soils, careful control has to be used to allow dissipation of excess pore pressures created during the compaction. In cohesive soils, the reduction of settlements due to dynamic compaction is more distinct than the increase in bearing capacity. The tampering produces a true pre-settlement of soils, well beyond the settlement that would have occurred as a result of construction weight only, without any preliminary consolidation. For cohesionless soils, dynamic compaction densifies loose soils.

Dynamic compaction is conducted using a closely spaced grid pattern, selected for a given site. Preliminary test is done to determine grid spacing and weight, height, and number of drops at every point. Typically 5 to 10 drops are made on each grid point.

Experience shows that after compaction, the bearing capacity of the soils can be improved by up to 200% to 500%, and soil compressibility can be reduced by 200% to 500%. The influence depth of dynamic compaction in the soil can be up to 10 m.

2.10.2 Objectives of Deep Dynamic Compaction (DDC)

The primary goal of deep dynamic compaction (DDC) is to transform the heterogeneous soil into one that has more uniform and better engineering properties, e.g. increasing the soil strength and decreasing the compressibility and settlement as a result of densification. DDC can be used to solve a series of foundation problems listed bellow:

- To increase in-situ density and in this way to improve the bearing capacity of soil foundations, or the stability of slopes and excavations with respect to static and/or dynamic loading;
- To increase in-situ density and in this way to increase soil stiffness to reduce total and different deformations and settlements that may be caused by static, cyclic or dynamic loading;
- To reduce lateral earth pressure against retaining structures provided that compaction is carried out prior to their installation;
- To mitigate liquefaction hazard in loose, saturated granular soils below the ground water level as a result of dynamic and cyclic loading (e.g. caused by earthquakes);
- To lower soil permeability in, below or adjacent to dams and waterfront structures;
- To generally improve geotechnical properties of heterogeneous soils.

The two most common applications of DDC are the improvement of reclaimed land for infrastructure projects such as ports or airports, and the mitigation of liquefaction risk in seismic areas.

2.10.3 The Mechanism of Deep Dynamic Compaction (DDC)

For the moment, the exact mechanism of soil consolidation by DDC is not completely known. And the understanding is based on experience and analysis of monitoring data.

There are three different mechanisms of deep compaction to densify soil foundations: dynamic compaction, dynamic consolidation, and dynamic replacement, which depend on the soils type and the construction technology.

2.10.3.1 Dynamic Compaction

Dynamic compaction is commonly used to densify coarse, unsaturated soils by vibrating the soil for soil particles rearrangement thereby decreasing the void volume and make the soils denser. The densification process in unsaturated soils is the process of expelling air out from the voids during the soil particles rearrangement. Experience shows that under the application of shock/vibration energy, on the ground surface the settlement and collapse will happen immediately. After one pass of compaction, the depth of the crater caused by compaction can be 0.6 to 1.6m and a layer of hardpan will be formed at the bottom of the crater. The new bearing capacity of soils can be 2 to 3 times of the original.

2.10.3.2 Dynamic Consolidation

The mechanism of densification of saturated soils by compaction is based on dynamic consolidation. The shock wave produced by compaction in soils, destroys the soil structure and causes liquefactions in local areas and as a result cracks in the soil to let rapid pore water flow out. After the dissipation of the pore water pressure, the soils are consolidated. Due to the thixotropy of soft soils, the strength of the soil will be improved.

The shock wave caused by the deep compaction can be classified as volumetric wave and boundary wave according to their way of propagation in the soils and influence on the soils. Volumetric waves can be classified as compression wave and shear waves (or horizontal wave and vertical wave). The compacted energy is transmitted from the ground surface to the deeper layers by propagating the shear and compression waves, which force the soil particle to a denser state. The boundary waves propagate along the ground surface, which can not densify the soil particle and therefore make the ground surface loose.

As a result of deep dynamic compaction, three different areas are formed with depth as shown in figure 2.86. The loose area is formed in the topsoil due to the disturbance of boundary waves and shear waves. Consolidation area is formed at some depth below the loose area, due to the densification caused by the compression wave. Below the consolidation area, the shock waves decrease with depth and can not provide enough energy to cause plastic deformation and hence densification in the soil. This area is called elastic area.

Based on relationship between pore water pressure in soils and time and that of stress and strain during the deep dynamic compaction processes, the densification processes in the consolidation area caused by shock waves can be classified into three phases: loading phase, unloading phase and dynamic consolidation phase as shown in figure 2.87.

(a) Loading phase (OA or O'A'). It refers to the short time of compaction. Intensive vibration and dynamic stress σ appears in the soils due to the compaction by the heavy weight. During this period, dynamic stress σ and pore water pressure u increase rapidly and generally maximum dynamic stress is larger than that of pore pressure, namely $\omega_{\max} > \mu_{\max}$. The structure of the soils will then be destroyed due to the plastic deformation caused by the effective dynamic stress. For sand, the energy brought by compaction will force the soil into denser state by rearranging the soil particles. For clayey soils, the soil structures will be

compressed during the compaction process. During the compaction, as the dynamic stress difference between soil and water is larger than the absorbed energy, parts of bound water and capillary water between soil particels will be expelled out due to the different vibration effects caused by water and soil particels separately. The water expelled out will then accummulate and form the drainage path in the soil.

(b) Unloading phase (AB or $A'B'$). Total dynamic stress disappears immediately as the dissipation of the compaction energy into the soils. However, the pore pressure in soils still is at high level and the value of pore pressure is larger than that of effective stress, which causes liquefaction in sand. In clayey soils, when maximum pore pressure is larger than the sum of minimum principal stress σ_3, static lateral soil stress and anti-tension strength of soils, cracks will appear in soils and soil permeability increases rapidly, and then pore pressure goes down quickly.

(c) Dynamic consolidation phase (BC or $B'C'$). After unloading, some pore pressure still exists in the soil, by which the soil is drained in a consolidation process. In sand, pore pressure dissipates very quickly, in about 3 to 5 minutes and the sand is forced into a denser state. In clayey soils, the pore pressure dissipates slowly and generally it will take about 2 to 4 weeks.

If consolidation drainage can happen, the soil particles are forced to closer and new water membrane and new soil structures are formed, which cause the soil strength to go back up and soil foundations are improved. If the maximum pore pressure in the loading and unloading phases separately can not cause the cracks in soils, and also can not expel out the absorbed water and capillary water, so that after unloading, the pore pressure can not be drained quickly and pore pressure stays at high level, which will damage soil structures to decrease soil shear strength and to increase soil compressibility.

When saturated clayey soils are chosen for deep compaction, suitable compaction energy should be determined according to the characteristics of the shock waves propagating in soils and foundation soils properties. At the same time, drainage path should be set up and conditions should be created for restoring soil thixotropy. Before construction, dynamic consolidation tests are carried out to determine the range of densifying soils for deep compaction, to choose suitable compaction energy and suitable compaction ways, and to check whether dynamic drainage consolidation and thixotropy restoring would appear during compaction process. It is very difficult to cause dynamic consolidation in saturated clayey soils by DDC, instead, maybe the expected effects can not be obtained.

2.10.3.3 Dynamic Replacement

Dynamic replacement can be divided into integral replacement and pile type replacement. The integral replacement is to push the crashed stone integrally into muck soils as shown in figure 2.88 (a). Pile type replacement is to place the crashed stone into soils, and some gravel piles are compacted into soft soil at intervals to form pile type stone column as shown in figure 2.88 (b). It mainly depends on interval friction angle and lateral soil pressure between the stone columns to keep balance. It works with soils between stone columns as composite foundations.

2.10.4 Design of DDC

2.10.4.1 Depth of influence in DDC

The maximum depth of influence that can be achieved by dynamic compaction is an important factor for selecting the preferable ground treatment. Menard and Broise (1975) suggested that the depth of influence of dynamic compaction could be calculated by $D = \sqrt{W \cdot h}$, in which W is the weight of the tamper and H is the drop height. Recently, many researchers suggested that the equation proposed by Menard and Broise (1975) should be adjusted by multiplying a factor to account for other factors that affect the depth of improvement, other than the mass of the tamper and the drop height. Leonards et al. (1980) suggested that it should be multiplied by 0.5, and Gambin (1987) suggested it should be multiplied by 0.5 to 1.0. In China, some scholars (Ye et al., 1992) suggested that for cohesive soils, the adjusted factor could be 0.5, and for loess, it can be 0.35 to 0.5. The FHWA suggested the following equation (Lukas and Schexnayder, 1986) for the determination of improvement depth by DDC.

$$D = n\sqrt{W \cdot h} \tag{2.6}$$

where:

D = depth of improvement (m);
W = weight of tamper (ton);
H = drop height (m)
n = empirical coefficient that is less than 1.0

Figure 2.91 based on Mayne et al. (1984) presented the relationship between apparent maximum depth of influence and energy per blow. The maximum influence depth that can be achieved by dynamic compaction depends on several factors, such as the geotechnical properties of the soil layers to be compacted, the dynamic soil properties in and below the layer to be compacted (e.g. a soft clay layer below the layer to be densified can significantly reduce the compaction effect), the ground water level, the compaction grid, the number of compaction passes and the time interval between passes. Table 2.5 summarizes the n values for different soil types recommended by Lukas and Schexnayder (1986). Based on the analysis of both cone penetration testing (CPT) and seismic cone penetration testing (SCPT), Hajduk et al. (2004) verified the validation of the use of n equal to 0.5 for the replacement fill at U.S. route 44, Massachusetts.

2.10.4.2 Tamper and Drop Height

Unit impact energy E_{unit} is the potential energy of the drop, being equal to the product of the tamper's mass M multiplied by the drop height, namely $E_{unit} = W \times H$. The heavier the tamper and the larger the drop height, better will be the effect of the deep compaction to a certain limit. The applied impact energy *AE* is the total impact energy divided by the total densified areas:

$$AE = \frac{N \times W \times H \times P}{S^2} \tag{2.7}$$

Where:

N = number of drops
P = number of passes
W = mass of tamper
H = drop height
S = grid spacing

The determination of the unit impact energy of deep dynamic compaction should be based on the soil type, structure type, loading intensity, and required influence depth. Lukas and Schexnayder (1986) recommended that for the compaction of pervious coarse-grained soils, the applied unit impact energy should be about 200 to 250 kJ/m^3; For semipervious fine-grained soils, it is about 250 to 300 kJ/m^3; for landfills, it is about 600 to 1100 kJ/m^3.

The tamper used for deep dynamic compaction shall be made of steel and welded or bolted so that it can sustain the specified drop impacts. The adopted tamper weight is about 5 to 40 tons. There are two types of plane shapes of tamper available, circlular and square as shown in figure 2.89. Based on its structure, it can be divided into air-void type and sealed type as shown figure 2.90. Ye et al. (1992) pointed out that the circular tamper with air-void is preferable than the square tamper. Their explanation is that the circular shaped tamper creates circular indentation upon impact, which closely overlaps the contact area of subsequent impacts with the soil. However, a square tamper creates circular indentations which do not allow for a good contact area with subsequent impacts inducing larger loss of energy impact. The air-voids penetrate the tamper from the top to the bottom and their diameters typically range between 250 to 300mm, which can decrease suction pressure when lifting the tamper. The bottom area of the tamper has direct influence on the compaction results. For tampers having the same weight, the one with a smaller contact area will produce larger pressure on the ground surface, causing a deeper crater. For saturated fine granular soils, this will increase the resistance to the tamper and can not improve the compaction effects. The bottom area of the tamper should be chosen therefore based on the soil properties. The pressure acting on the contact area of the tamper can be 25 to 41 kPa. For fine granular soil, it is better to aim at the lower values. For sandy soils, the contact area of the tamper with the soil is 3 to 4 m^2, and for clayey soils it should not be smaller than 6 m^2. Typically the depth of the crater should be less than half of the width of the tamper. Otherwise, some of impact energy will be lost. As deeper crater are created by deep dynamic compaction in fine granular soils, tampers with large contact areas should be used under such conditions.

Figure 2.92 based on Mayne et al. (1984) presents the relationship between the tamper's mass and height for various cases. The drop height can be determined based on the required single impact energy. The typical selected drop height is about 50 to 100 feet (Ye et al. 1992). For the same impact energy, larger drop heights can be adopted. Larger drop height cause larger impact velocity resulting with much of impact energy being transmitted into the deeper soil layers to be densified. The percent of impact energy causing plastic deformation in the topsoil decreases under such conditions.

2.10.4.3 Spaced Grid Drop Pattern

1. Grid Drop Pattern The determination of the grid pattern for the compaction locations can be based on the type of structure to be constructed. For structures with large

foundation area, the grid patter can adopt equilateral triangular pattern or square pattern. For the foundations of office buildings or residential buildings, the grid pattern can be designed along the bearing wall. For factory buildings, the allocation of drop pattern can be based on column locations.

The areas for compaction should be larger than the footprint of the buildings because of the lateral diffusion of stress or when needed to eliminate liquefaction.

2. Grid Spacing The grid spacing refers to the center to center distance between impact locations. The grid spacing is commonly determined according to the soil properties and the required influence depth of the compaction. A drop point spacing of 1.5 to 2.5 times the diameter or width of the tamper is common (Lukas and Schexnayder, 1986). In order to densify the deep soil layers, the grid spacing for the first pass should be the largest; otherwise the impact energy can not be transmitted into the deeper layers. The grid spacing of the second pass is commonly positioned at the middle point of the former grid spacing. The last pass is used with lower energy impacts make use of a special tamper with lesser pressure to compact the disturbed materials at shallow depth. The grid spacing should not be too small. As otherwise, a layer of hardpan can be formed in the shallow depth due to the overlapping of the impact energy at these areas. This hardpan layer will keep the impact energy from being transmitted into deeper layers. For clayey soils, cracks will appear around the craters caused by compaction, which is the result of dynamic consolidation.

2.10.4.4 Drops and Passes

1. Drops The number of drops at grid points should be determined according to the relationship between drops and settlements caused by compaction at the site. Example of such relations for various soil types is presented in figures 2.93 and 2.94 based on Lukas and Schexnayder (1986). At the same time, it should meet the requirements listed as bellow:

- The total settlement caused by the last two drops should be less than 50mm. and it should be less than 100 mm when single impact energy is larger than 1.6 MJ/m^3;
- Large heave should be prevented from appearing around the craters;
- The depth of the crater should not be too large so that it is too difficult to lift the tamper out of the crater.

The drops at grid points should maximize the soils' compression and minimize lateral movement. Normally, 7 to 15 drops of high level energy are applied at each point (Lukas and Schexnayder, 1986).

2. Passes The selection of compaction passes should be based on the soils' properties. Commonly soils are compacted 2 to 3 passes and finally compacted with low energy pass. For fine granular soils with low permeability, if necessary, more passes should be used.

2.10.4.5 Blanket

Prior to commencement of compaction, a granular stiffer blanket should be placed over the treated area so that it can sustain compaction equipments. At the same time, a layer of stiffer granular material can help the dissipation of the impact energy into the deep layers and increase the distance between the underground water and ground surface. When

underground water table level is 2m below the ground surface, the sand-gravel layers can be compacted directly without a blanket. For saturated clayey soils and saturated loose sand susceptible of liquefaction, with underground water level close to ground surface, a blanket is necessary for compaction. The thickness of a blanket is determined by the geologic condition at the site, tamper weight and shape, and so on. The blanket thickness is commonly 0.5 to 2.0m. Clayey soils can not be one part of blanket because they can not provide enough bearing capacity for the heavy compaction equipments.

2.10.4.6 Time Interval

Some time interval is required between the passes. The time interval between two passes is determined by the time required for the pore pressure water dissipation in the treated soils. For sandy soils, the peak value of the pore pressure appears just after deep dynamic compaction. The dissipation time of pore pressure in sand is very short, only 2 to 4 minutes. So for sandy soils with higher permeability, the compaction can be carried out continuously. For clayey soils, the pore pressure dissipates slowly, typically in about 2 to 4 weeks, and the pore pressure increases with the increasing in the impact energy. If drain piles are used in clayey soils to accelerate the speed of pore pressure dissipation, the time interval between passes can be shortened.

2.11 FINITE ELEMENT METHOD (FEM)

2.11.1 Introduction

The following write up about finite element method (FEM) is based on the book entitled *"Finite Element Analysis in Geotechnical Engineering"* edited by Zhang (1995). In the finite element method (FEM), the continuum of the real problem is approximated by a number of finite or discrete lumps whose mechanical behavior is selected to simulate that of the continuum (elastic, plastic, visco-elastic, etc.). The method was originally developed in 1955 in the aircraft industry and has been used more and more frequently in structural analysis in general. In its original form, the finite element represented real structural elements, beams, and columns, and the operational equations were developed on a physical basis. This approach is not convenient in the application of the technique to continuum mechanics, and, consequently, the formulations are based on the energy stored and work produced by the system.

The method is formulated in terms of a plane strain problem, although there are no additional difficulties in considering a general three-dimensional situation. In structural example, the identification of the discrete elements with parts of the structure (springs) is obvious. The visualization of a structure as an assemblage of elementary components is therefore not difficult for many types of real structures. In soil mechanics, we are largely involved with the representation of soil masses or continua, and therefore it is necessary to set out a technique for handling stresses and displacement problems in continua.

The approach is to overlay the region of interest with an assemblage of polygons, which has common vertices and sides. Although four-sided polygons may and frequently are selected, it is convenient to use triangles in many soil engineering applications. Triangles are easily adopted to a variety of boundary and internal geometries. Examples are shown in

figure 2.95(a) and 2.95(b) for two soil mechanics problems. In figure 2.95(a), it is appropriate, although not necessary, to use a regular triangular network, whereas in figure 2.95(b), a regular rectangular pattern, adaptable to the boundary conditions, is employed. It is desirable to use smaller rectangles in the region of interest. For example, near the footing, where stress concentrations are expected to occur. In figure 2.95(b), the footing is also represented by finite elements for the case in which its flexibility is of interest. Should it be assumed rigid in comparison with the soil, the elements are omitted. Instead, the appropriate mesh points at the ground surface are all given the same displacement.

2.11.2 Outline of a FEM Solution

The method of solving the problem is then to assume a displacement field for each triangular (or other shape) discrete element, equivalent to the assumption of a given rotation θ, such that a node point common to several triangles undergoes the same displacement when it is calculated from the displacement field for each of the connected triangles. It will be recognized that this is an application of the idea of consistent deformations. In line with the above, the displacement fields selected must match the known boundary displacements, as essential conditions. Next, the strains in each triangle are calculated from its displacement field, which contains unknown constants whose values will be eventually obtained. At this stage, the material behavior enters the calculation, so that stresses in each element can be derived from the strains. The potential energy, which can be written in a form independent of the constitutive relations of the material, can be specialized for the particular material properties of interest, in terms of strains or stresses. Substituting the calculated strains, for example, of one triangular element into the energy expression gives an equation for the energy of that element. Since the potential energy includes provisions for boundary forces and body forces, these will be included for any triangle that is subjected to a boundary load at a node point and all triangles if body forces are important. When this is done for all the triangles, their potential energies are added together to give the total potential energy for the whole region as expressed in equation 2.8:

$$\pi = \frac{1}{2}k_1 a^2\theta^2 + \frac{1}{2}k_2 c^2\theta^2 - Pb\theta \qquad (2.8)$$

where: k_1, k_2 = spring factor
a, b = length
θ = rotation angle
P = force
b = displacement

The values of the unknown constants that characterize the displacement fields can then be evaluated. These values have to be such as to minimize the total potential energy. This minimum is obtained by differentiating the total potential energy expression with respects to each unknown constant, or, more conveniently, to each node displacement in turn and setting the resultant equation equal to zero, as done in the Ritz method. However in Ritz method, the results were only a few equations in terms of force equaling stiffness time deflection. When the problem to be solved is a two or three dimensional continuum one, use of the Ritz method is still possible. However, if the problem region is divided into smaller domains, the use of Ritz method is difficult. In the general finite element case, there are

hundreds or thousand of node points, each of which has two components of displacement in the plane problem, the differentiation process leads to one equation for each component at each node point. Thus we will have a system of many algebraic equations that have to be solved simultaneously to give the nodal displacements. Once the displacement at each node of a triangle has been obtained, the constants in the displacement field for that triangle can be calculated and consequently the strains and stresses can then be computed. The evaluation of the system of simultaneous equations requires a large digital computer. A variety of programs are available for carrying out the required operations extremely rapidly.

Each of the equations obtained by the differentiation of the total potential involves forces and displacements. However, in general, each equation includes the displacement components and forces at several node points. The coefficient multiplying θ in equation 2.8 is a stiffness. Consequently, in the full set of equations the system of coefficients multiplying the displacement component represents the stiffness of the entire system and is called the stiffness matrix.

$$P = \frac{k_1 a^2 + k_2 c^2}{b}\theta = k\theta \tag{2.9}$$

It will be recognized that each equation resulting from the differentiation of the total potential energy expression with respect to a displacement component is an equilibrium equation in the direction of the component. The system of equations therefore also represents the equilibrium of the problem region expressed through the equilibrium of the force components at every nodal point. Consequently, the procedure outlined above has taken into account all necessary elements of analysis: consistency of deformations, constitutive relations, and equilibrium.

It must be noted that the representation of the area of the problem by means of the network of triangles is a conceptual procedure only. It does not correspond to a model representation, for example, in which, the real region might be represented by a number of real triangles pinned together at their nodal points. The actual displacements of a plane solid triangular element subjected to loads at its nodes are complicated and are not what is assumed to occur in the present approach. Rather consistency of deformation requires that not only the nodal points of triangles but also the sides of adjacent triangles remain attached. Consequently, the assumed displacement for any triangle must give displacements along its sides, which are identical with the displacements along the continuous sides of adjacent triangles, derived from their displacement fields. In selecting the displacement field, this requirement must be satisfied.

The simplest displacement field that meets these requirements is one in which the displacements are assumed to be linear functions of the coordinates in each triangle, so that the triangle with the coordinates of figure 2.96(a) is assumed to deform as shown in figure 2.96(b). With this assumption, the displacements in the nth triangle become:

$$\begin{aligned} u_n &= a_n x + b_n y + c_n \\ v_n &= d_n x + e_n y + f_n \end{aligned} \tag{2.10}$$

in which the a_n, b_n, c_n, d_n, e_n, and f_n are constant holding for triangle n only, and x and y are the coordinates of points in the triangle, including the vertices. The linear equations 2.10 allow the triangle to displace, rotate, stretch, and deform, but lines which were straight before straining remain straight afterward. Once the coefficients a_n, b_n, c_n, d_n, e_n, and f_n have been

determined, the following calculation gives the displacement of triangle n. Each corner of the triangle has two degrees of freedom, in the x- and y-directions, and so its total displacement requires six constants (a_n, b_n, c_n, d_n, e_n, and f_n) for its description. If a rectangular element was to be employed with four corners, eight degrees of freedom are involved and eight constants must be used. In this case, equations identical to equation 2.10, each with the addition of a term in xy multiplied by another constant, are needed.

Other displacement functions, such as parabolic, may also be employed. Since they give more degrees of freedom to the element, compatibility must be ensured by adding nodal points, for example, at the midpoints of the triangle sides.

With the displacements given by equation 2.10, the strains in triangle n are given by equation 2.11:

$$\begin{aligned}\left(\varepsilon_x\right)_n &= \frac{\partial u_n}{\partial x} = a_n ; \left(\varepsilon_y\right)_n = \frac{\partial v_n}{\partial y} = e_n \\ \left(\gamma_{xy}\right)_n &= \frac{1}{2}\left[\frac{\partial u_n}{\partial y} + \frac{\partial v_n}{\partial x}\right] = \frac{1}{2}\left(b_n + d_n\right)\end{aligned} \tag{2.11}$$

From equation 2.10 and equation 2.11, the stresses in triangle n can be computed. We assume here that the problem is in plane strain, so that $\varepsilon_Z = 0$.

$$\pi = \frac{5}{16}a_1^2 + \frac{2}{3}a_1 a_2 + \frac{5}{8}a_2^2 - a_1 - a_2 \tag{2.12}$$

$$\left(\sigma_x\right)_n = \frac{E}{(1+\nu)(1-2\nu)}\left[(1-\nu)\left(\varepsilon_x\right)_n + \nu\left(\varepsilon_y\right)_n\right] = \frac{E}{(1+\nu)(1-2\nu)}\left[(1-\nu)a_n + \nu e_n\right] \tag{2.13}$$

$$\left(\sigma_y\right)_n = \frac{E}{(1+\nu)(1-2\nu)}\left[(1-\nu)\left(\varepsilon_y\right)_n + \nu\left(\varepsilon_x\right)_n\right] = \frac{E}{(1+\nu)(1-2\nu)}\left[(1-\nu)e_n + \nu a_n\right] \tag{2.14}$$

$$\left(\tau_{xy}\right)_n = G\left(\gamma_{xy}\right)_n = \frac{E}{2(1+\nu)}\left(b_n + d_n\right) \tag{2.15}$$

Thus, the strains and stresses are constant in each triangle but are different from one triangle to another. Specifically, the stresses are never zero at the external boundaries of the triangles, even where there is no boundary load. This occurs because stress is not an essential condition.

Considering the nodal points of triangle n, we see that their displacements can be written from equation 2.10 in terms of the constants a_n, b_n, since the coordinates of vertices are known. This gives six equations as bellow:

$$\begin{aligned}u_i &= a_n x_i + b_n y_i + c_n \\ v_i &= d_n x_i + e_n y_i + f_n \\ u_j &= a_n x_j + b_n y_j + c_n \\ v_j &= d_n x_j + e_n y_j + f_n \\ u_k &= a_n x_k + b_n y_k + c_n \\ v_k &= d_n x_k + e_n y_k + f_n\end{aligned} \tag{2.16}$$

At some of the nodal points of triangles in a given problem, (such as those shown in figures 2.95(a) and 2.95(b), the displacements will be specified by the boundary conditions. For example, in figure 2.95(a) we might require that the vertices occurring along the base of the dam has zero displacements in both x and y directions. This would represent the effects of a rigid foundation to which the dam is bonded. In other situations, such as along the centerline (axis of symmetry) of figure 2.95(b), the horizontal displacement would be required to be zero if the foundation and soil are homogeneous. These conditions are made use of , by solving equation 2.16 for the coefficients a_n, b_n, c_n, d_n, e_n, and f_n in terms of the displacements of the triangle vertices, some of which in general may be known and some not. The solution of equation 2.16 can be carried out by determinants to give:

$$a_n = \frac{\begin{vmatrix} u_i & y_i & 1 \\ u_j & y_j & 1 \\ u_k & y_k & 1 \end{vmatrix}}{2A_n}$$

$$b_n = \frac{\begin{vmatrix} x_i & u_i & 1 \\ x_j & u_j & 1 \\ x_k & u_k & 1 \end{vmatrix}}{2A_n} \qquad (2.17)$$

$$c_n = \frac{\begin{vmatrix} x_i & y_i & u_i \\ x_j & y_j & u_j \\ x_k & y_k & u_k \end{vmatrix}}{2A_n}$$

$$d_n = \frac{\begin{vmatrix} v_i & y_i & 1 \\ v_j & y_j & 1 \\ v_k & y_k & 1 \end{vmatrix}}{2A_n}$$

$$e_n = \frac{\begin{vmatrix} x_i & v_i & 1 \\ x_j & v_j & 1 \\ x_k & v_k & 1 \end{vmatrix}}{2A_n} \qquad (2.17)$$

$$f_n = \frac{\begin{vmatrix} x_i & y_i & v_i \\ x_j & y_j & v_j \\ x_k & y_k & v_k \end{vmatrix}}{2A_n}$$

Where A_n is the area of triangle n. Thus for each triangle, the coefficient a, b, c, d, e, and f are expressed in terms of the displacements of vertices.

The next step is to write the expression for the potential energy of the system. In this case, we must develop the equation for the potential energy of one triangle, n, in plane strain

and then sum the energy for all the triangles. For a linearly elastic, isotropic body, the strain energy density U can in terms of strains as follows (plane strain case):

$$U = \frac{\nu E}{2(1+\nu)(1-2\nu)}\left(\varepsilon_x+\varepsilon_y\right)^2 + \frac{E}{2(1+\nu)}\left(\varepsilon_x^2+\varepsilon_y^2\right) + \frac{2E}{2(1+\nu)}\gamma_{xy}^2$$

$$= \frac{E}{2(1+\nu)(1-2\nu)}\left[(1-\nu)\left(\varepsilon_x^2+\varepsilon_y^2\right) + 2\nu\varepsilon_x\varepsilon_y + 2(1-2\nu)\gamma_{xy}^2\right] \tag{2.18}$$

$$= \frac{E}{2(1+\nu)(1-2\nu)}\left\{(1-\nu)\left[\left(\frac{\partial u}{\partial x}\right)^2+\left(\frac{\partial v}{\partial y}\right)^2\right] + 2\nu\frac{\partial u}{\partial x}\cdot\frac{\partial v}{\partial y} + \frac{(1-2\nu)}{2}\left[\frac{\partial u}{\partial y}+\frac{\partial v}{\partial x}\right]^2\right\}$$

Considering that the state of strain is constant in any one triangle n, for example, the total strain energy U_y for that triangle is equal to the strain energy density times the area of the triangle, A_n. The terms $\partial u/\partial x, \partial v/\partial y$, etc; appearing in equation 2.16 have been evaluated in equation 2.10. For the displacements of equations 2.10 in triangle n, so that equation 2.17, multiplied by the area, and with the replacement gradients from equation 2.11, gives U_{vn}, the strain energy in the triangle n:

$$U_{vn} = \frac{EA_n}{2(1+\nu)(1-2\nu)}\left\{(1-\nu)\left[a_n^2+e_n^2\right] + 2\nu a_n e_n + \frac{(1-2\nu)}{2}\left[b_n+d_n\right]^2\right\} \tag{2.19}$$

The total potential energy includes a term W in the work done by the surface and body forces as the strained region moves from its initial to its final displaced position. For a single triangular element n, this quantity is given by the expression:

$$W_n = \int A_n\left(Xu_n + Yv_n\right)dxdy + \int S_n\left(T_x u_n + T_y v_n\right)ds \tag{2.20}$$

in which X and Y are the components of the body force per unit of area (in the two-dimensional problem) in the x and y directions and the first integral is carried out over the area of the element. T_x and T_y are the components of the surface force (applied load) per unit of length of the boundary and the integration is carried out over the length of the boundary S_n. many triangles in atypical problem with an edge forming one of the boundaries of the region will have no surface load acting. In general, there are no surface loads on internal angles. Consequently, the second term in equation 2.20 will only appear in the energy expression for a few triangles in atypical problem. In many problems body forces per unit of volume are neglected and in these cases the first integral in equation 2.20 will not appear in the formulation of the problem.

Considering $\pi = U_v - W$, we can put equations 2.19 and 2.20 together to get the total potential energy of the nth element in the following equation as bellow:

$$\pi_n = \frac{EA_n}{2(1+\nu)(1-2\nu)}\left\{(1-\nu)\left[a_n^2+e_n^2\right] + 2\nu a_n e_n + \frac{(1-2\nu)}{2}\left[b_n+d_n\right]^2\right\}$$

$$-\int_{A_n}\left\{X\left(a_n x+b_n y+c_n\right)+Y\left(d_n x+e_n y+f_n\right)\right\}dxdy \tag{2.21}$$

$$-\int_{S_n}\left\{T_x\left(a_n x+b_n y+c_n\right)+T_y\left(d_n x+e_n y+f_n\right)\right\}ds$$

Following the procedure in the simple example given before, we sum up potential energies, π_n, of each triangle to give the total potential energy of the region under study, π.

Next we must take the derivative of the resulting potential energy expression with respect to each unknown nodal displacement, $\partial\pi/\partial u_i$ '$\partial\pi/\partial v_i$, etc, and equate each derivative to zero. This is equivalent to obtaining the equation of equilibrium in each of the two coordinate directions at each node point. Since there is one equation for each unknown displacement component, we will now have a set of simultaneous algebraic equations in the unknown nodal displacement. The term for the strain energy includes the squares of the coefficients a_n, b_n, c_n, d_n, e_n, and f_n. These coefficients are linear in the displacements u_i, v_i,…, etc., so that the final form of the total energy expression includes the squares of the unknown displacements, in its strain energy term, whereas the body and surface force terms are linear in these displacements. Consequently, the differentiation with respect to the displacements produces a system of simultaneous algebraic equations, linear in the unknown u_i, v_i, etc., and with constant coefficients as follows:

$$\begin{aligned}
&k_{11}u_1 + k_{12}v_1 + k_{13}u_2 + k_{14}v_2 + \ldots + k_{1(2m)}v_m = C_1\\
&k_{21}u_1 + k_{22}v_1 + k_{23}u_2 + k_{24}v_2 + \ldots + k_{2(2m)} = C_2\\
&k_{31}u_1 + k_{32}v_1 + k_{33}u_2 + k_{34}v_2 + \ldots + k_{3(2m)} = C_3\\
&\ldots\ldots\ldots\ldots\ldots\ldots\ldots\ldots\ldots\ldots\ldots\ldots\ldots\ldots\ldots\ldots\ldots\ldots\ldots\ldots\\
&\ldots\ldots\ldots\ldots\ldots\ldots\ldots\ldots\ldots\ldots\ldots\ldots\ldots\ldots\ldots\ldots\ldots\ldots\ldots\ldots\\
&k_{(2m)1}u_1 + k_{(2m)2}v_1 + \ldots\ldots + k_{(2m)(2m)}v_m = C_{(2M)}
\end{aligned} \tag{2.22}$$

$$k = \begin{bmatrix}
k_{11} & k_{12} & k_{13} & k_{14} & \ldots & k_{1(2m)}\\
k_{21} & k_{22} & k_{23} & k_{24} & \ldots & k_{2(2m)}\\
k_{31} & k_{32} & k_{33} & k_{34} & \ldots & k_{3(2m)}\\
k_{41} & k_{42} & k_{43} & k_{44} & \ldots & k_{4(2m)}\\
\ldots & \ldots & \ldots & \ldots & \ldots & \ldots\\
k_{(2m)1} & k_{(2m)2} & k_{(2m)3} & k_{(2m)4} & \ldots & k_{(2m)(2m)}
\end{bmatrix} \tag{2.23}$$

In general, the set of simultaneous algebraic linear equation 2.22 is solved by means of large computer. Efficient computer programs exist for the solution of such equations when there are only a few terms in each equation and the matrix is symmetric. The point will not be dealt with further here, but the solution is facilitated by careful numbering of the nod points in a given problem, so that the nonzero terms in each equation in equation 2.22 are closer together and the stiffness matrix is banded. When the solution is obtained in terms of the nodal displacements at all the nodes of the problem net, the coefficients a_n, b_n, c_n, d_n, e_n, and f_n, can be obtained from equation 2.17, and the stresses in each triangle from equations 2.13 and 2.14.

2.11.3 FEM and Geotechnical Engineering

Many finite element programs have been developed for different applications. For example, FLAC has been developed successfully for application in structure analysis, and

PLAXIS has been developed successfully for application in geotechnical engineering. The finite element method is used to simulate various geotechnical engineering problems. Finno and Harahap (1991) simulated the construction of a 40-feet deep braced excavation in saturated clays in Chicago by using a coupled finite element formulation. Ng and Lings (1995) and studied the application of two relatively simple models: a linear elastic-perfectly plastic Mohr-Coulomb and a nonlinear "brick" model for simulating the top-down construction of a multi-propped excavation in the overconsolidated stiff fissured Gault clay by using finite element method. Ou et al. (1996) proposed a nonlinear, three dimensional finite element technique to study the effects of the existence of the corner on the wall behavior of a deep excavation in clayey subsoil stratum.

2.11.4 PLAXIS

The PLAXIS computer code is based on the finite element method. On one hand, PLAXIS is based on advanced scientific developments in the field of geomechanics and numerical methods. On the other hand, PLAXIS is meant for practical applications in the geotechnical engineering practice, professional geotechnical education and geotechnical research. Hence, PLAXIS is designed to build and maintain a bridge between theory and practice.

PLAXIS is a finite element code for the analysis of deformation and stability of geotechnical structures. The name PLAXIS is an acronym for Plasticity Axissymmetric, and the computer code may also be used to solve plane strain problems. Two different PLAXIS versions have been released; an introductory version and a professional version. The introductory version may be used to study the stability and displacements of simple geotechnical structures. This version is, in fact, intended to serve as a demonstration program and may only be used to solve problems with 28, or less, high order 15-noded triangular elements. The professional version is suitable for detailed calculations of complex geotechnical structures. Large number of elements can be used to deal with complex geometries. It is possible use up to 200 high order 15-noded triangular elements, or alternatively 800 lower order 6-noded triangular elements. It covers a wide range of geotechnical analyses such as an excavation for a tunnel, consolidation, and groundwater flow. PLAXIS also can analyze dynamic problems such as subjected to pile driving. The mechanical behavior of soils may be modeled at various degrees of accuracy. Hook's law of linear elasticity, for example, may be thought of as the simplest available soil model. This two parameters model, however, is generally too crude to capture the features of soil behavior that is practically important, although it is often appropriate for the modeling of structural elements or strong bedrock layers. The Mohr-Coulomb model is a good first-order approach for soils. The soft soil and hard soil models may be thought of as more sophisticated, second-order approximations of reality. In order to carry out high quality predictions, it is often tempting to use the most sophisticated model available. Ukritchon et al. (2003) developed both limit analyses and nonlinear finite element analyses to compute rigorous upper and lower bounds for short-term undrained stability in the braced excavation in clay. Ukritchon et al. (2003) pointed out the limit analysis predicted similar failure depths as the finite element calculations. FEM PLAXIS is employed in Route 44 to model the soil-wall interaction in peat.

Table 2.1 Summary of references related to laboratory experiments and field work on active earth pressure against retaining walls

Researcher	Year	Soil Type
Terzaghi	1920,1932, 1936	sand
Lambe and Whitman	1969	sand
Sims et al.	1970	ash
Casagrande	1973	sand
Coyle and Bartoskewitz	1970, 1974,1981	sand
Moore and Spencer	1972	clay
Jones	1973	sand
Fukuoka et al.	1977	cohesive soil
Sherif et al.	1982	Ottawa sand
Fang and Ishibashi	1986	sand
Tedd et al.	1981, 1983, 1984	clay
Carder and Symons	1989	clay
Gunn and Clayton	1992	clay
Symons et al.	1992	clay

Table 2.2 Summary of references related to laboratory experiments and field work on passive earth pressure against retaining walls

Researcher	Year	Soil Type
Terzaghi	1920	sand
Franzius	1924	sand
Streck	1950	sand
Brinch-Hansen	1953	cohesive soil
Tschebotarioff and Johnson	1953	sand
Rowe and Peaker	1965	sand
Mackey et al.	1967	sand
Narain and Nandakkumaran	1969	sand
Broms and Ingleson	1971	sand
Ingold	1979a	sand
Carder and Symons	1989	sands & clay
Fang et al.	1994, 1997	sand

Table 2.3 Summary of references related to laboratory experiment and field work on compaction-induced earth pressure against retaining walls

Researcher	Year	Soil Type
Terzaghi	1932, 1934	sand
Rowe	1954	sand
Whiffin	1954	sand
Sowers et al.	1957	sand
Forssblad	1963	sand
Davies and Stephens	1966	sand
Terzaghi and Peck	1967	sand
D'Appolonoa et al.	1969	sand
Broms	1971	sand
Youd	1972	Ottawa sand
Casaggrande	1973	sand
Jones	1973	sand
Aggour and Brown	1974	sand
Fukuoka et al.	1977	sand
Carder et al.	1977	sand
Ingold	1979b	sand
Carder et al.	1980	clay
Coyle and Bartoskewitz	1981	sand
Clayton et al.	1991	clay

Table 2.4 Summary of references related to pressure measurements against sheet pile walls

Researcher	Sheet pile type	Aim	Soil Type
DiBiagio (1977)	Propped	Excavation	Soft clay
Stille (1979)	Anchored	Excavation	Soft Clay
Tamano (1983)	Anchored	Excavation	Soft clay
Finno (1989)	Propped	Excavation	Soft clay
Kort et al. (2000)	Propped	Excavation	Clay with a thin peat layer
Endley et al. (2000)	Anchored	Excavation	Soft clay
Peck (2002)	Propped	Excavation	Soft clay

Table 2.5 Recommended n value for different soil types (FHWA, 1995)

Soil Type	**Degree of Saturation**	**Recommended n Value***
Pervious Soil Deposit-Granular soils	High	0.5
	Low	0.5 – 0.6
Semipervious Soil Deposits-Primarily silts with plasticity index of < 8	High	0.35-0.4
	Low	0.4-0.5
Impervious Deposits-Primarily clayey soils with Plasticity index of > 8	High	Not recommended
	Low	0.35 – 0.40 Soils should be at water content less than the plastic limit.

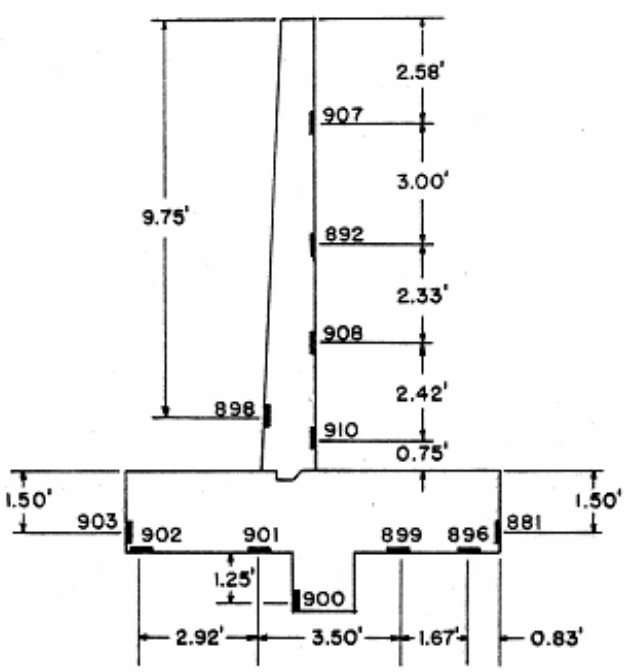

Figure 2.1 Locations of pressure cells (1 ft=0.305m) (Coyle and Bartoskewitz, 1974)

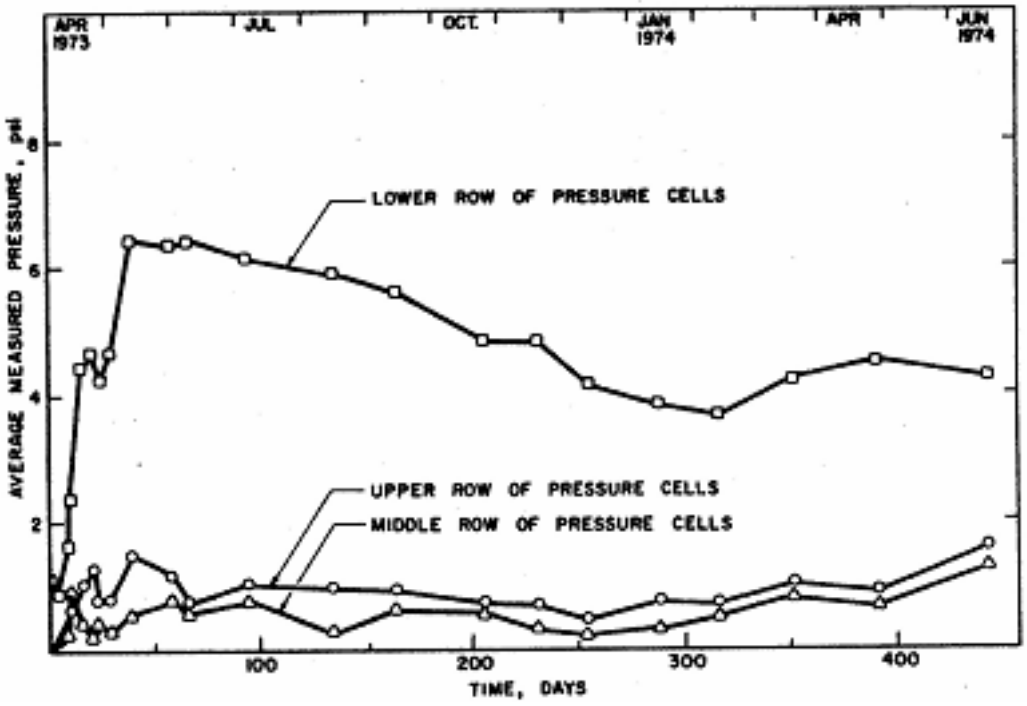

Figure 2.2 Average measured pressure on panel wall (Coyle and Bartoskewitz, 1974)

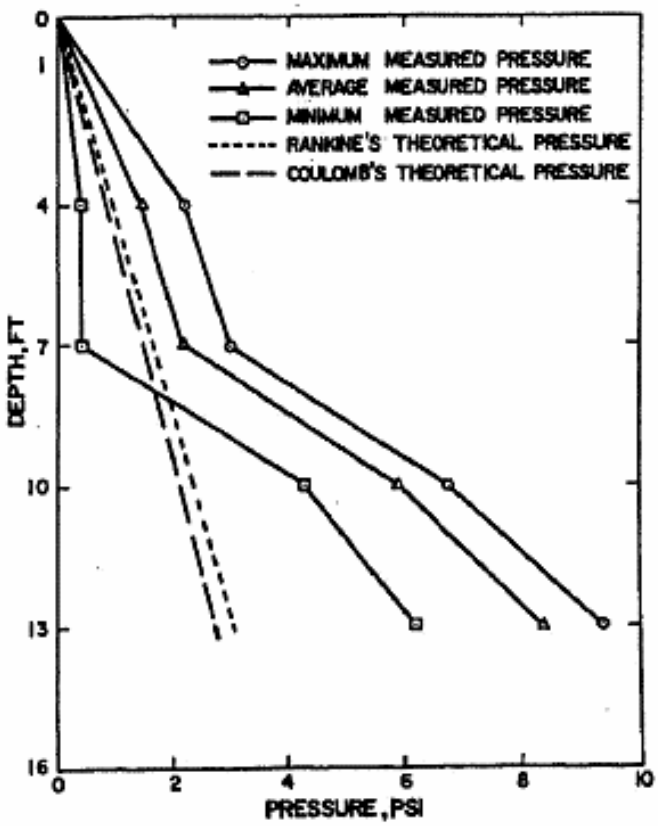

Figure 2.3 Measured and theoretical earth pressure values
(Coyle and Bartoskewitz, 1974)

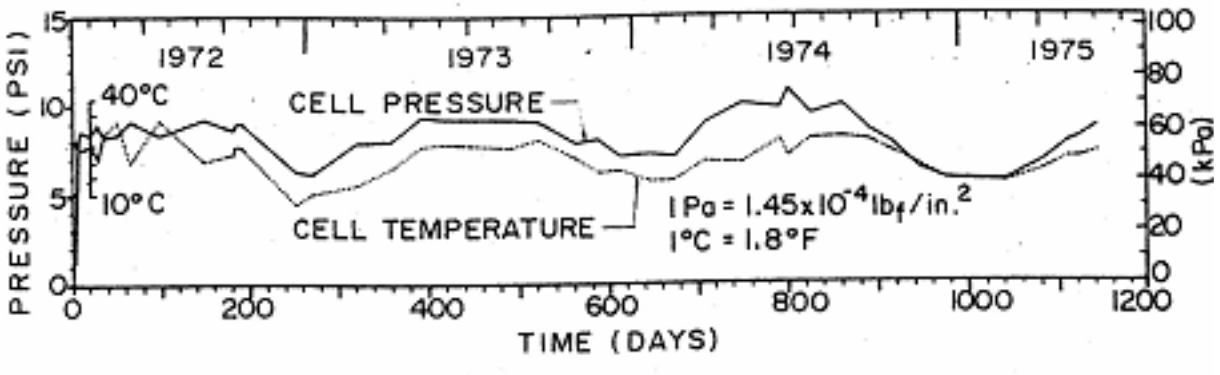

Figure 2.4 Pressure and time (temperature effects considered)
(Coyle and Bartoskewitz , 1974)

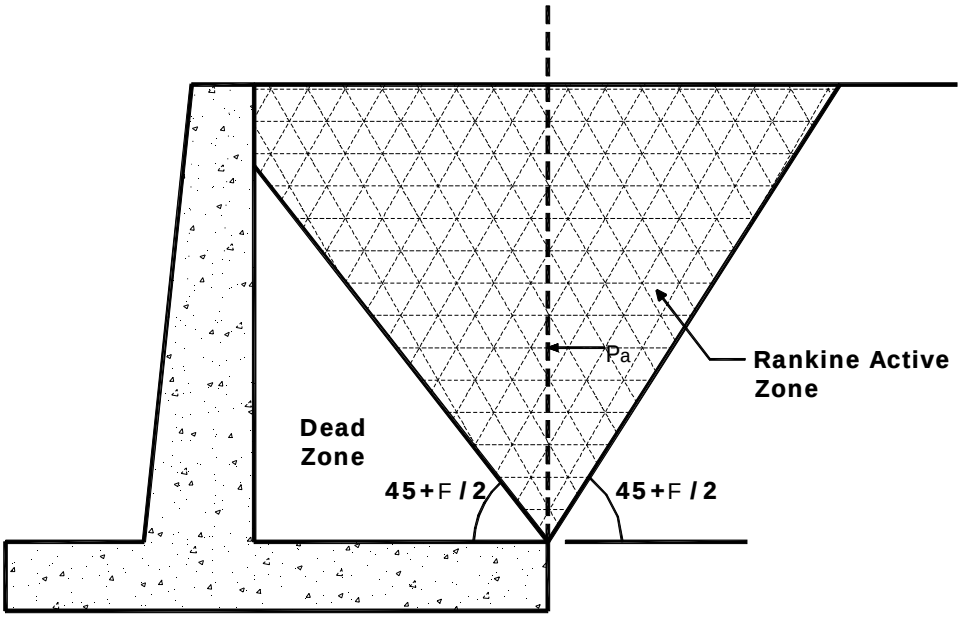

Figure 2.5 Failure of sand behind a cantilever retaining wall
(redrawn after Terzaghi, 1943)

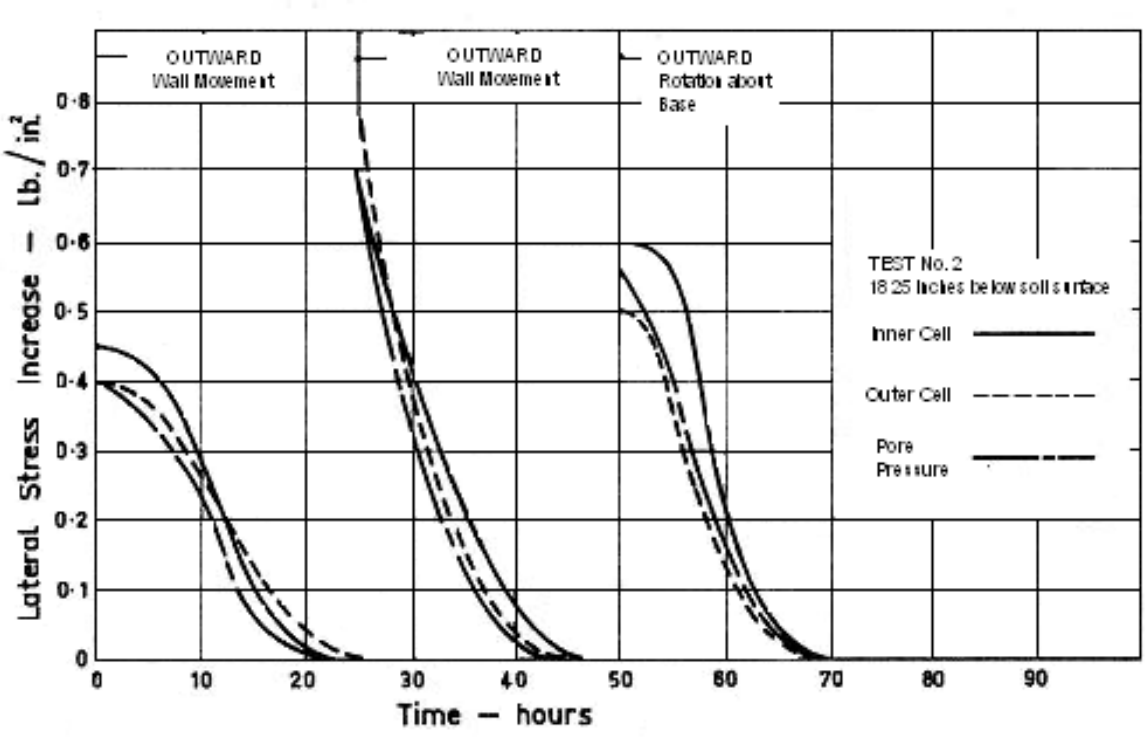

Figure 2.6 Earth pressure response following outward model wall movements
(1psi=6.9KN/m^2) (Moore and Spencer, 1972)

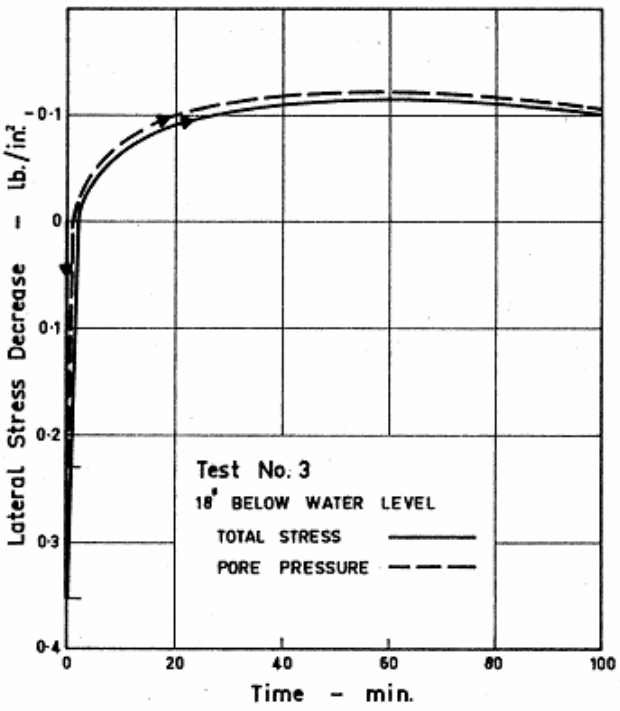

Figure 2.7 Earth pressure response following 1-in. wall model movements (1psi=6.9KN/m^2) (Moore and Spencer, 1972)

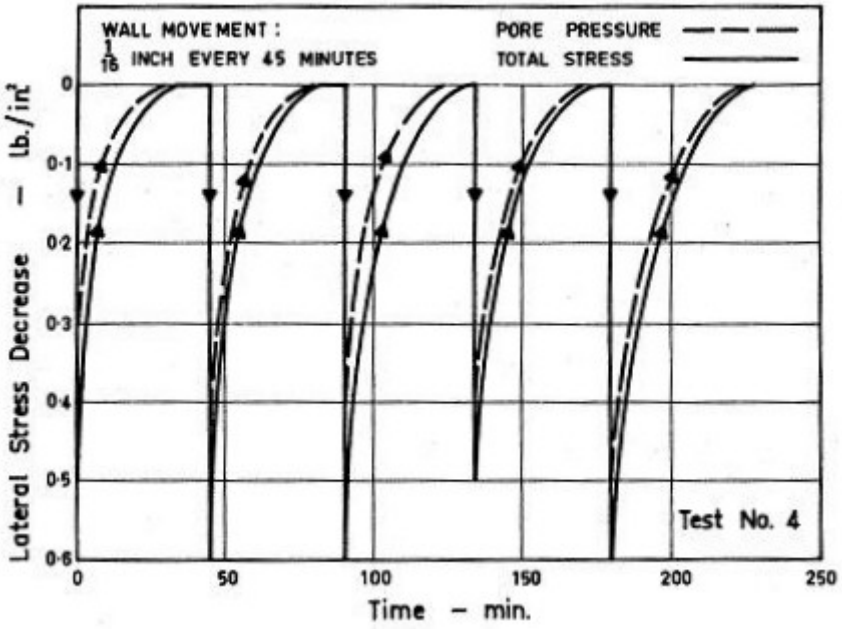

Figure 2.8 Response of lateral stress to repeated model wall movements (1psi=6.9KN/m^2) (Moore and Spencer, 1972)

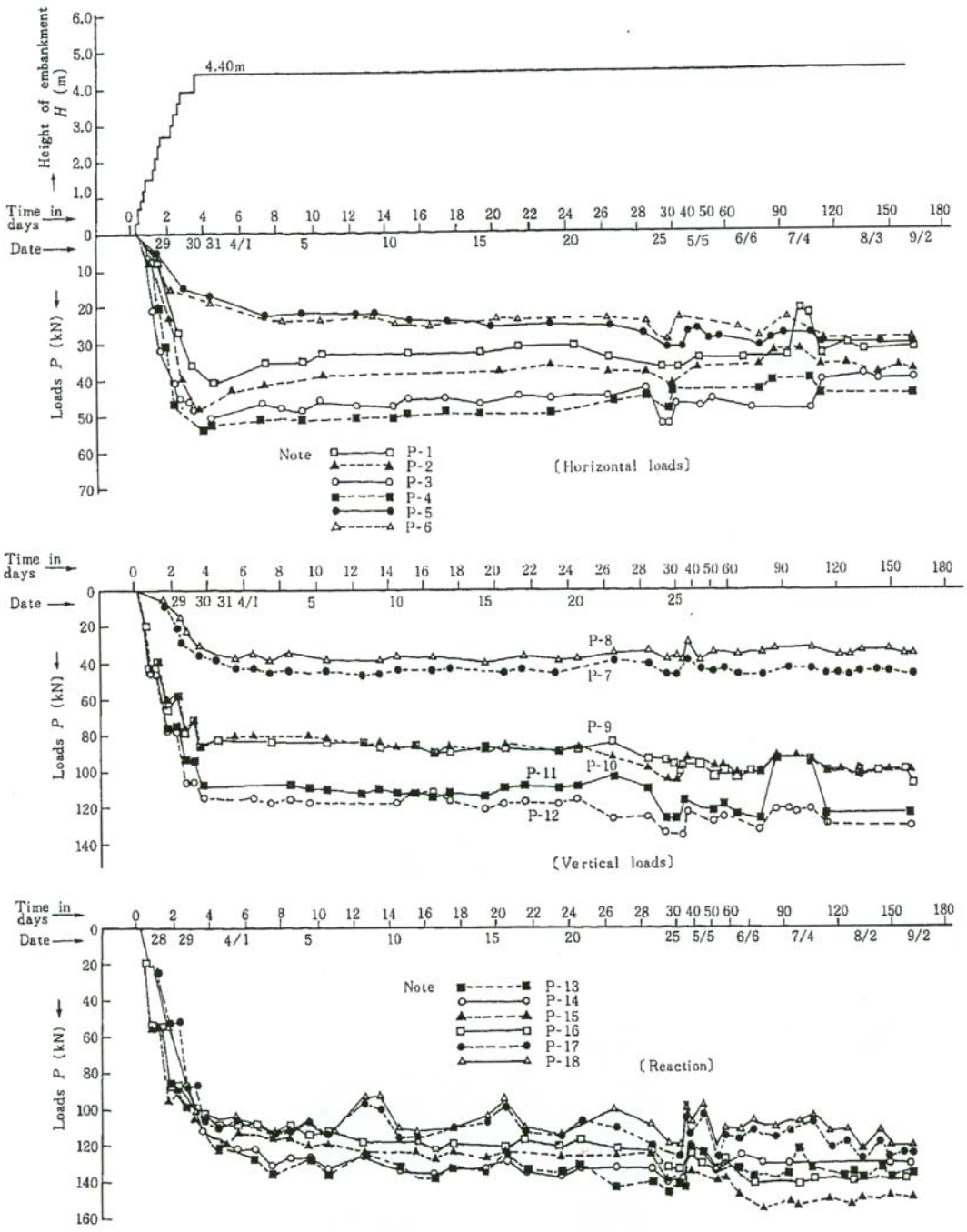

Figure 2.9 Result of field earth pressure measurement (before surcharge) (Fukuoka et al., 1977)

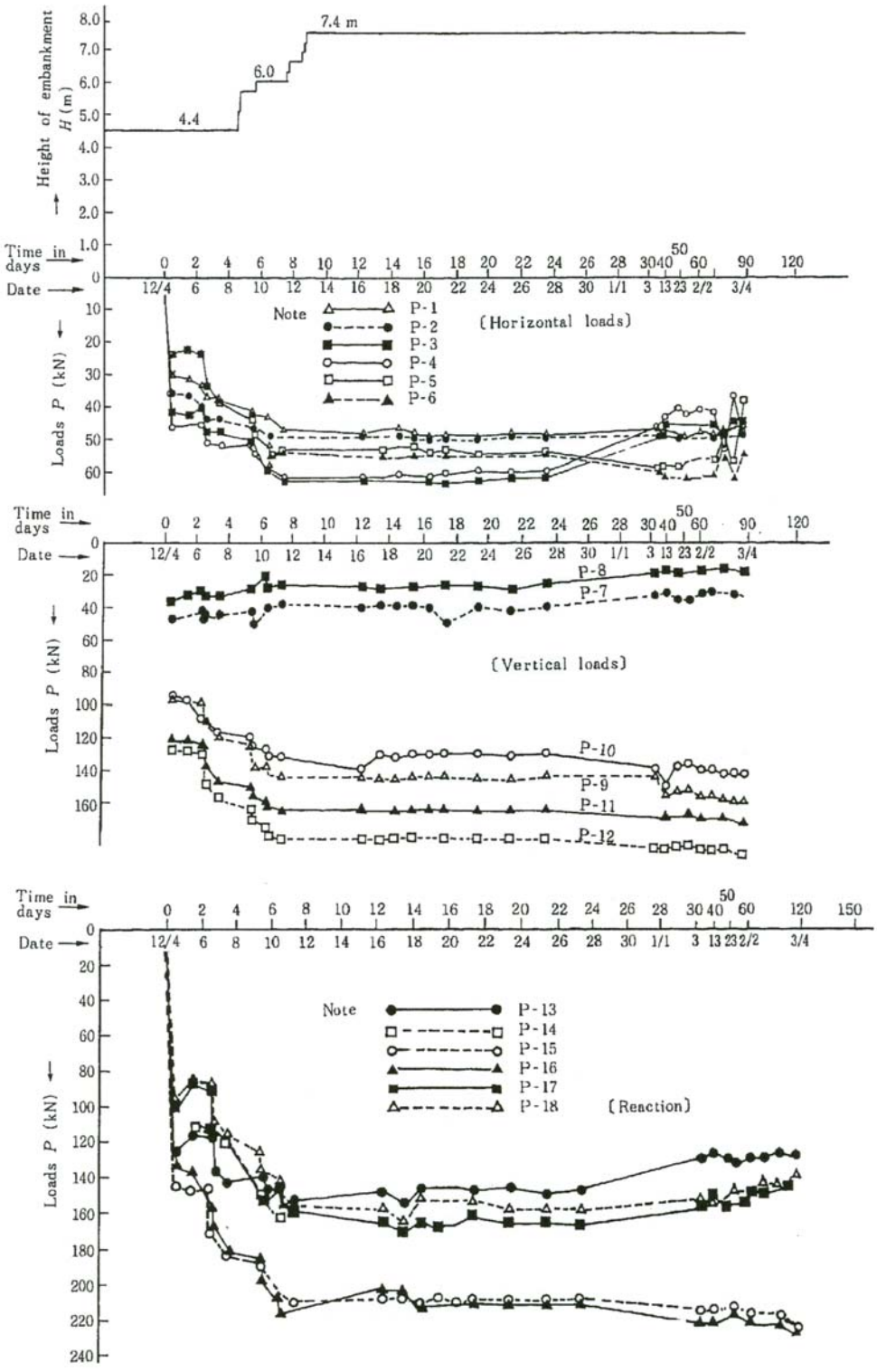

Figure 2.10 Result of field earth pressure measurement (after surcharge) (Fukuoka et al. 1977)

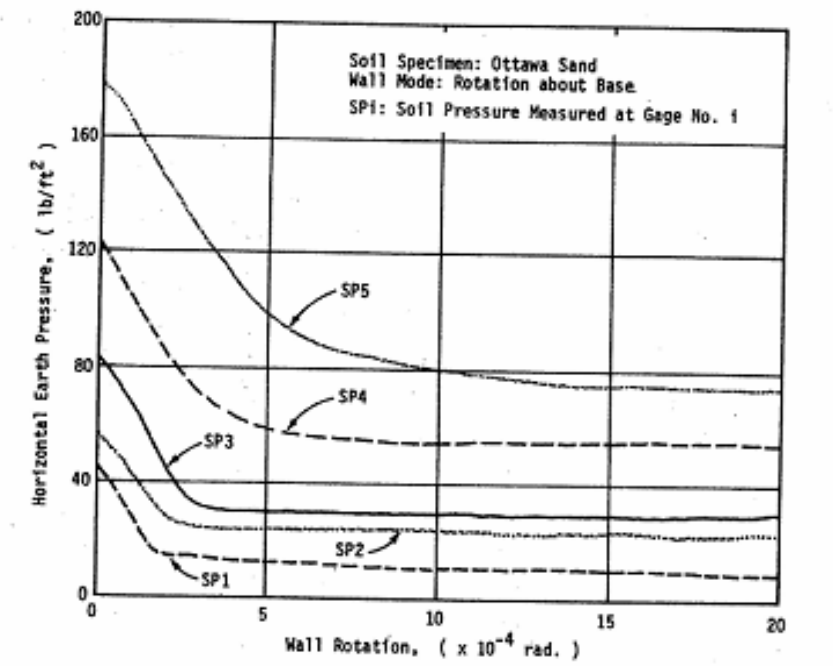

Figure 2.11 Variation of horizontal stresses behind rigid wall as a function of wall rotation about the base (Sherif et al., 1984)

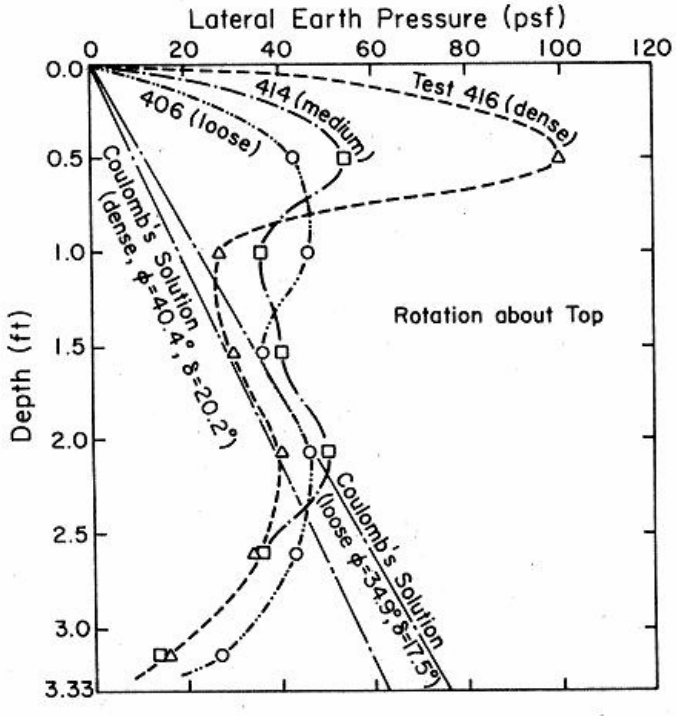

Figure 2.12 Distribution of horizontal earth pressure at active condition (rotation about top) (Fang and Ishibashi, 1986)

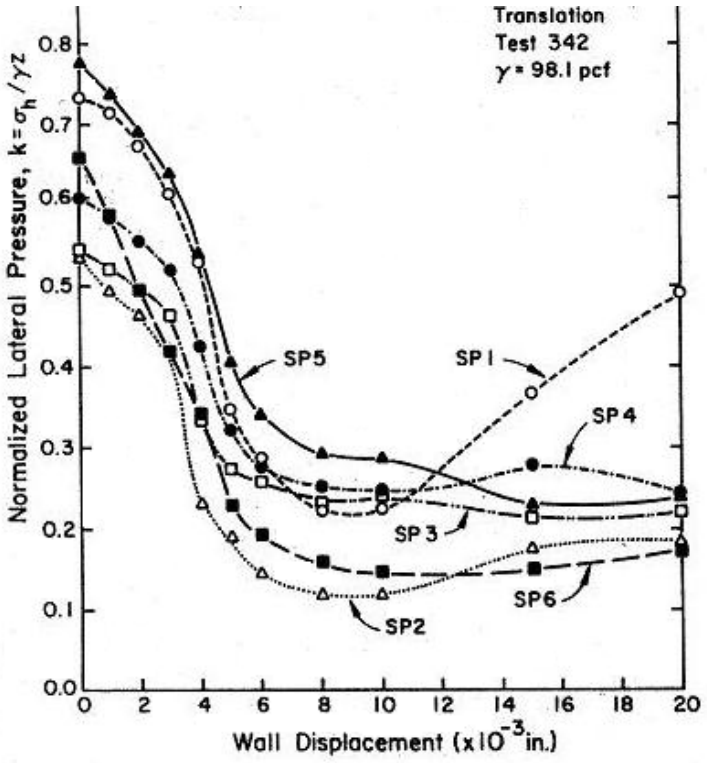

Figure 2.13 Change of normalized lateral pressure with translational wall displacement (Fang and Ishibashi, 1986)

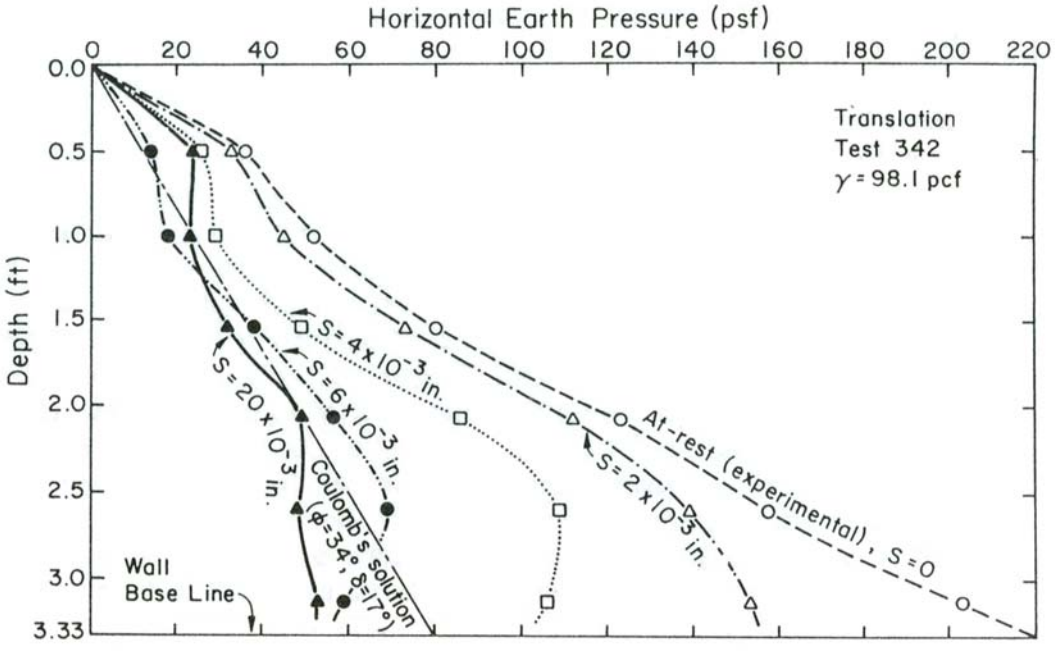

Figure 2.14 Distribution of horizontal earth pressure at different wall rotations (rotation about base) (Fang and Ishibashi, 1986)

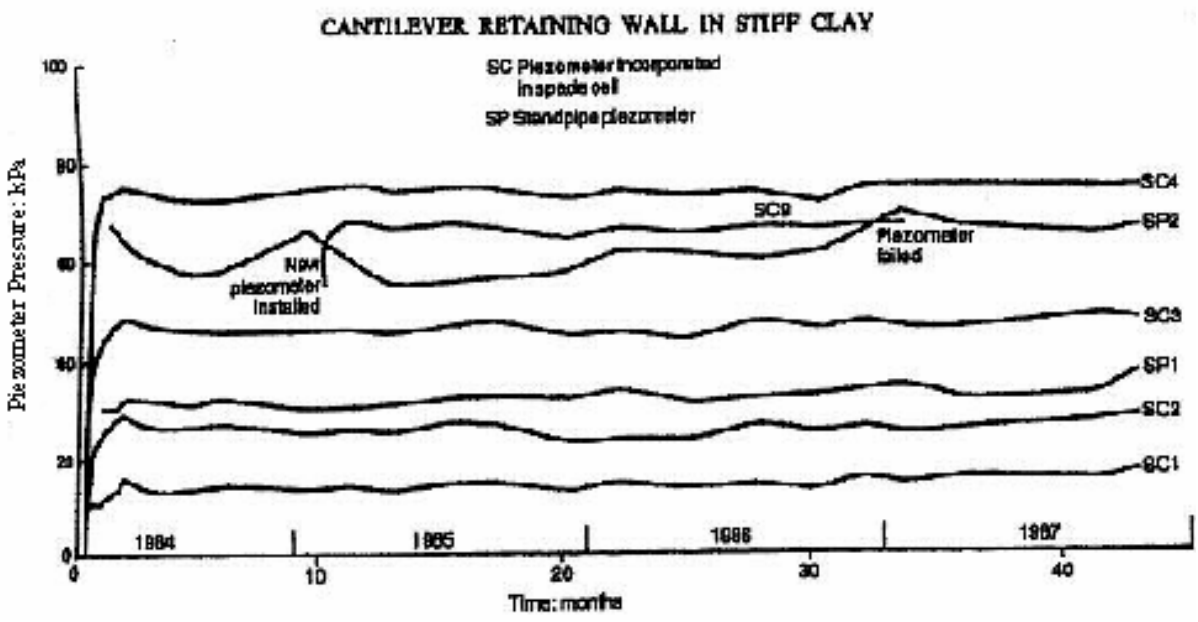

Figure 2.15 Variation of piezometer readings with time (Carder and Symons, 1989)

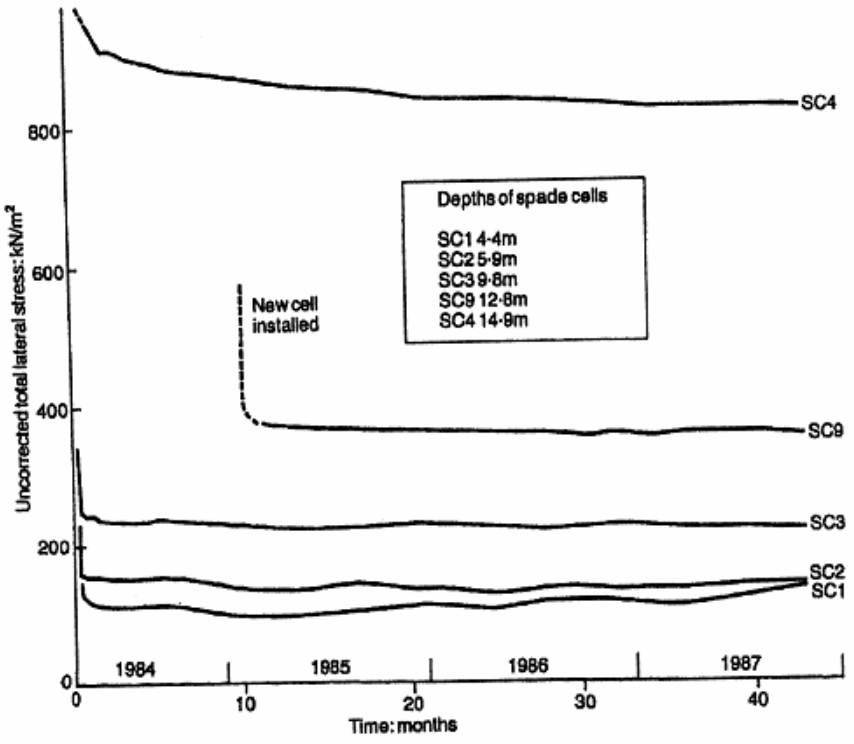

Figure 2.16 Variation of spade cell readings with time
(Carder and Symons, 1989)

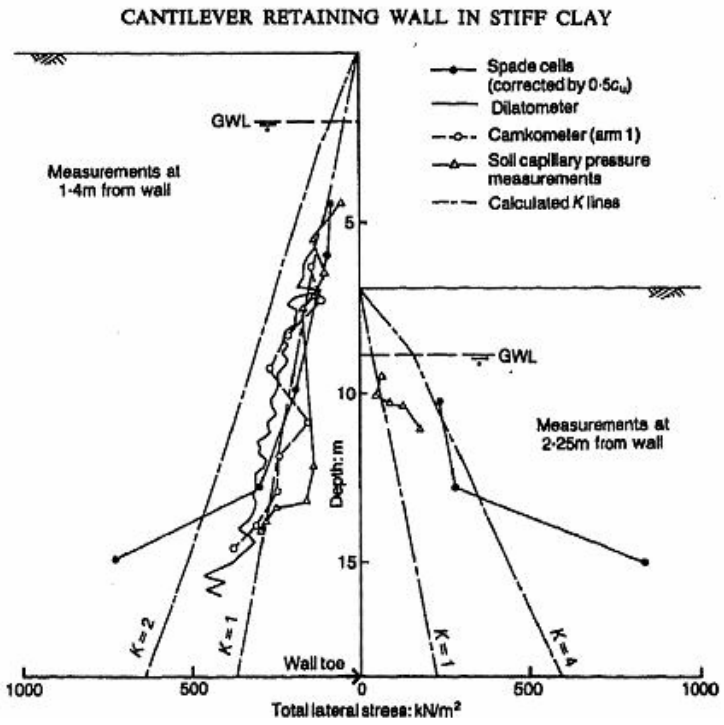

Figure 2.17 Lateral stress distribution at the retaining wall (Carder and Symons,1989)

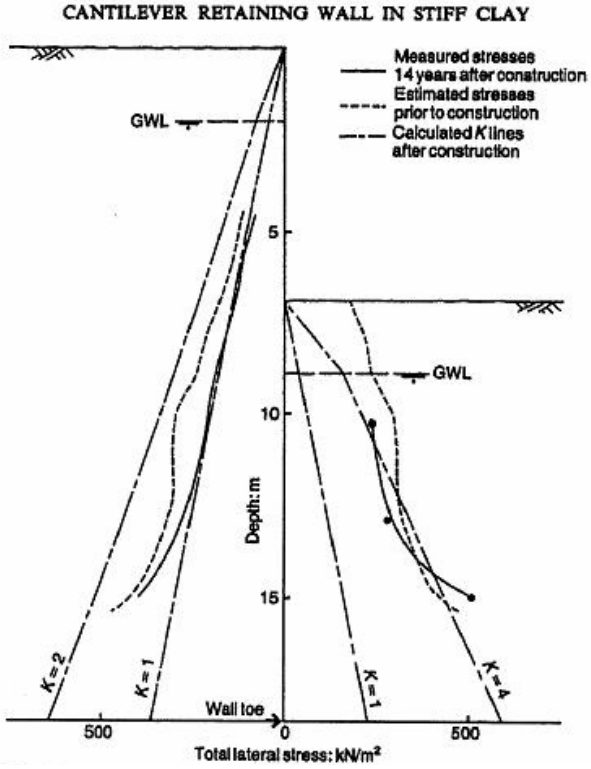

Figure 2.18 Summary of stresses near the retaining wall (Carder and Symons, 1989)

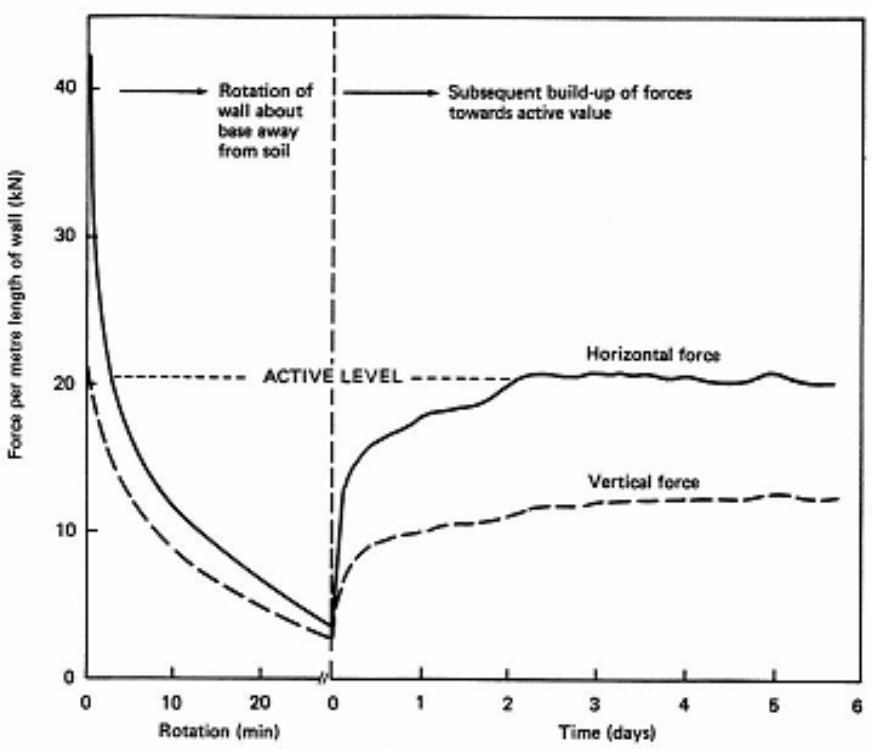

Figure 2.19 Force developed at the active condition (Carder and Symons, 1989)

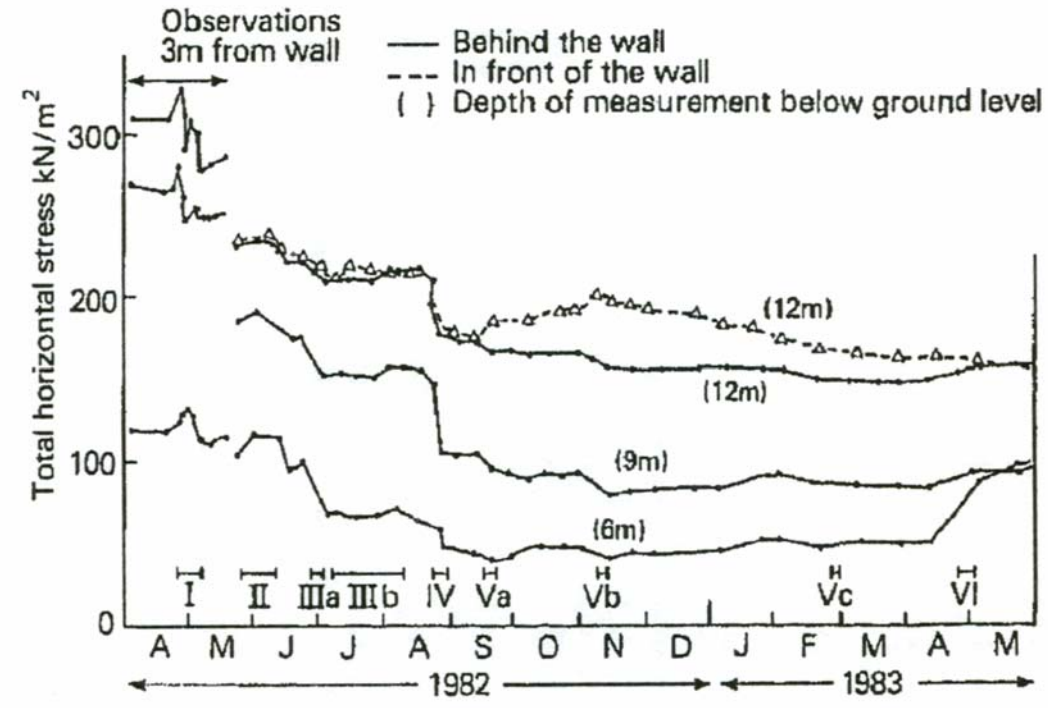

Figure 2.20 Change in total horizontal stress with time (Tedd et al., 1984)

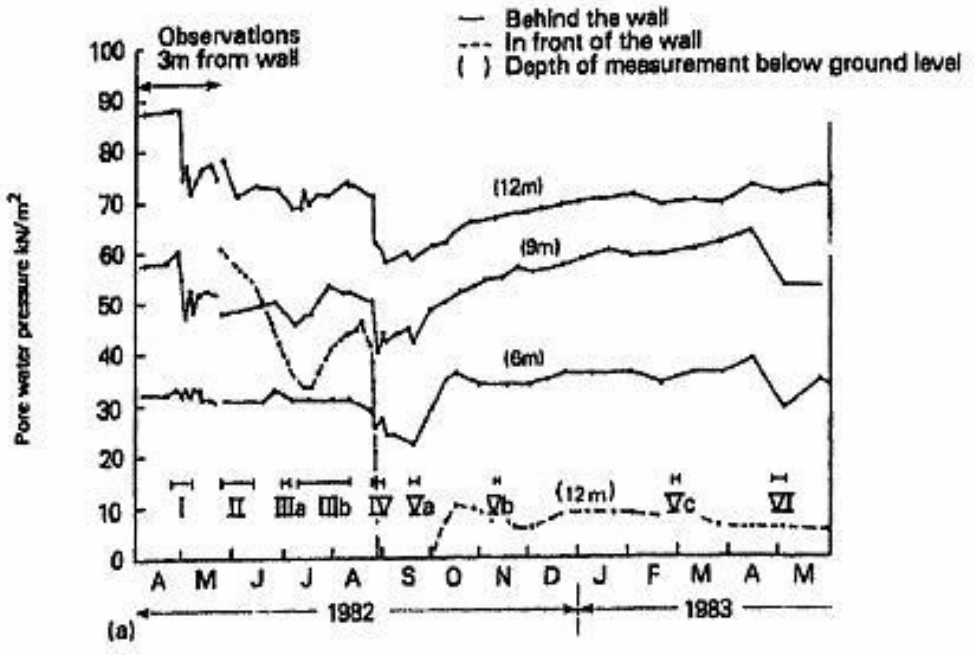

Figure 2.21 Change in pore water pressure with time (Tedd et al, 1984)

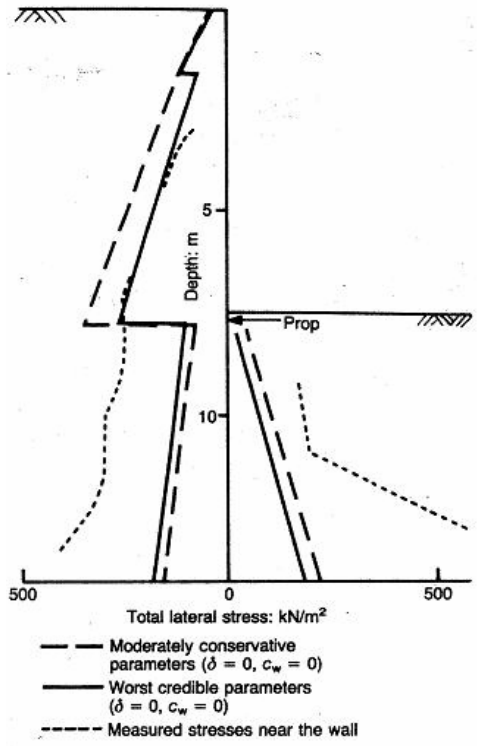

Figure2.22 Comparison of measured stresses at A3 site with those used in design based on linear seepage (Symons et al., 1992)

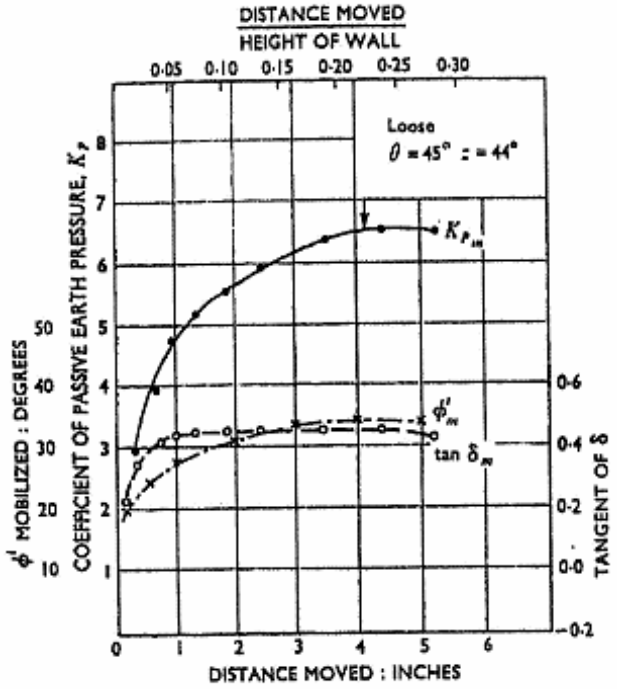

Figure 2.23 K_P and wall friction for loose sand (Rowe and Peaker, 1965)

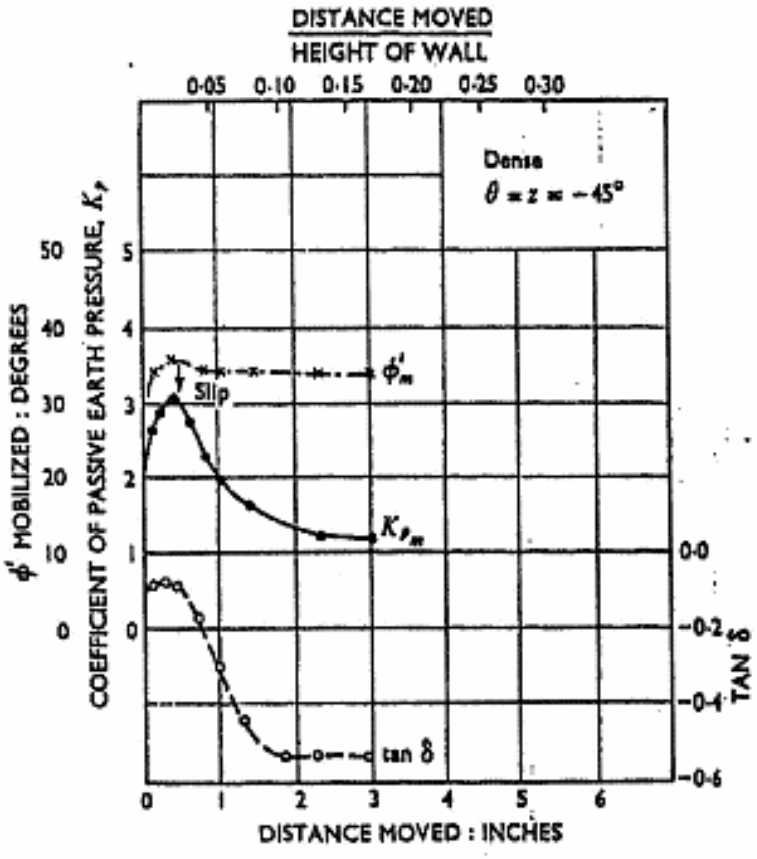

Figure 2.24 K_p and wall friction for dense sand (Rowe and Peaker, 1965)

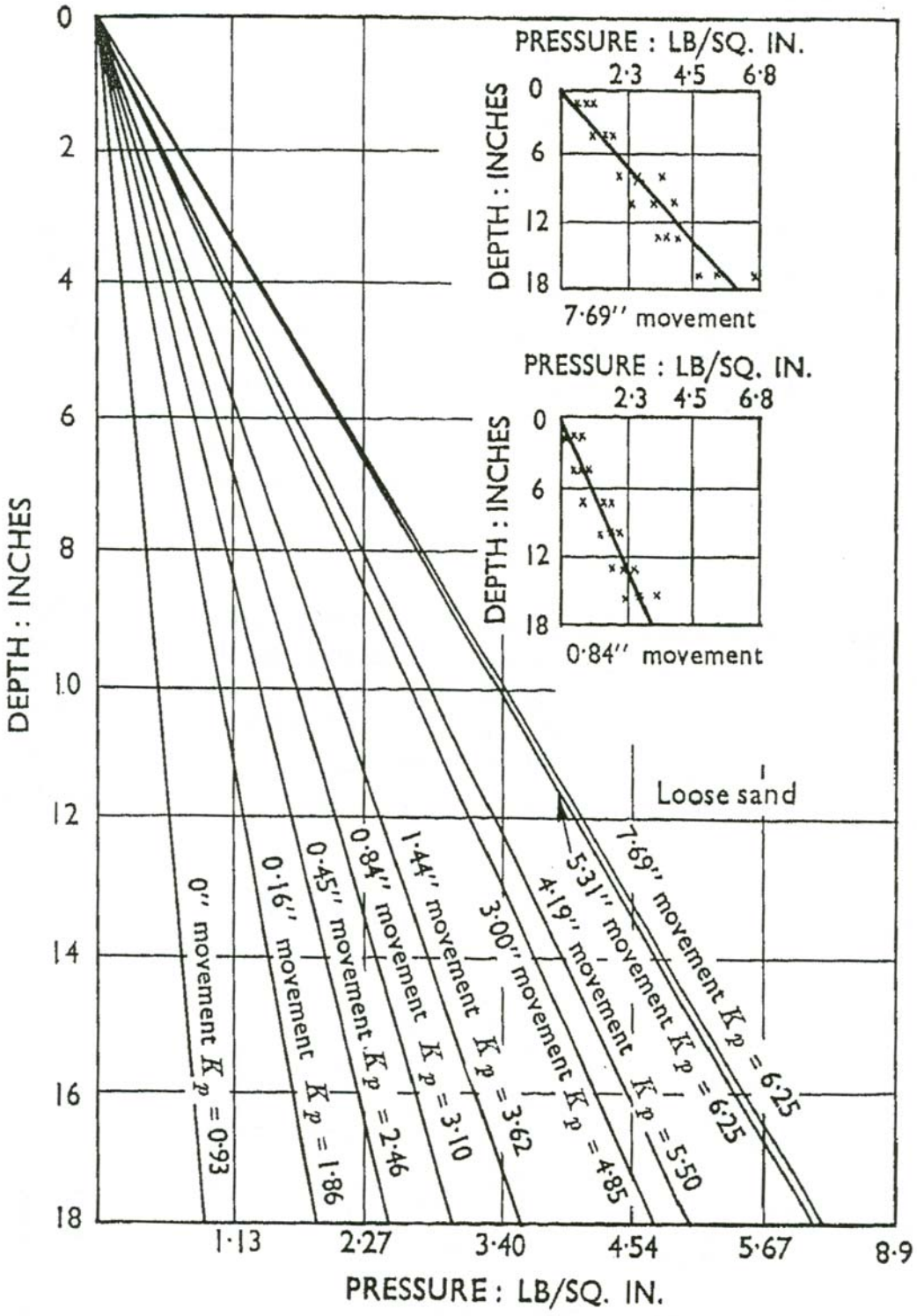

Figure 2.25 Typical pressure distribution (Rowe and Peaker, 1965)

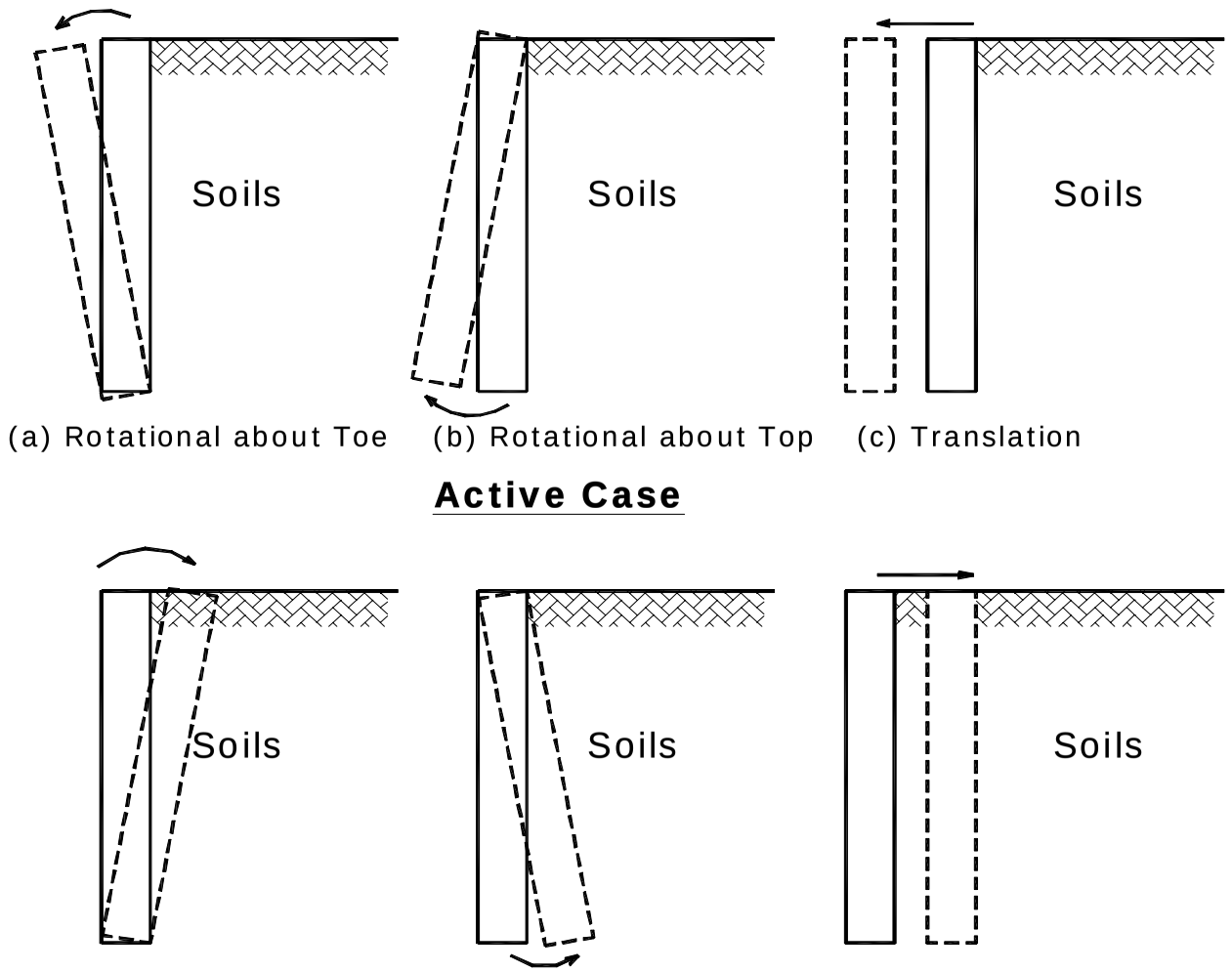

Figure 2.26 Rotational and translational wall retaining wall movement for active and passive cases (redrawn after Sherif et al., 1984)

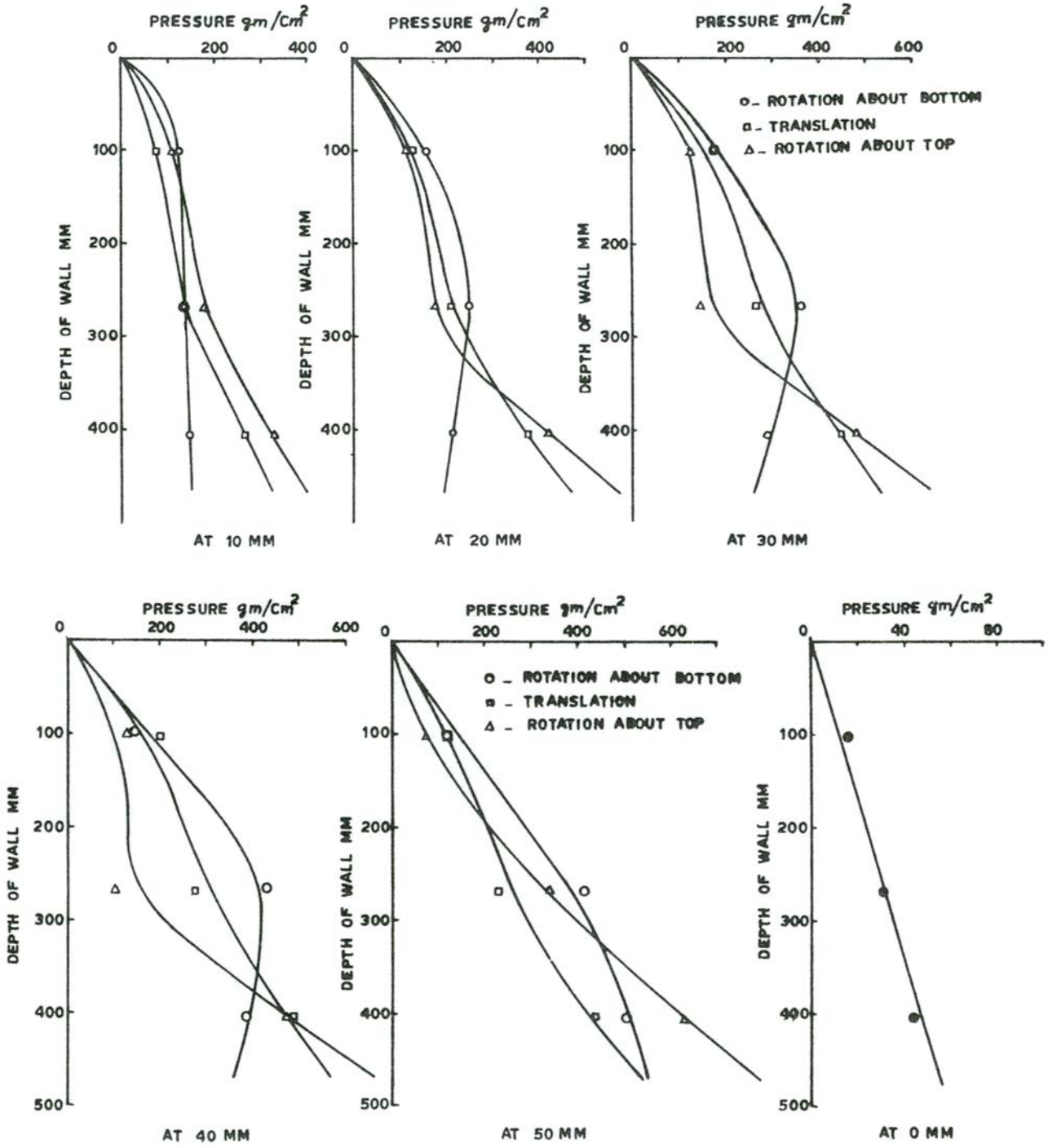

Figure 2.27 Pressure distribution on the wall at different wall movements (loose sand-passive case) (Narain and Nandakkumaran, 1969)

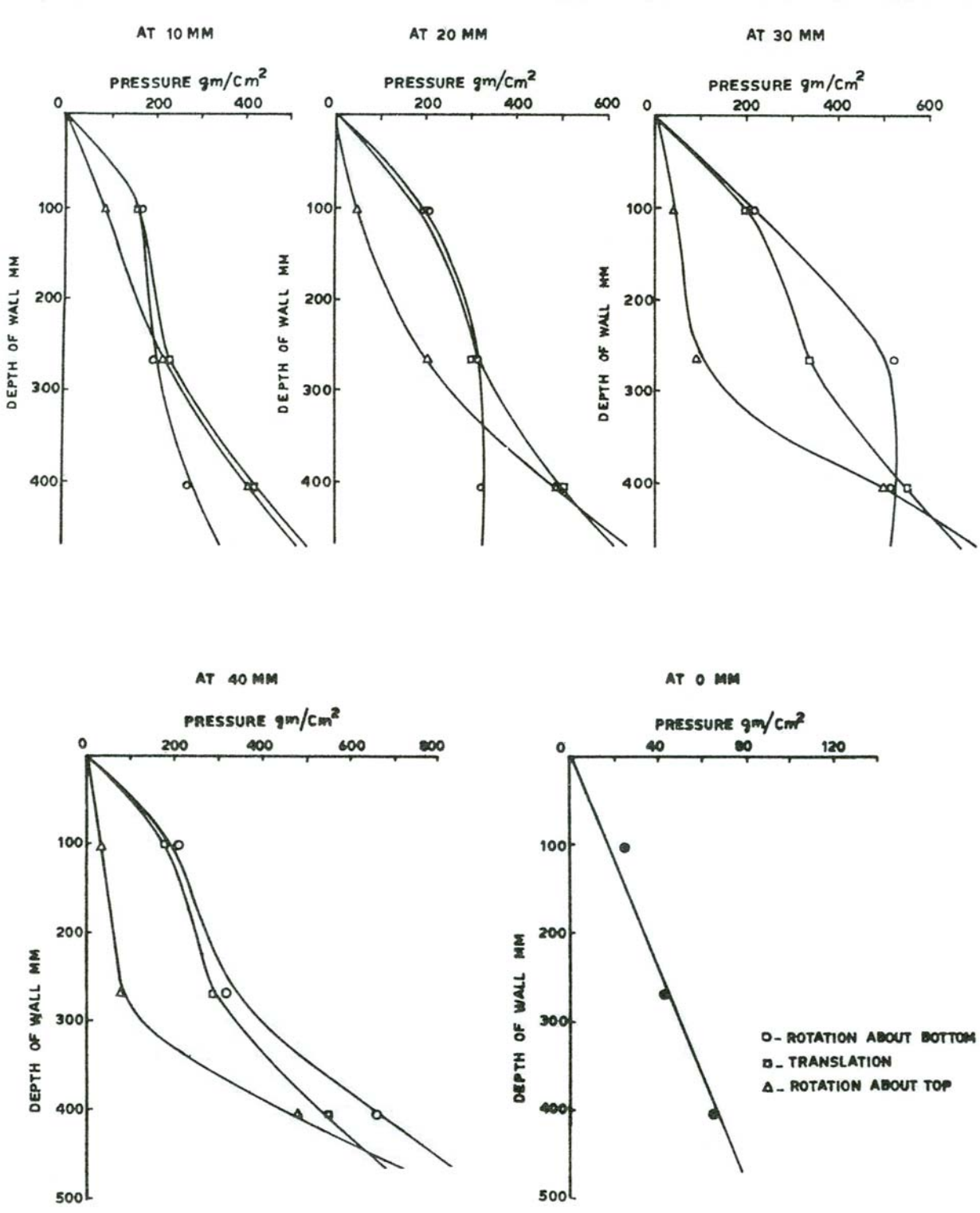

Figure 2.28 Pressure distribution on the wall at different wall movements (dense sand-passive case) (Narain and Nandakkumaran, 1969)

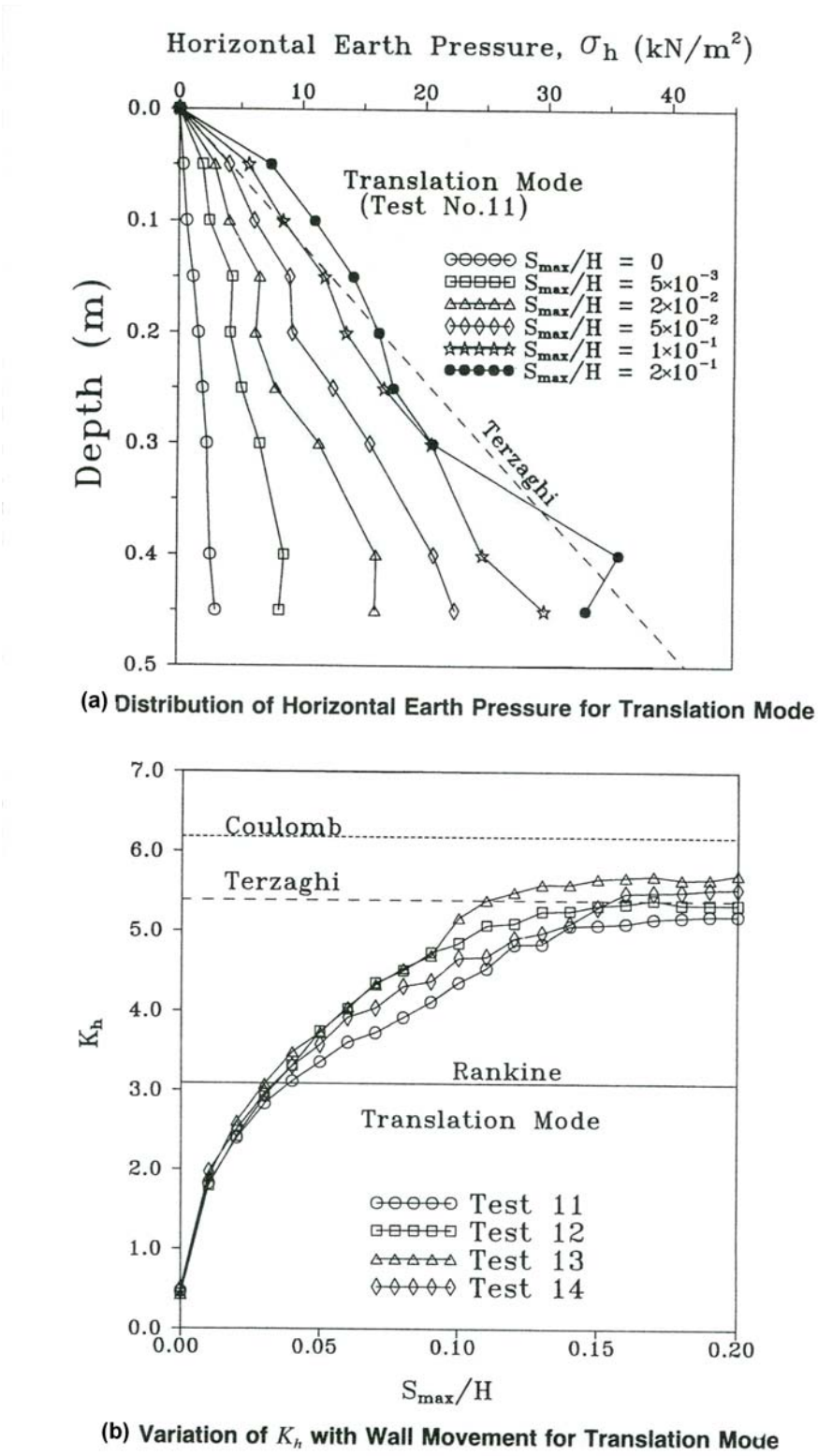

Figure 2.29 (a) Distribution of horizontal earth pressure for translation mode
(b) Variation of K_h with wall movement for translation mode
(Fang et al. 1994)

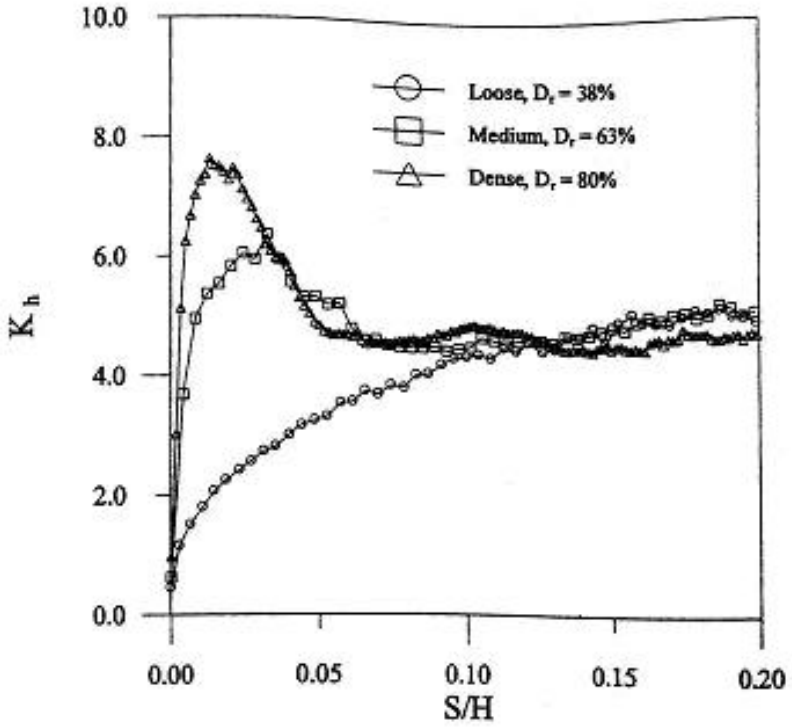

Figure 2.30 Variation of K_h with wall movement for loose, medium dense, and dense backfill (Fang et al., 2001)

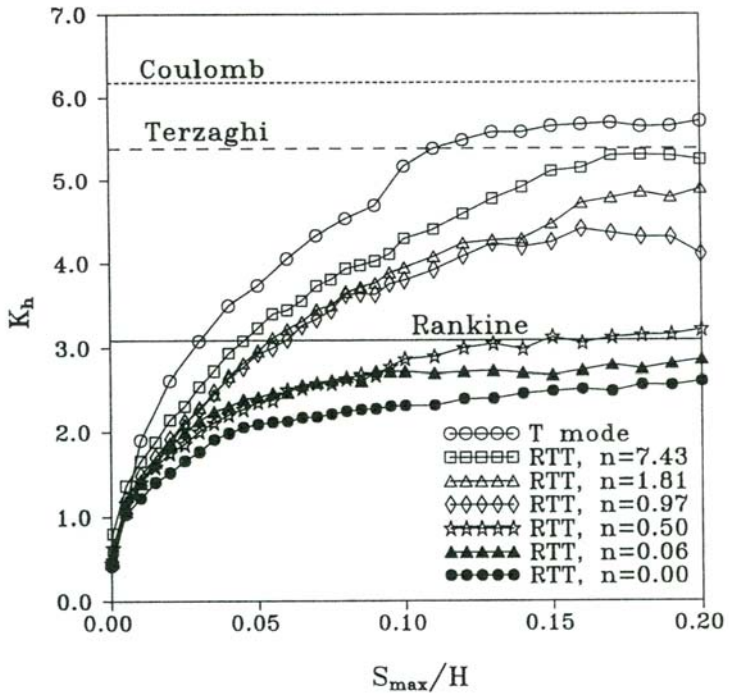

Figure 2.31 Variation of K_A with wall movement for RTT (rotation about a point above the top) mode (Fang et al. 1994)

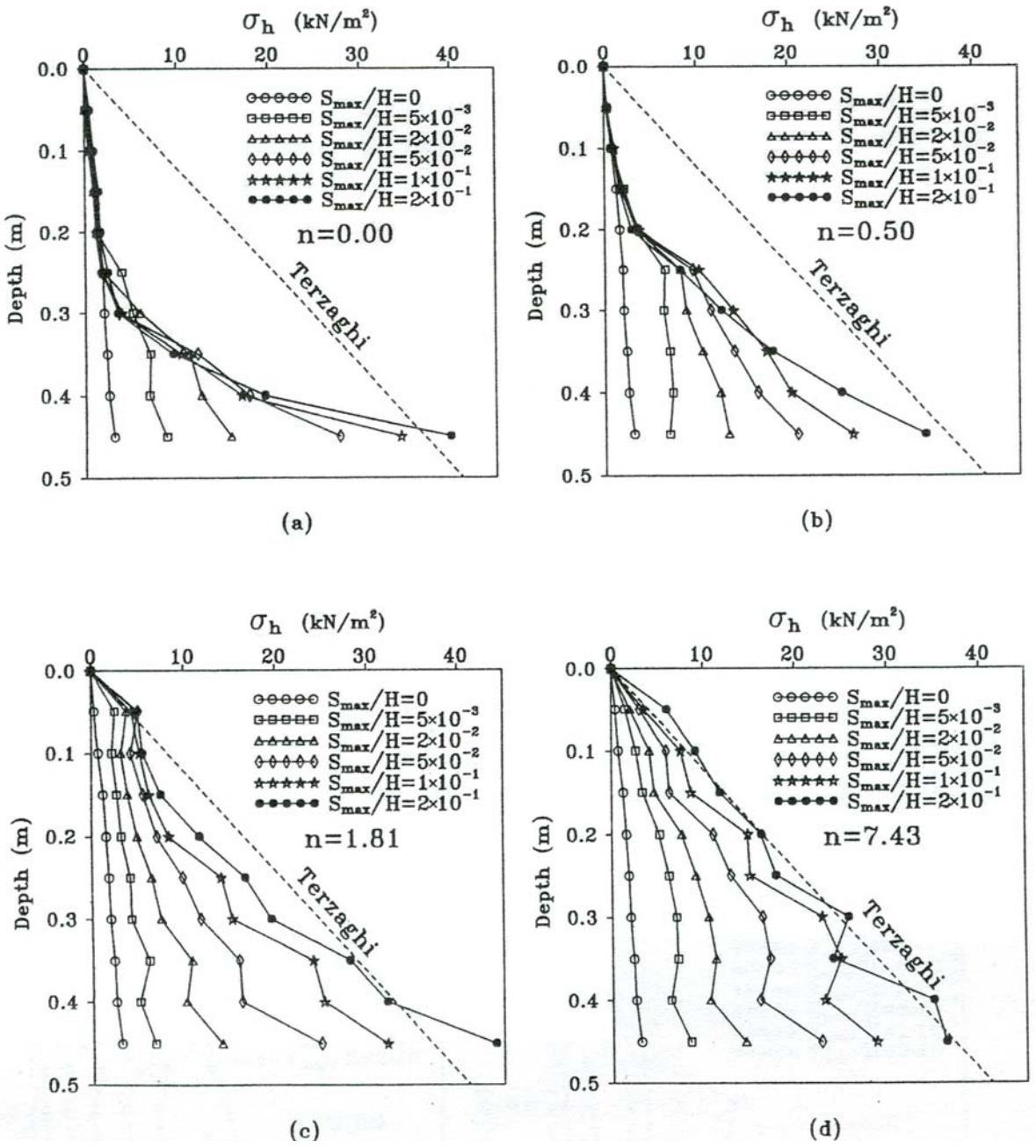

Figure 2.32 Distribution of horizontal earth pressure for RTT (rotation about a point above the top) mode (Fang et al. 1994)

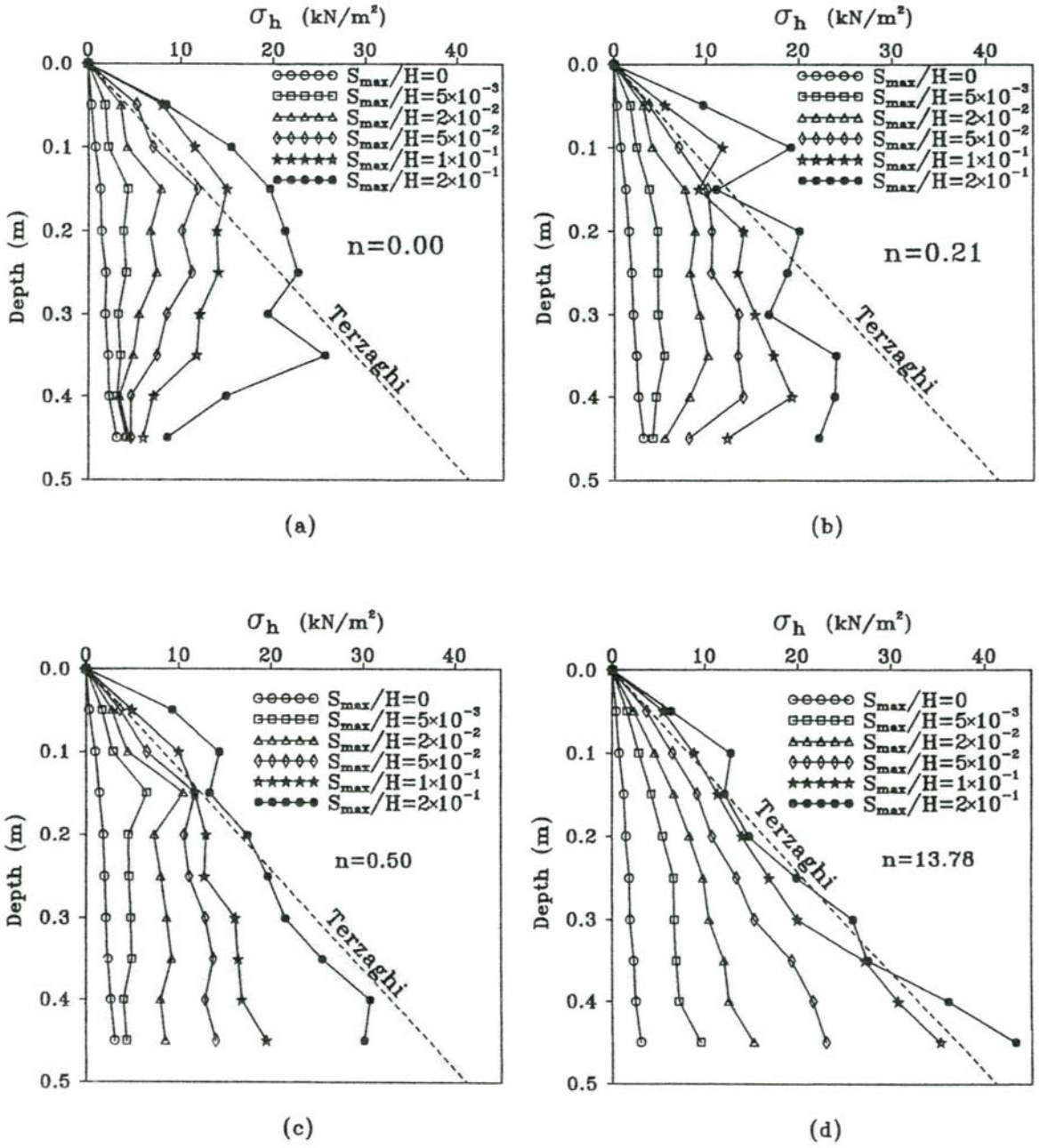

Figure 2.33 Distribution of horizontal earth pressure for RBT (rotation about a point below the wall base) mode (Fang et al., 1994)

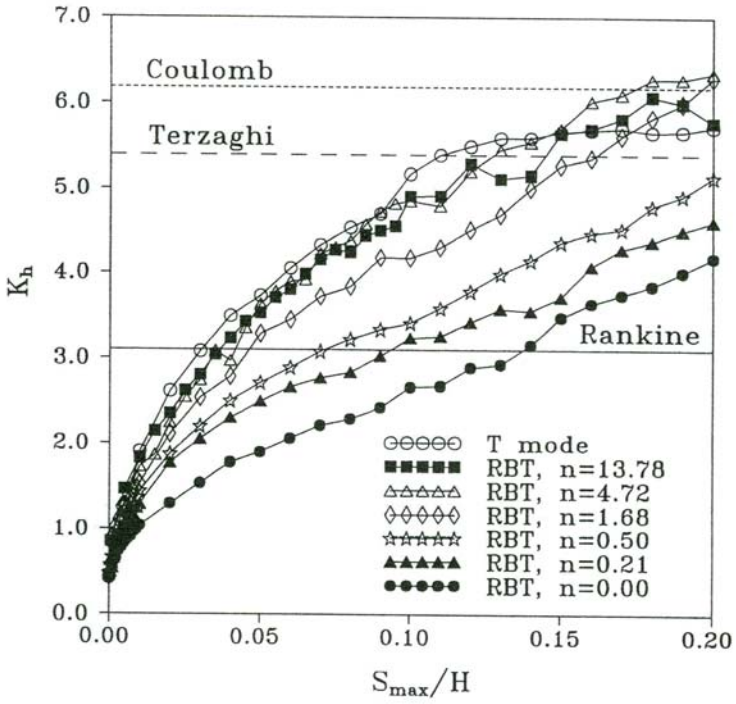

Figure 2.34 Variation of K_p with wall movement for RBT(rotation about a point below the wall base) mode (Fang et al. 1994)

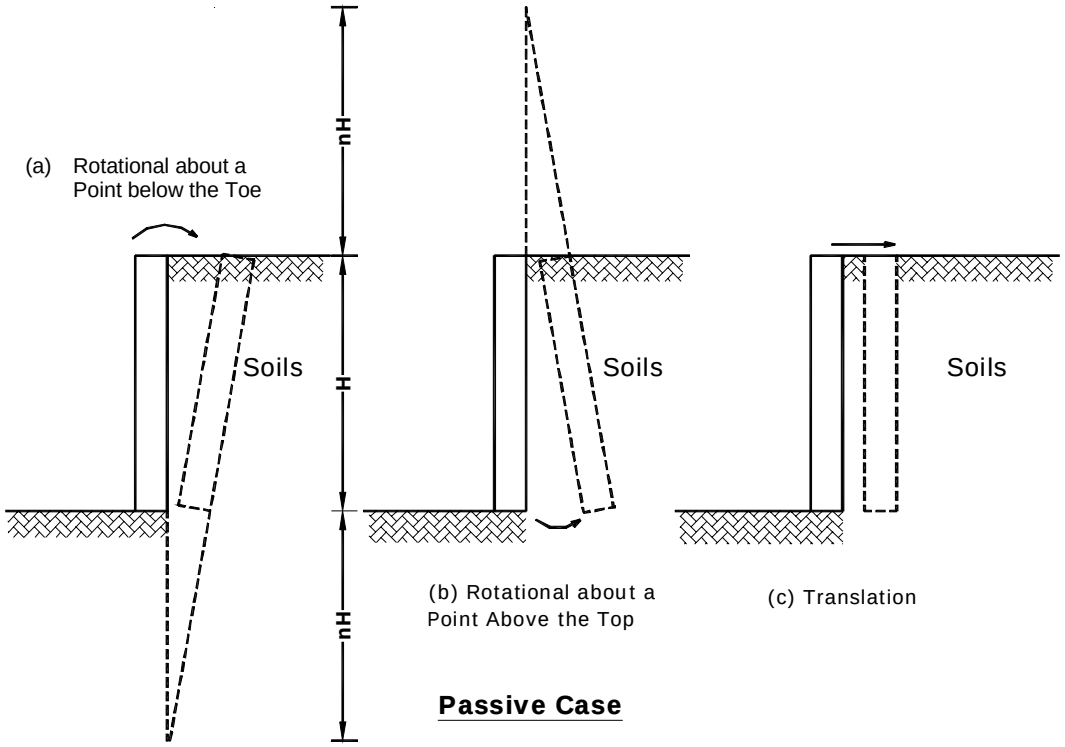

Figure 2.35 Passive wall movement modes (redrawn after Fang et al., 1994)

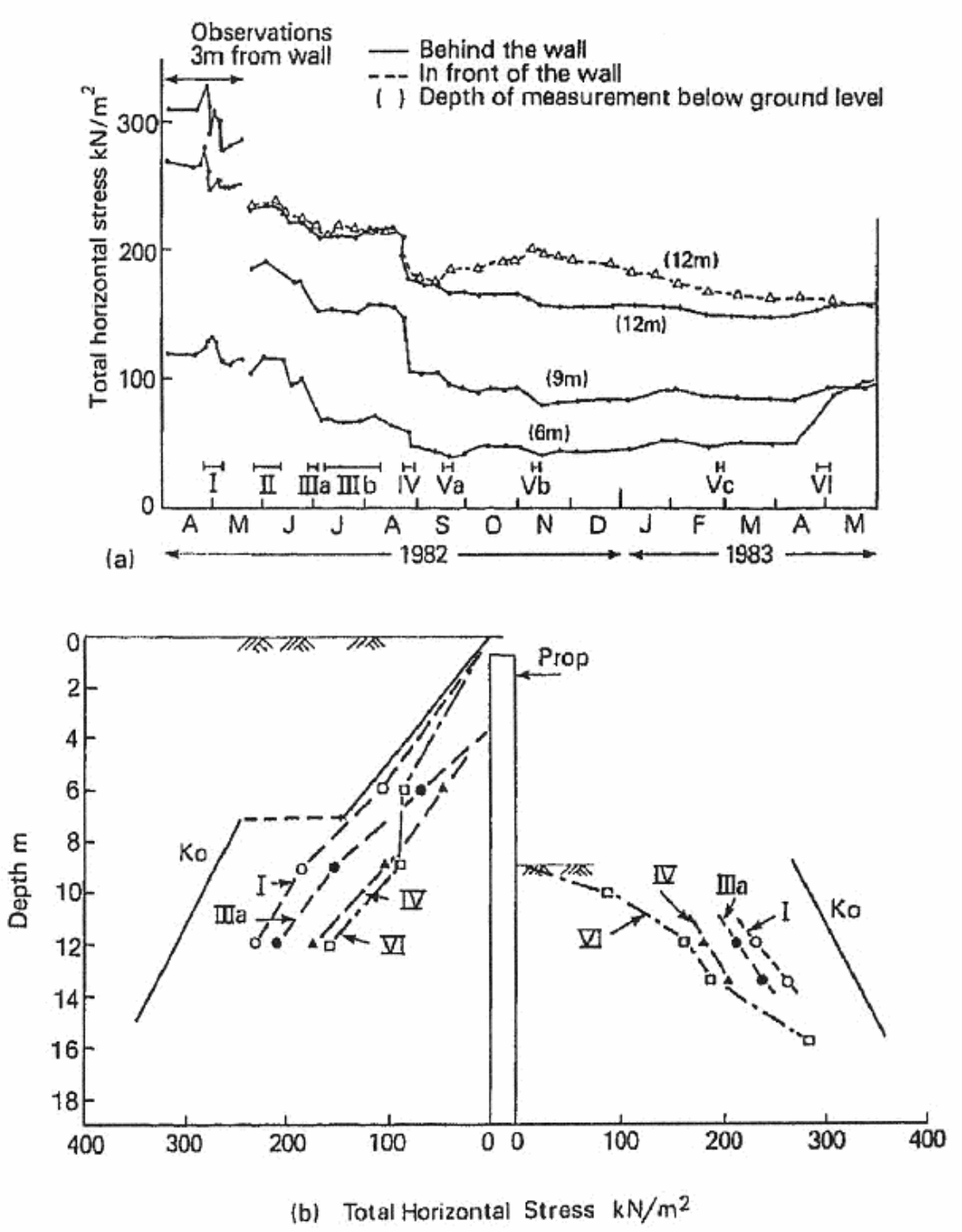

Figure 2.36 (a) Change in total horizontal stress with time
(b) Distribution of the total horizontal stress in the soil 0.6m from the wall at various stages of excavation (Tedd et al. 1984)

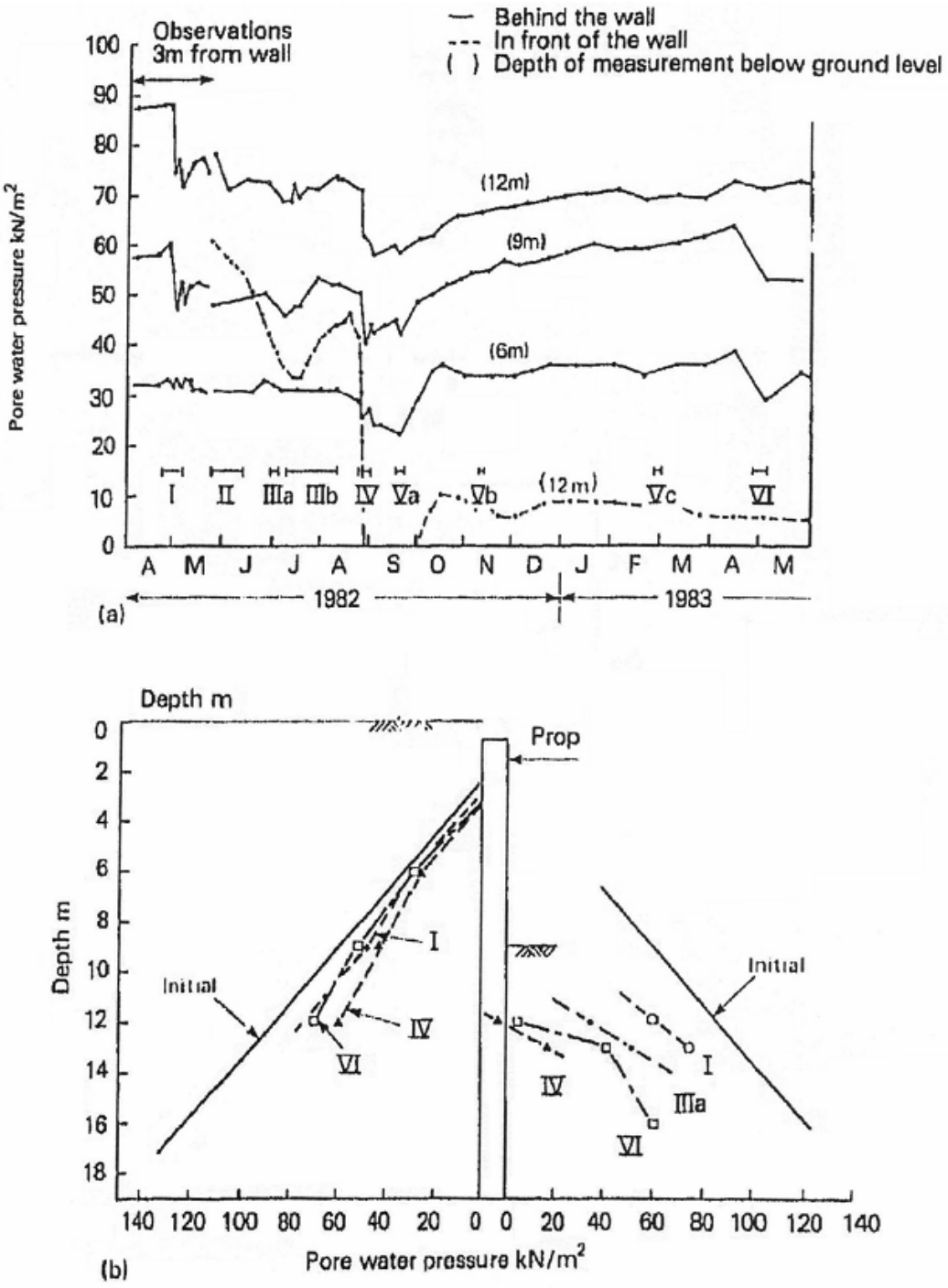

Figure 2.37 (a) Change in pore water pressure with time
(b) Distribution of pore water pressure 0.6m from the wall at various stages of excavation (Tedd et al. 1984)

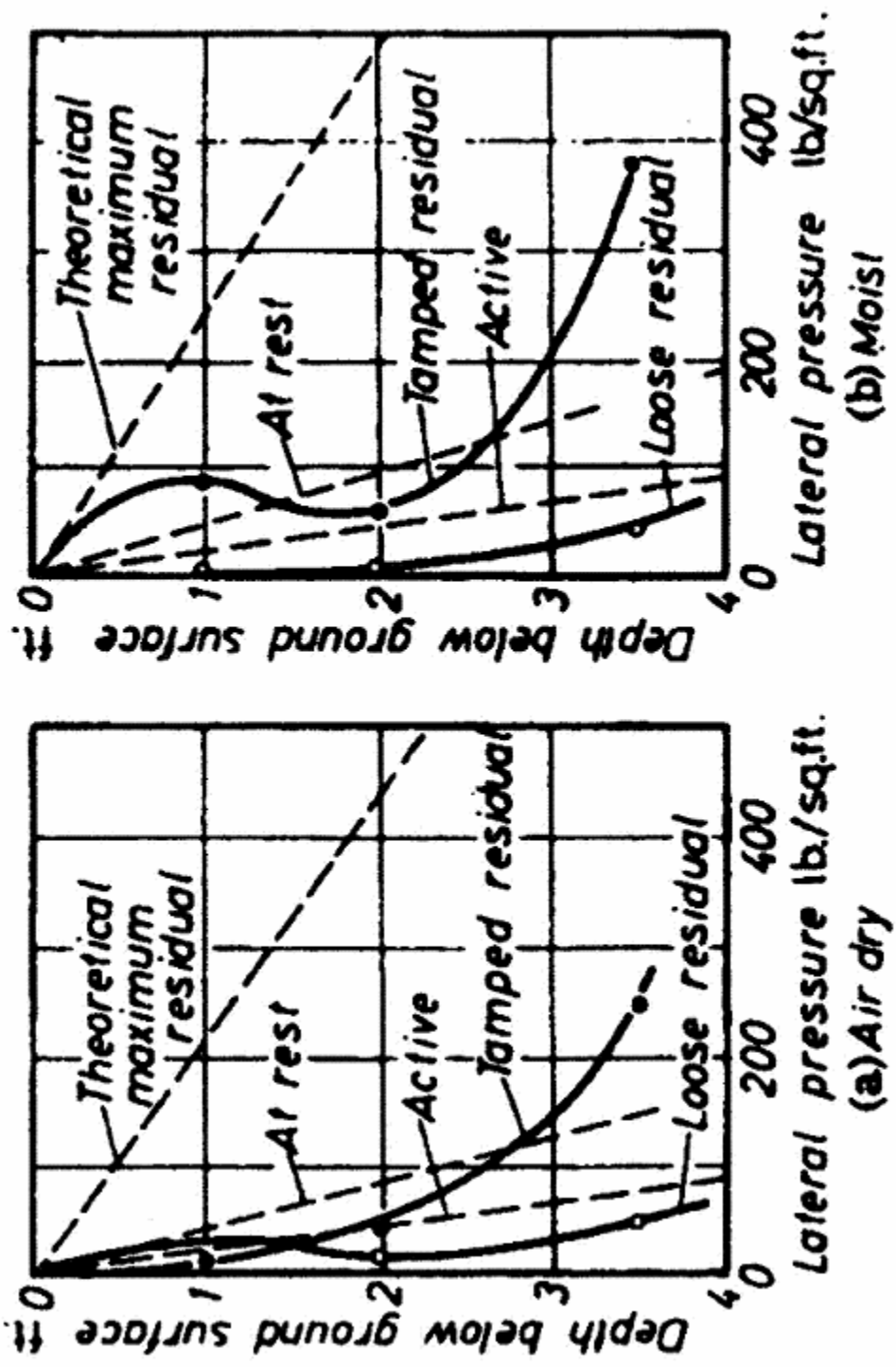

Figure 2.38 Residual lateral pressures as a functions of depth below the surface of river sand tampered and loosely placed behind a supported wall: (a) dry sand (b) at a moisture content of 14 percent (Sowers et al., 1957)

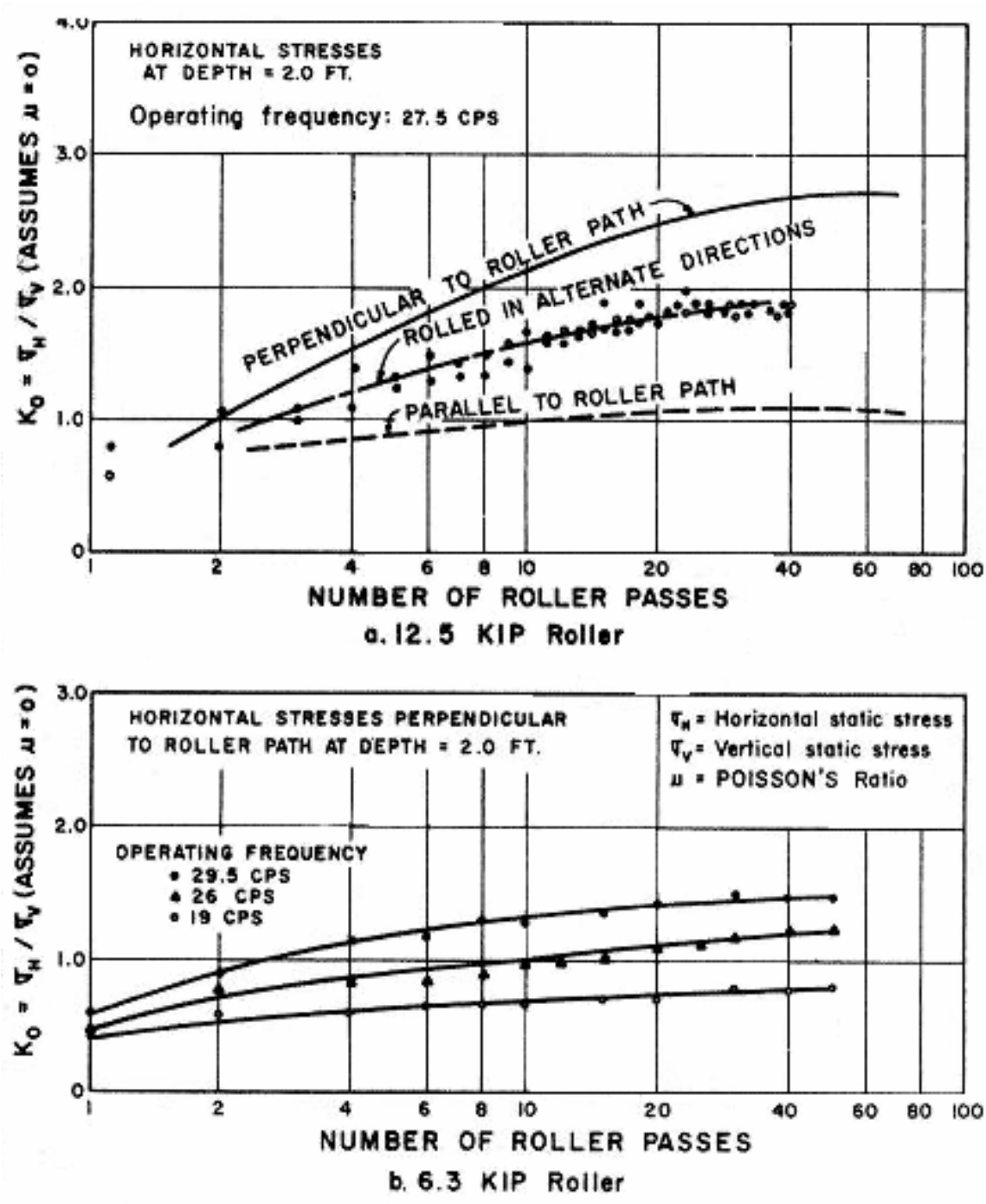

Figure 2.39 Variation of K_0 as a function of number of roller passes
(D'Appolonia et al., 1969)

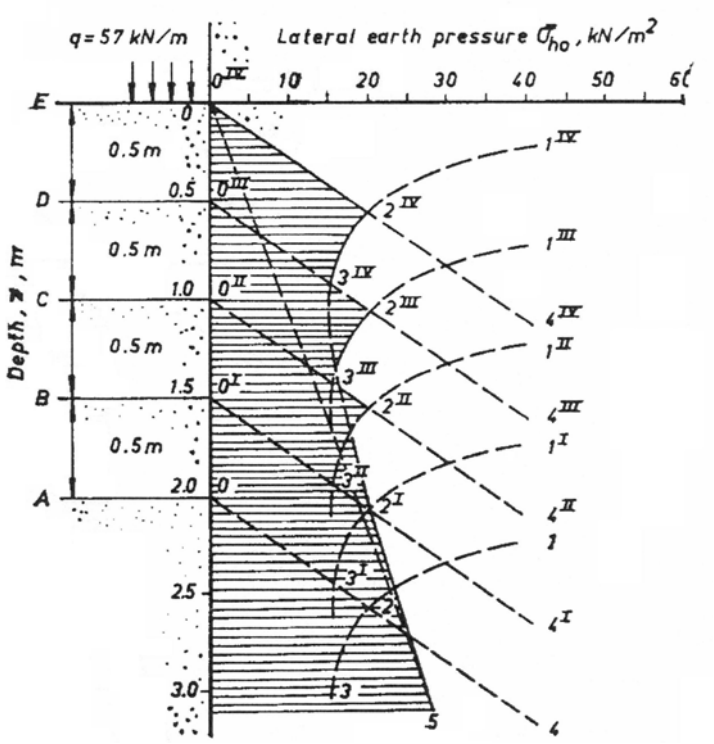

Figure 2.40 Earth pressure distribution for a 10.2 ton smooth-wheel roller (Broms, 1971)

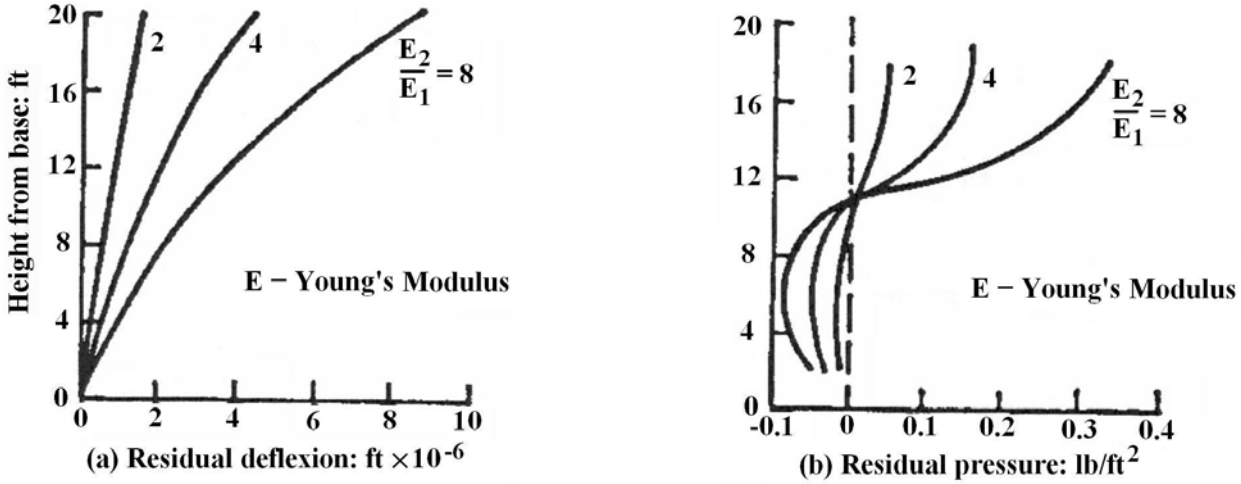

Figure 2.41 Residual effect of number of passes (Aggour and Brown, 1974)

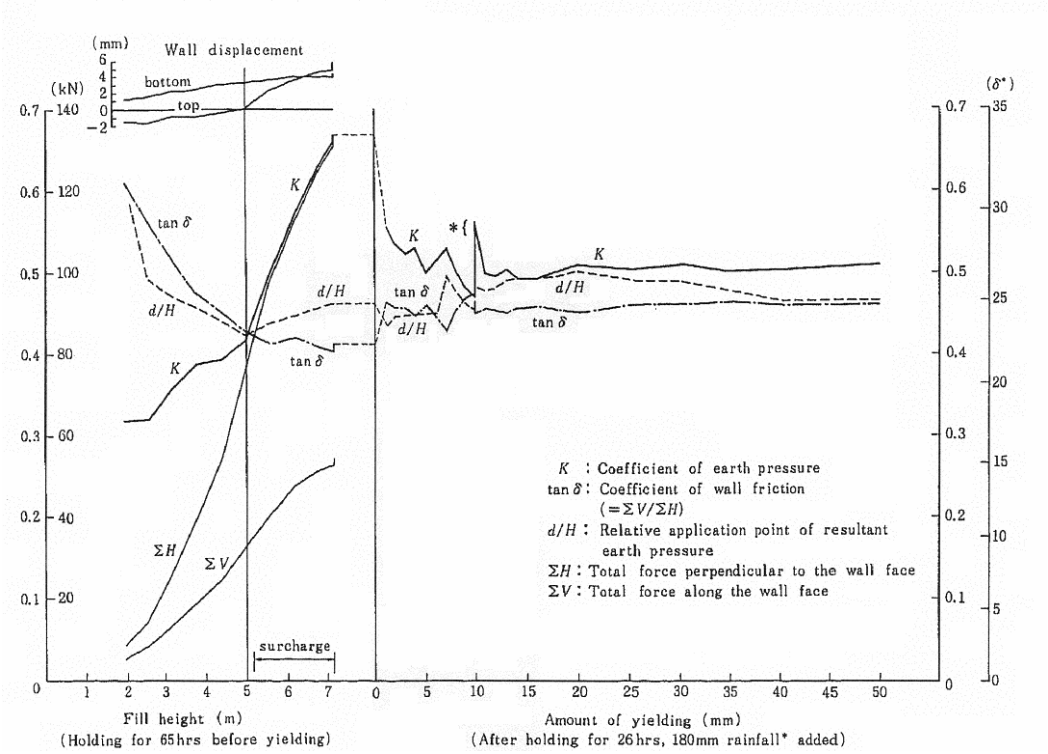

Figure 2.42 Coefficient of earth pressure at rest during the test (loose sand) (Fukuoka et al. 1977)

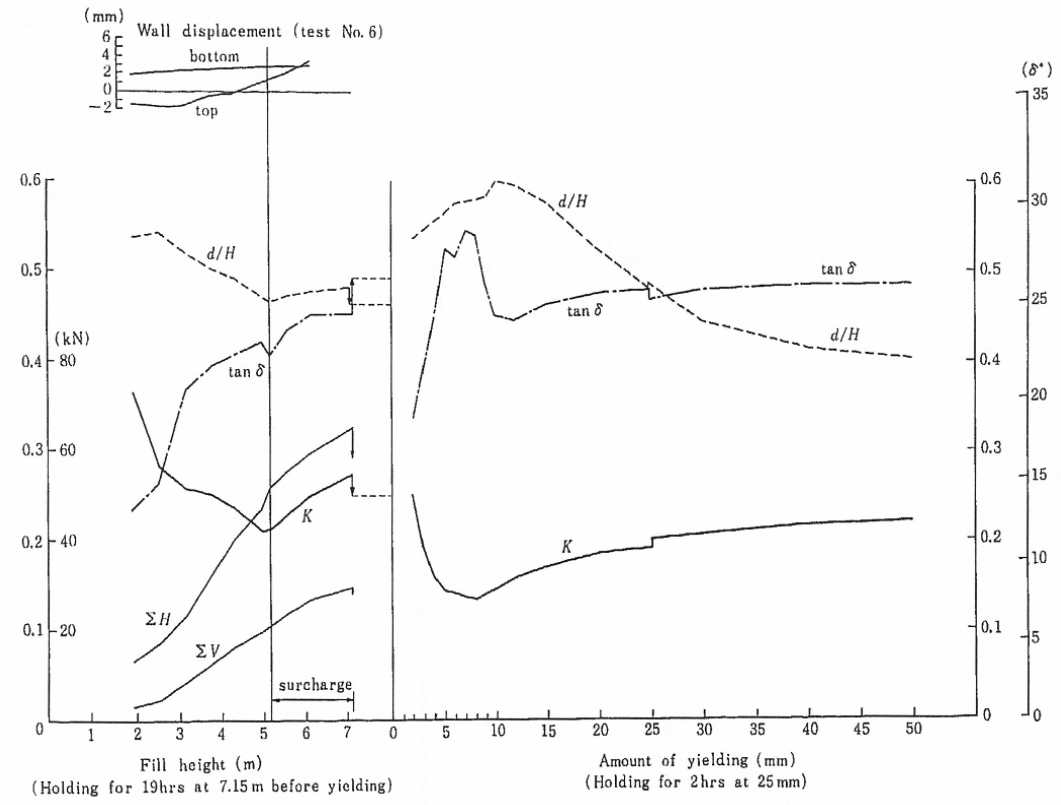

Figure 2.43 Coefficient of earth pressure at rest during the test (dense sand) (Fukuoka et al., 1977)

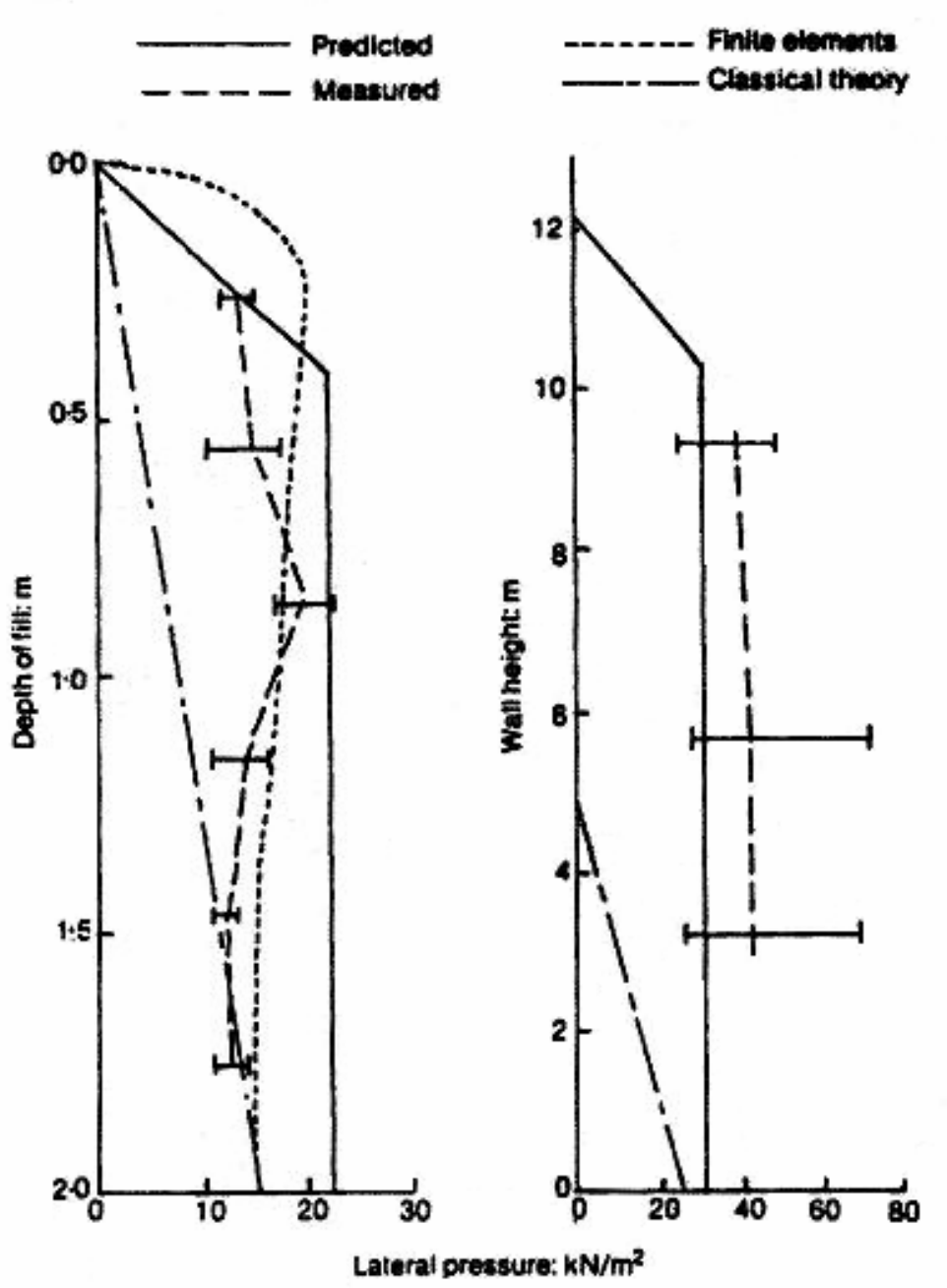

Figure 2.44 Comparison of predicted and observed lateral earth pressures (Ingold, 1979a)

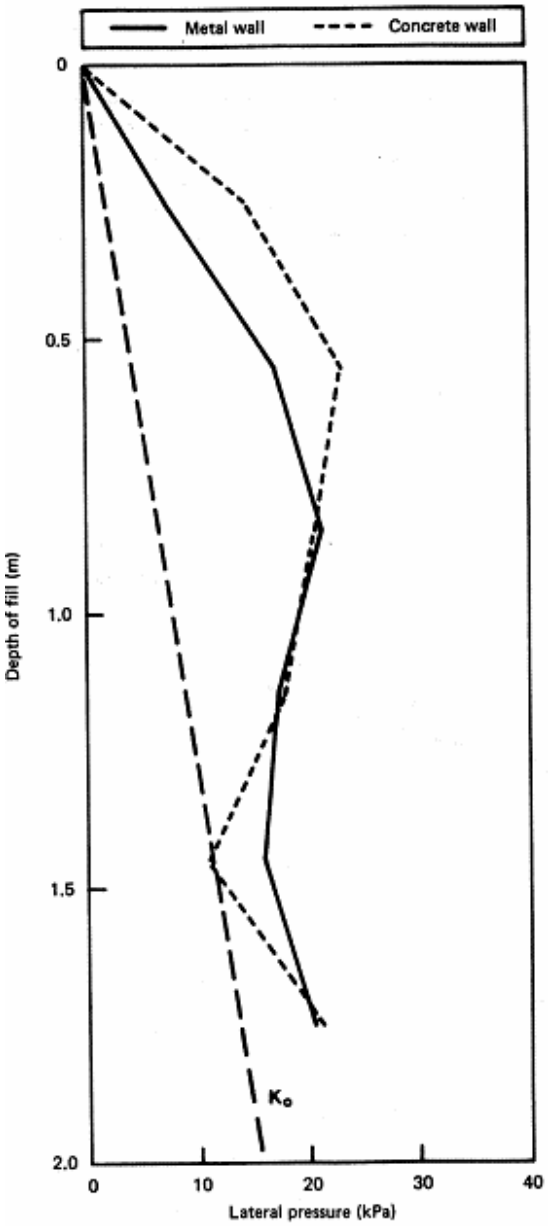

Figure 2.45 Wall pressure due to compaction of silty clay (Carder et al., 1980)

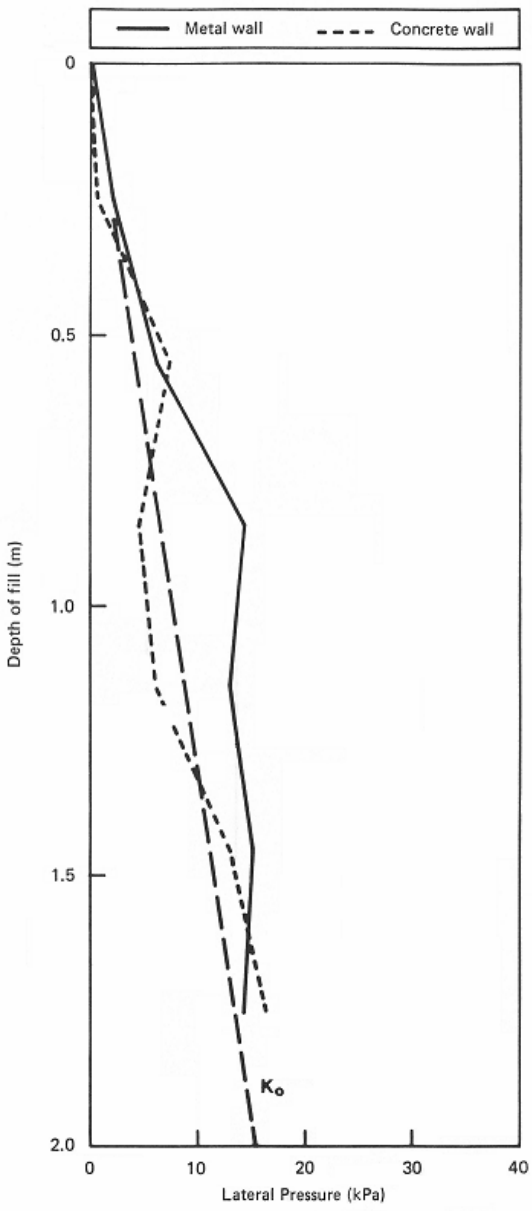

Figure 2.46 Stress distribution four months after completion of compaction (Carder et al., 1980)

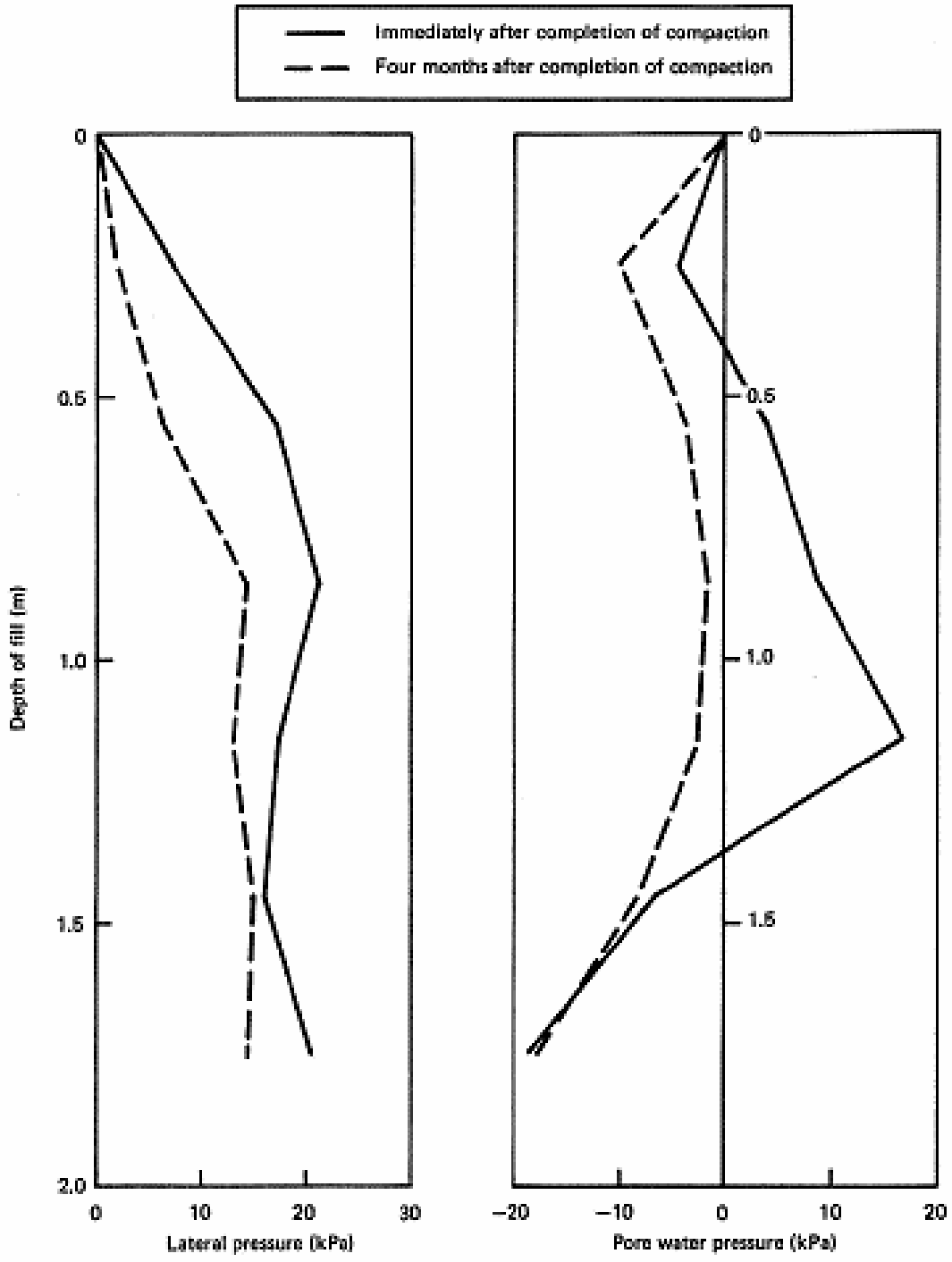

Figure 2.47 Comparison of changes in lateral pressure and pore water pressure for metal wall (Carder et al., 1980)

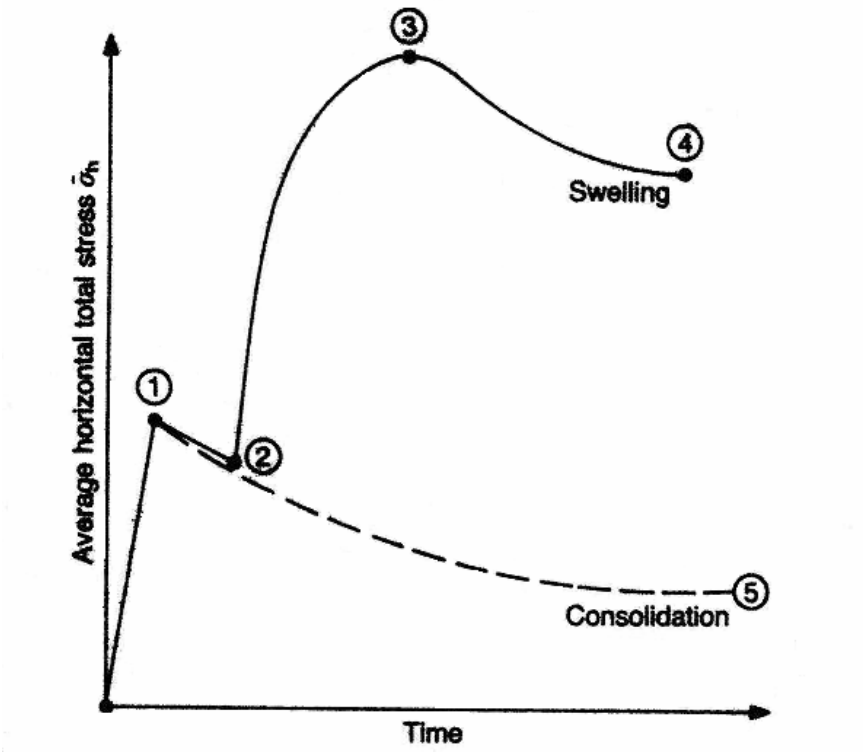

Figure 2.48 Variation in total horizontal stress in cohesive backfills (Clayton et al., 1991)

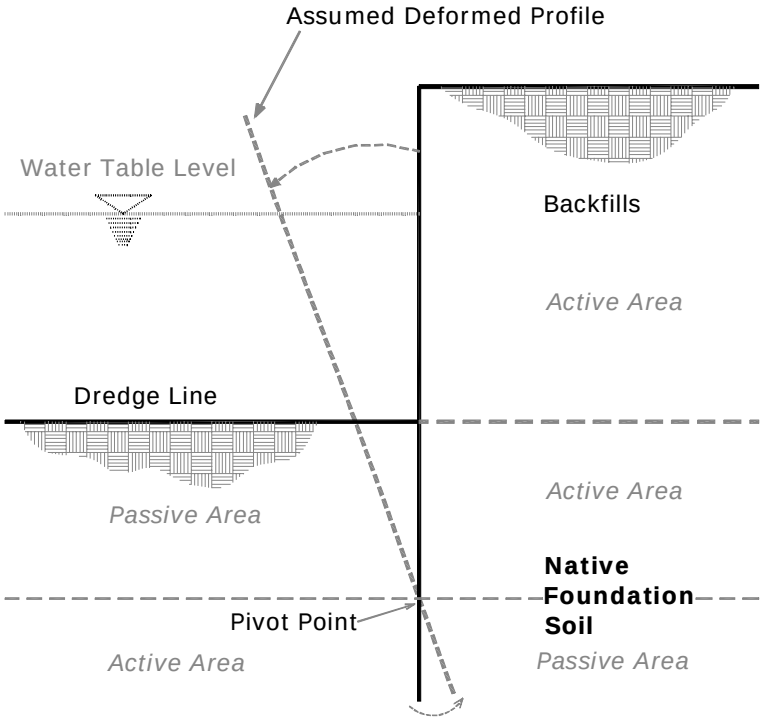

Figure 2.49 Assumed deformation profile of sheet pile (Clayton and Milititsky, 1983)

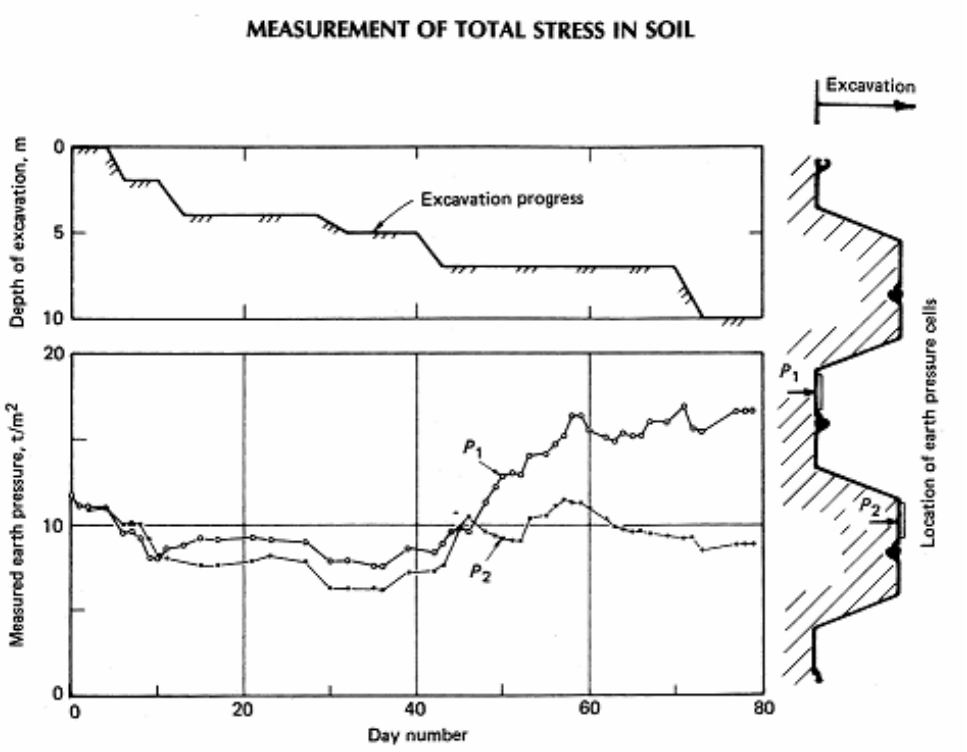

Figure 2.50 Variation in measured earth pressure on the corrugated surface of a sheet pile wall (DiBiagio, 1977)

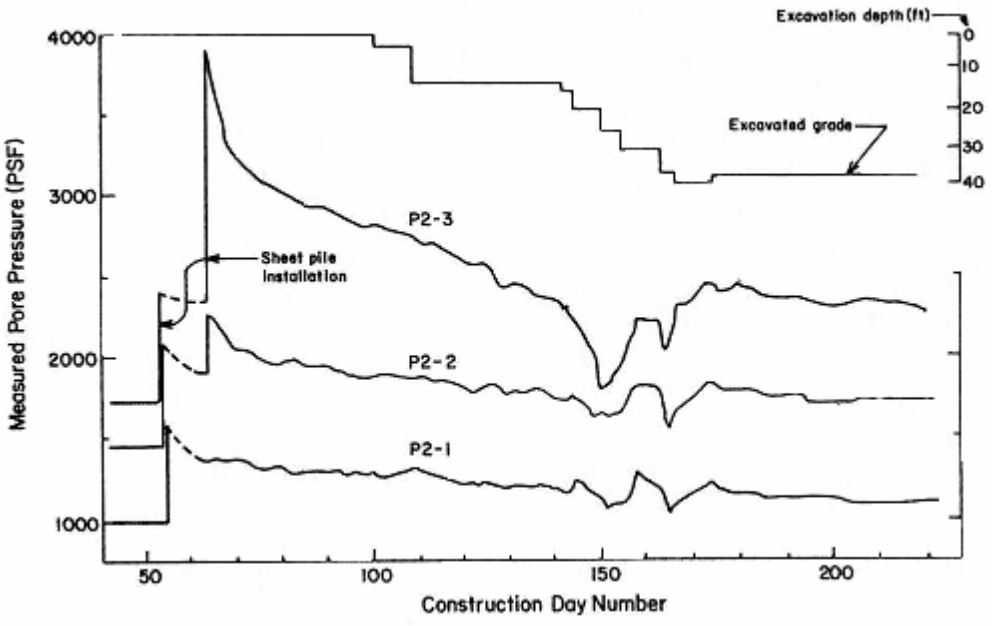

Figure 2.51 Pore water pressures from piezometer group 2 (Finno, 1989)

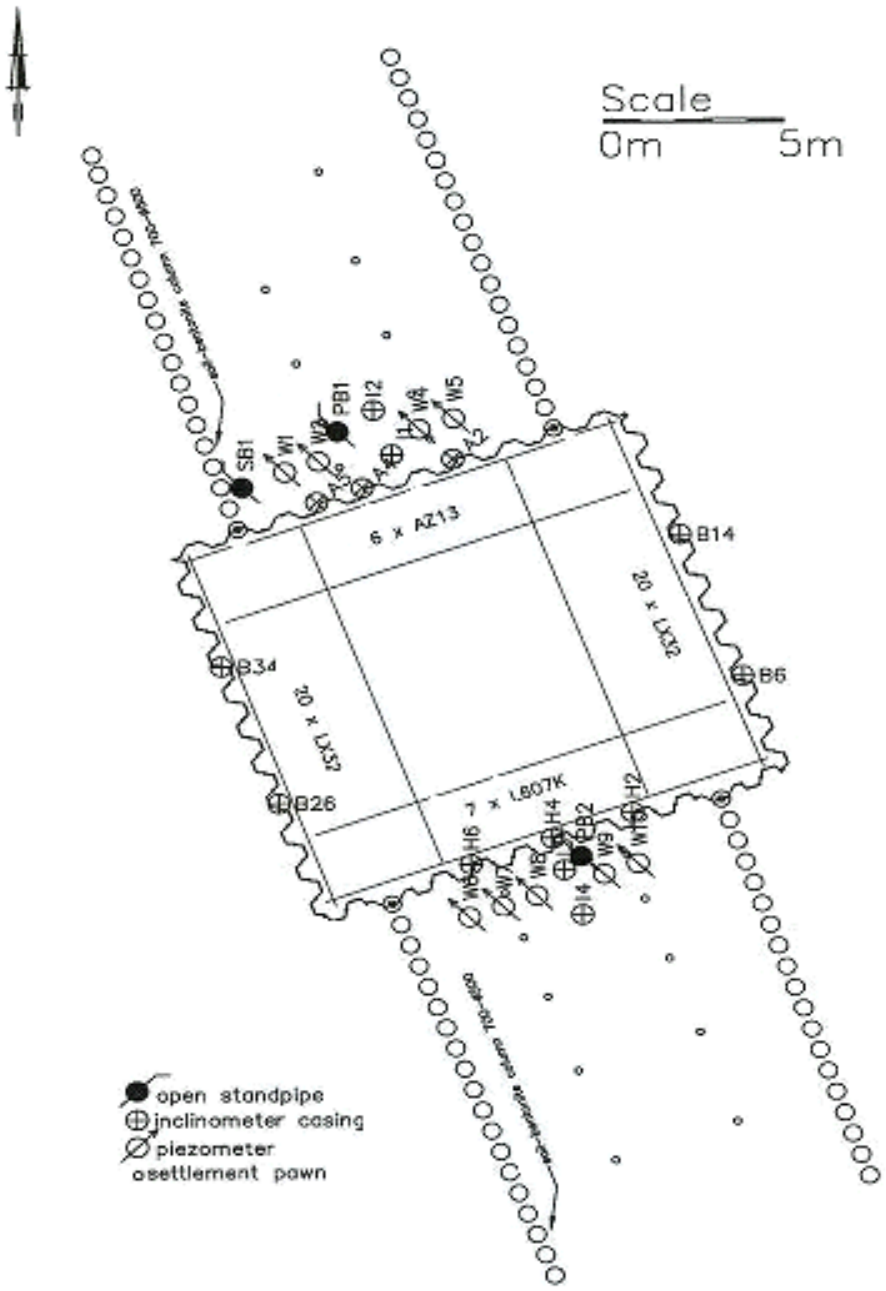

Figure 2.52 Layout of the Rotterdam sheet pile wall field test including all the measurement devices (Kort and Van Tol, 1999)

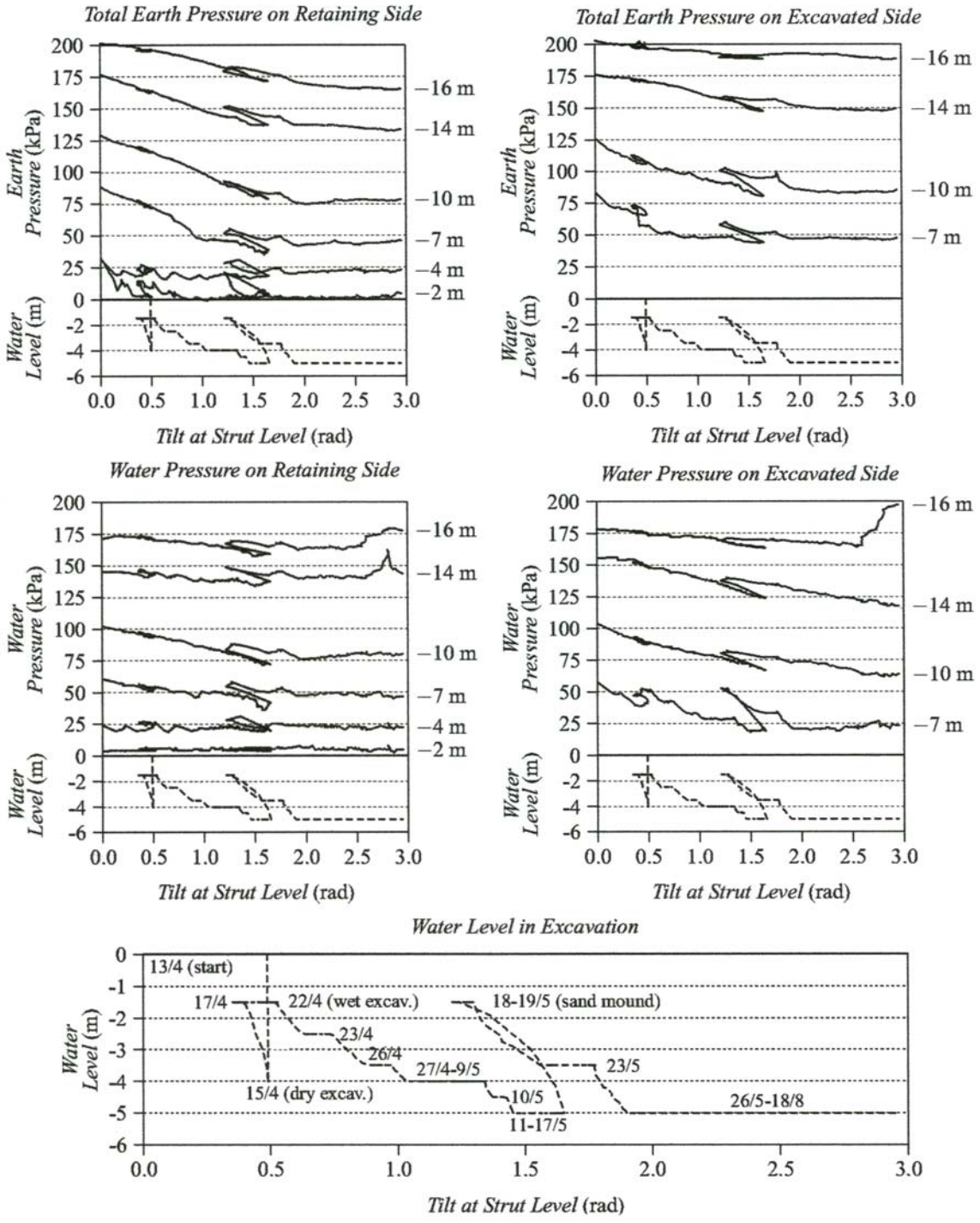

Figure2.53 Change of earth and water pressure at different excavation levels, as a function of the tilt at strut level (Kort et al., 2000)

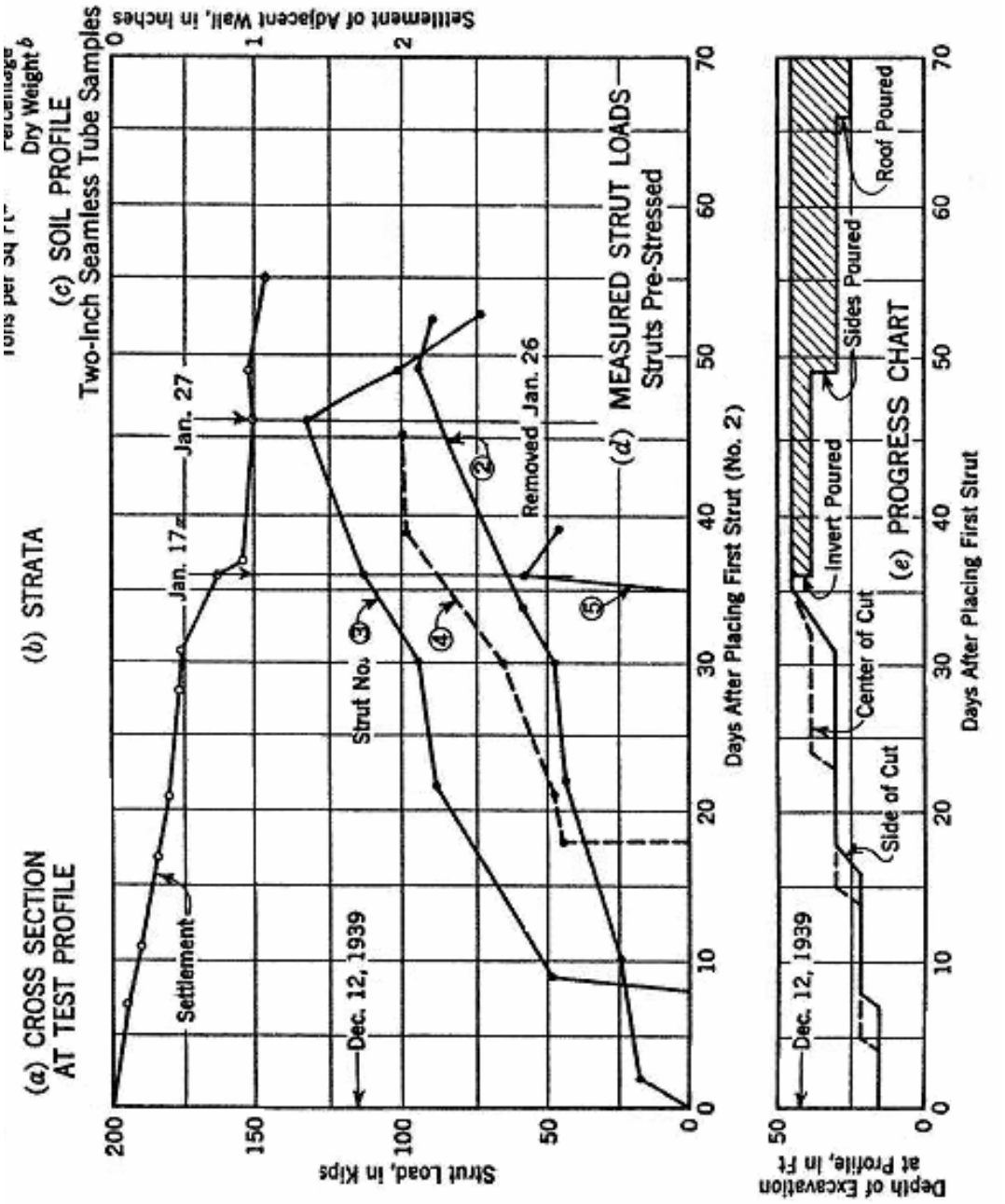

Figure 2.54 Strut load in open cut, contract S-4B (Peck, 2002

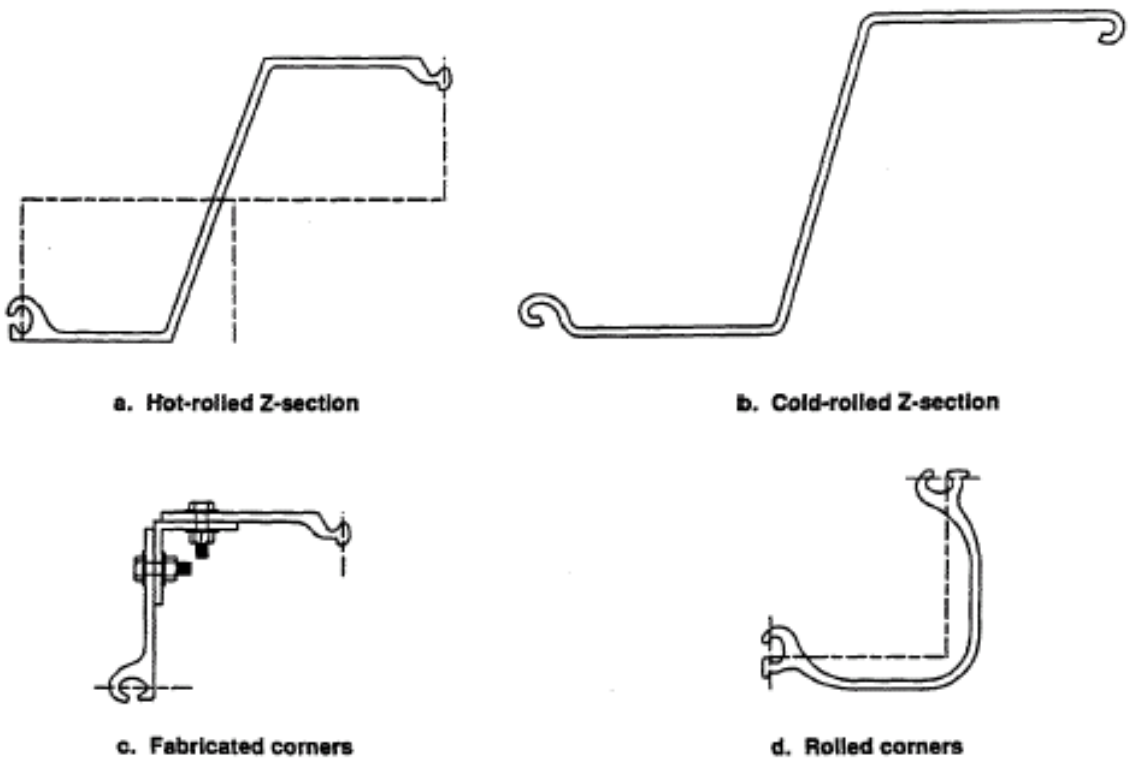

Figure 2.55 The configuration of heavy-gauge steel sheet pile (website of Atlantic Sheet Pile, Inc.)

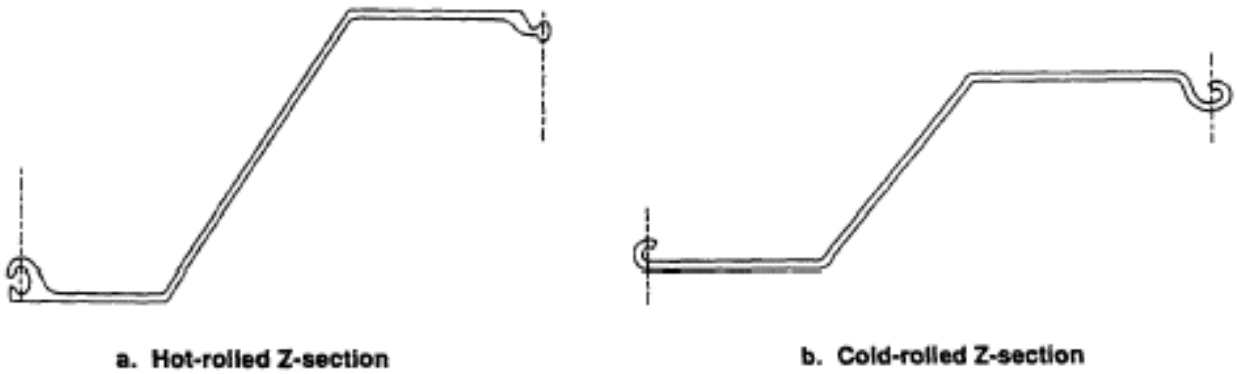

Figure 2.56 Configuration of typical light gauge steel sheet pile (website of Atlantic Sheet Pile, Inc.)

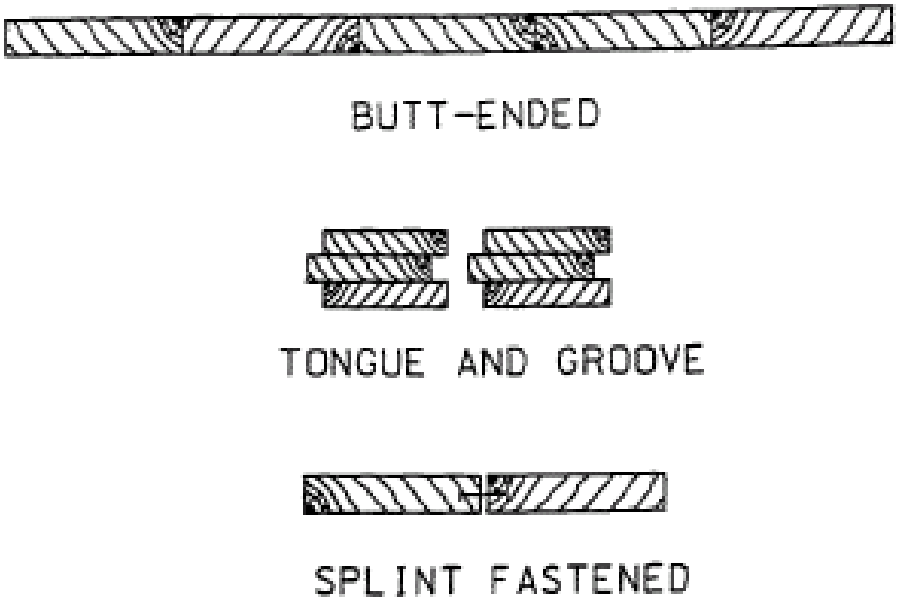

Figure 2.57 Typical wooden pile sections (website of Hercules Machinery Corporation)

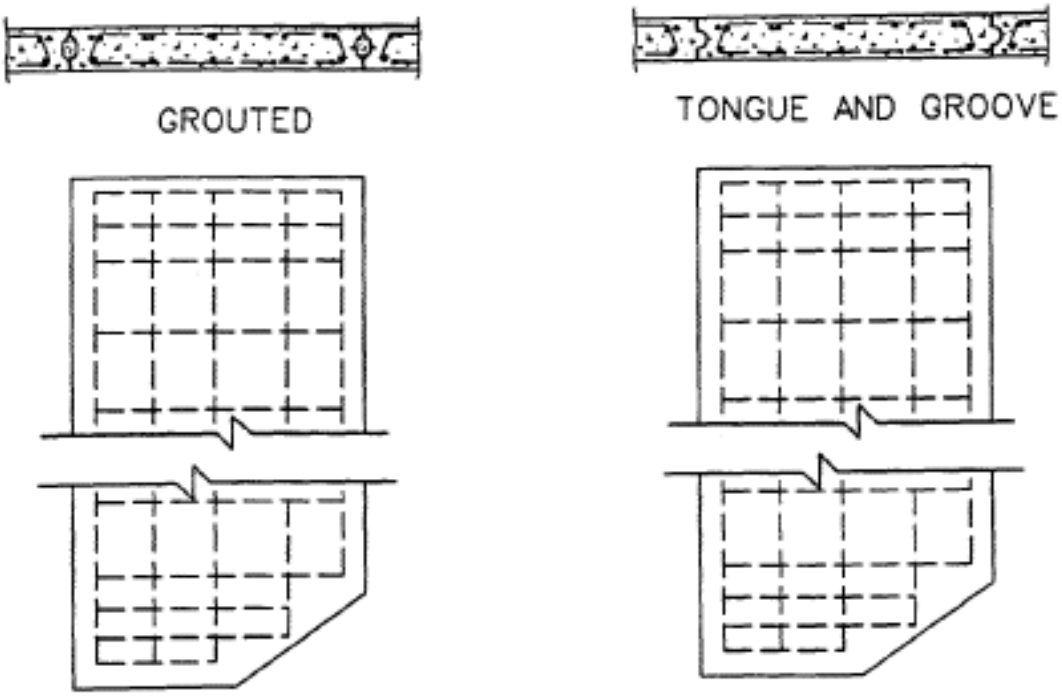

Figure 2.58 Typical cross sections of concrete piles (website of Hercules Machinery Corporation)

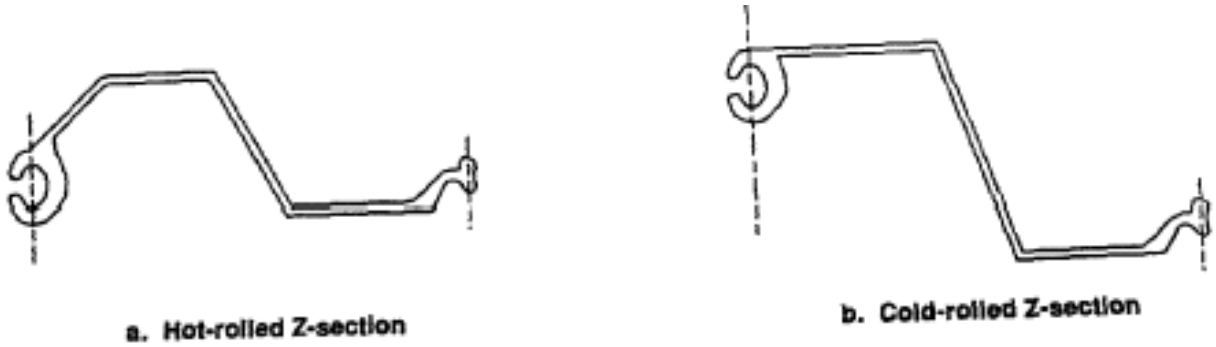

Figure 2.9 Typical sections of light-gauge aluminum sheet piles (website of Atlantic Sheet Pile, Inc.)

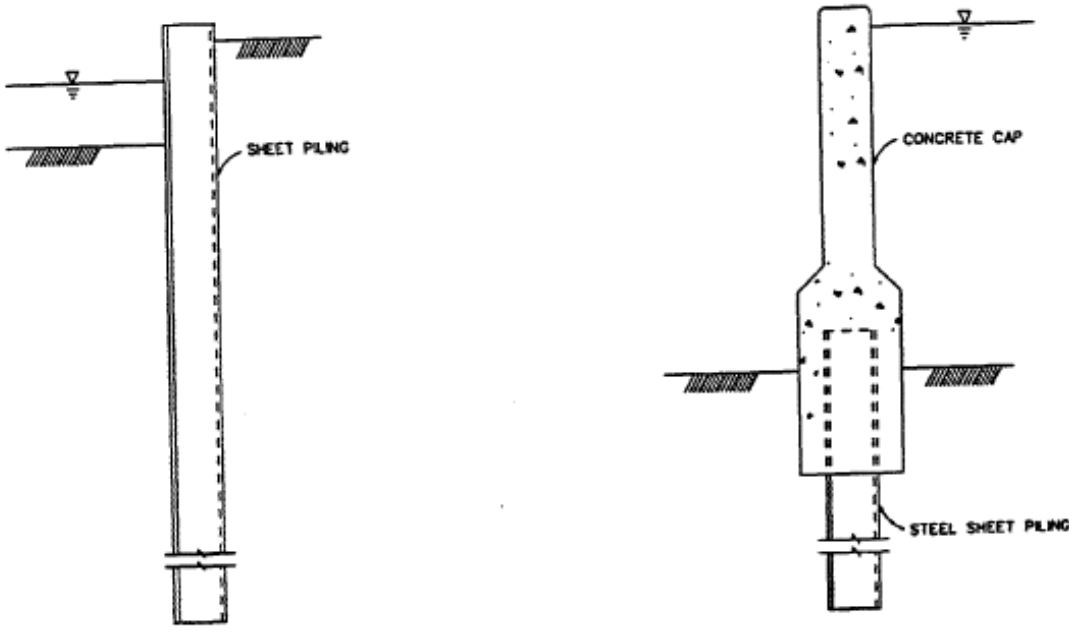

Figure 2.60 Typical cantilever walls (website of Atlantic Sheet Pile, Inc.)

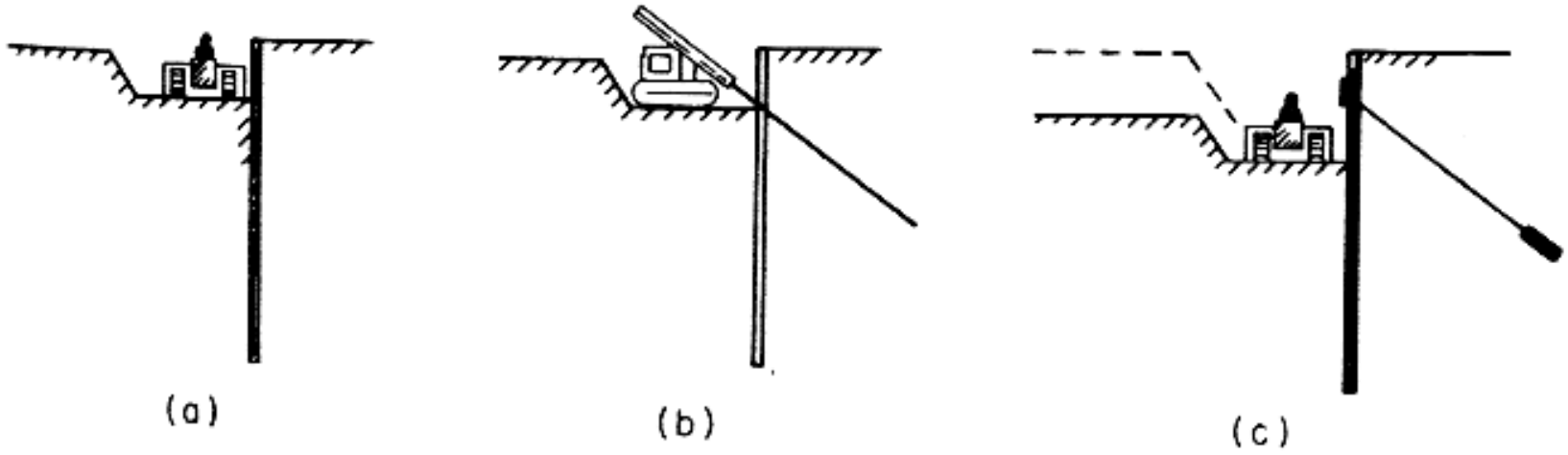

(a) Trench excavation after wall installed
(b) First anchor row installed
(c) Trench excavation for next row and excavation lowered

Figure 2.61 General procedures for anchor installation for support of a sheet pile wall (website of Atlantic Sheet Pile, Inc.)

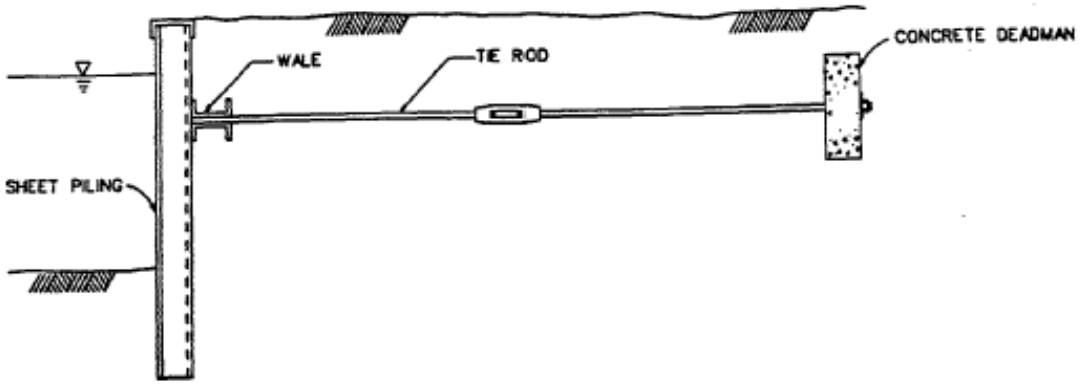

a. Tie rods and dead man

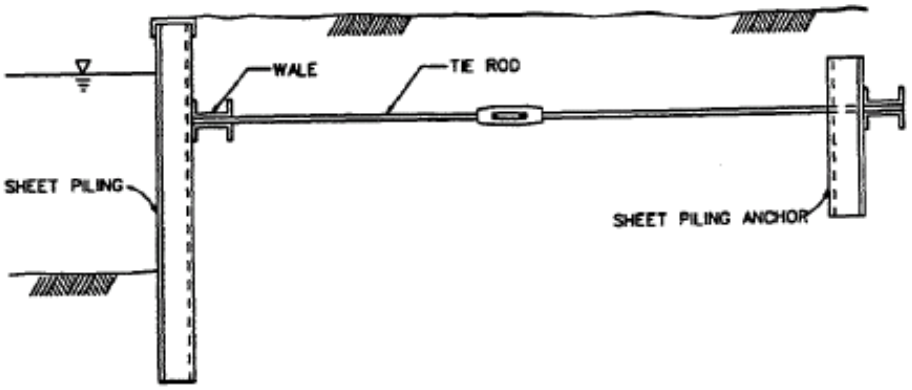

b. Tie rods and anchor wall

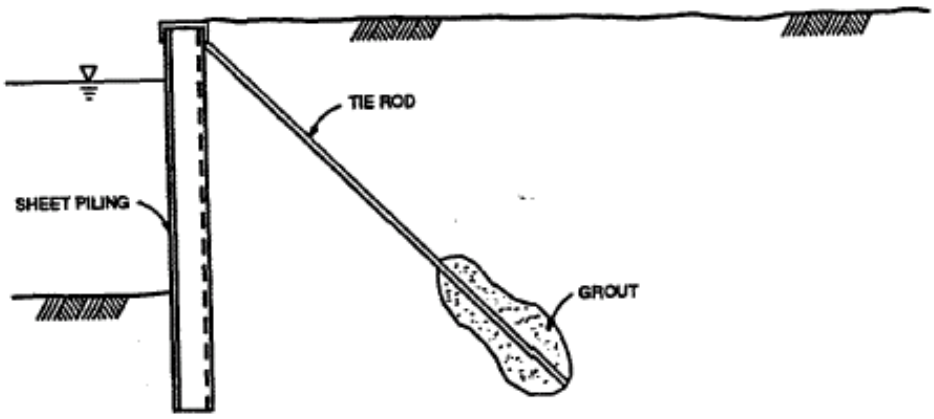

c. Tiebacks with grout anchor

Figure 2.62 Typical configurations of anchor walls (continued) (website of Hercules Machinery Corporation)

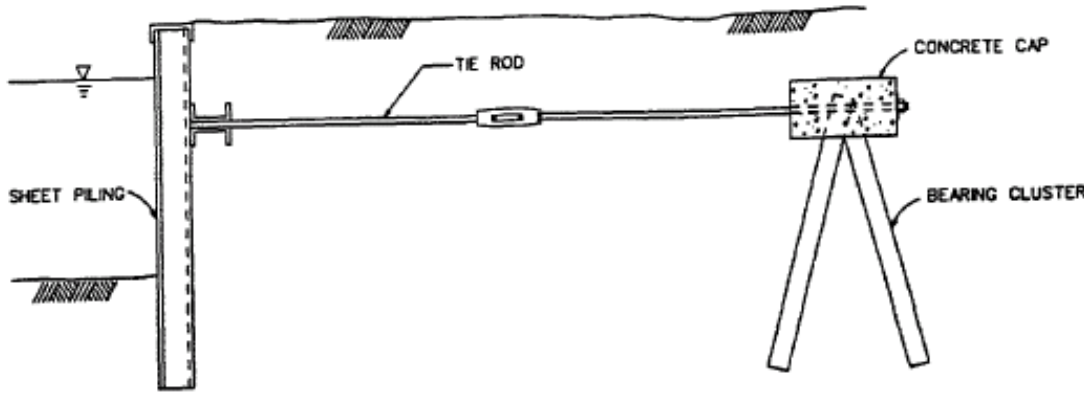

d. Tie rods and A-frame

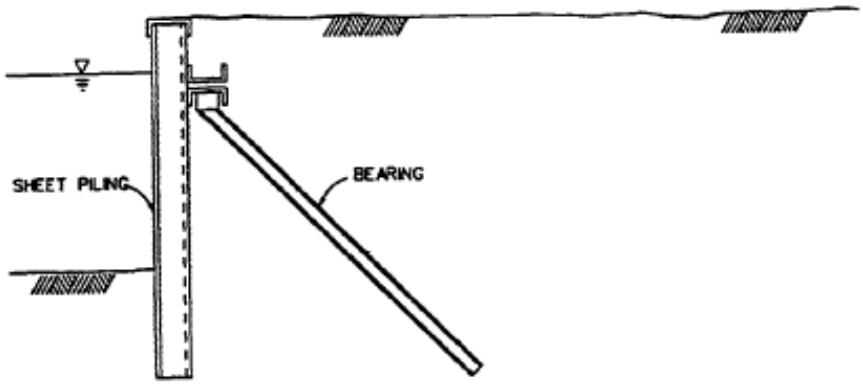

e. Steel H-pile tension anchors

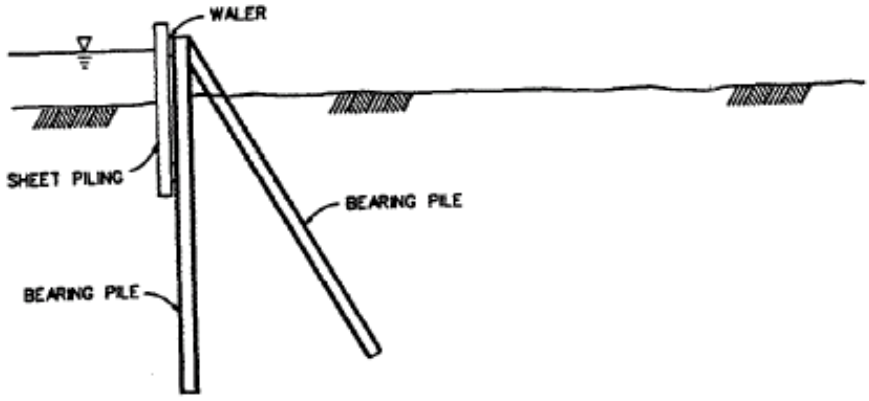

f. Steel H-pile anchors

Figure 2.62 Typical configurations of anchor walls (concluded) (website of Hercules Machinery Corporation)

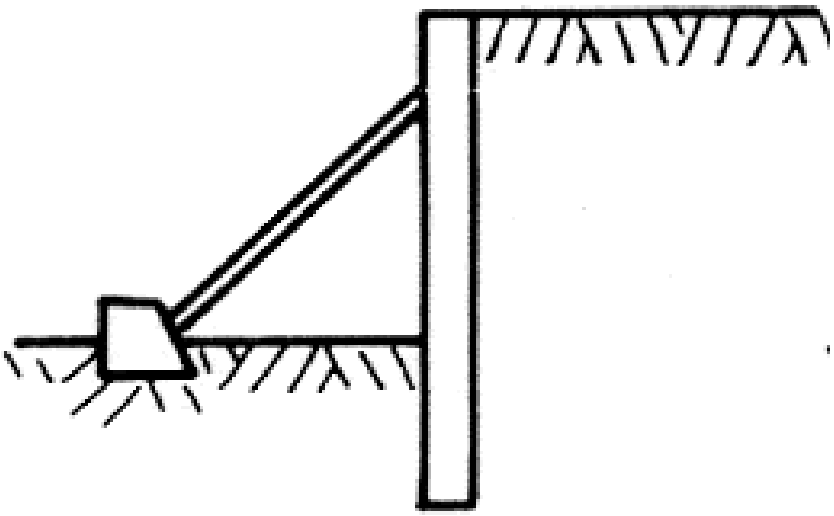

Figure 2.63 Typical configuration of propped sheet pile wall (website of Hercules Machinery Corporation)

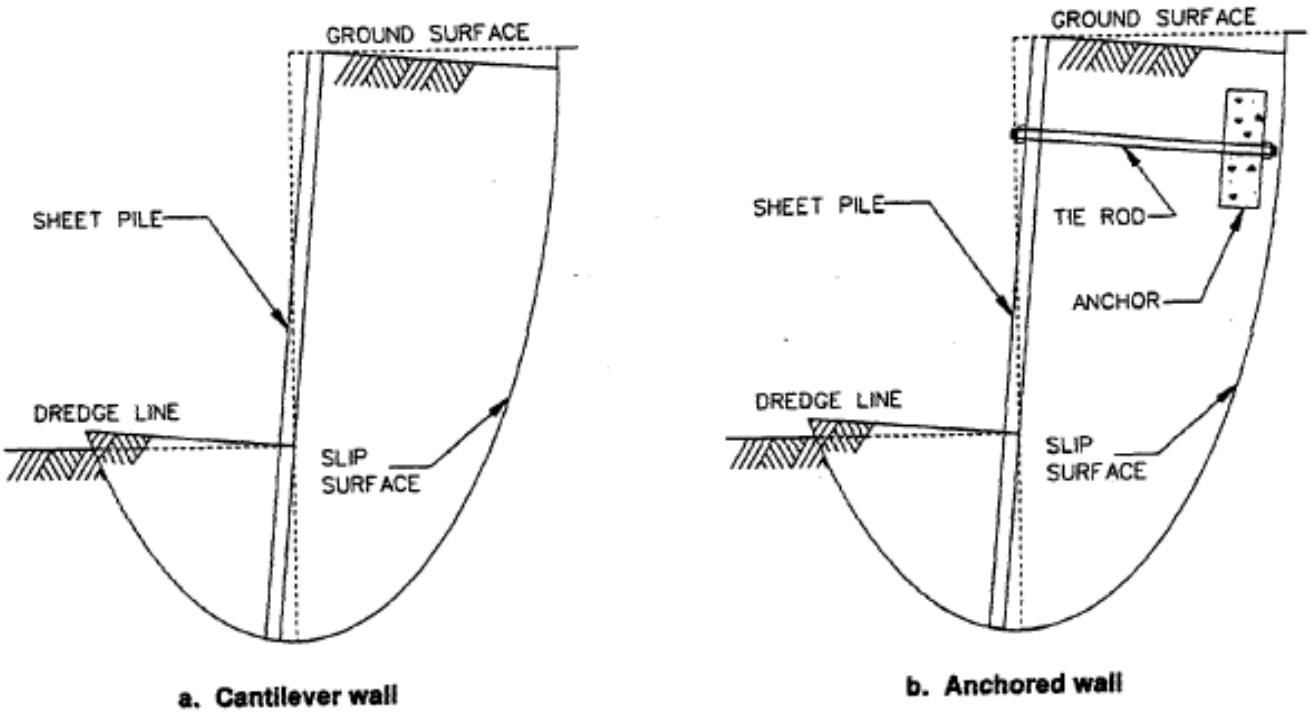

Figure 2.64 Deep-seated failure models (website of Hercules Machinery Corporation)

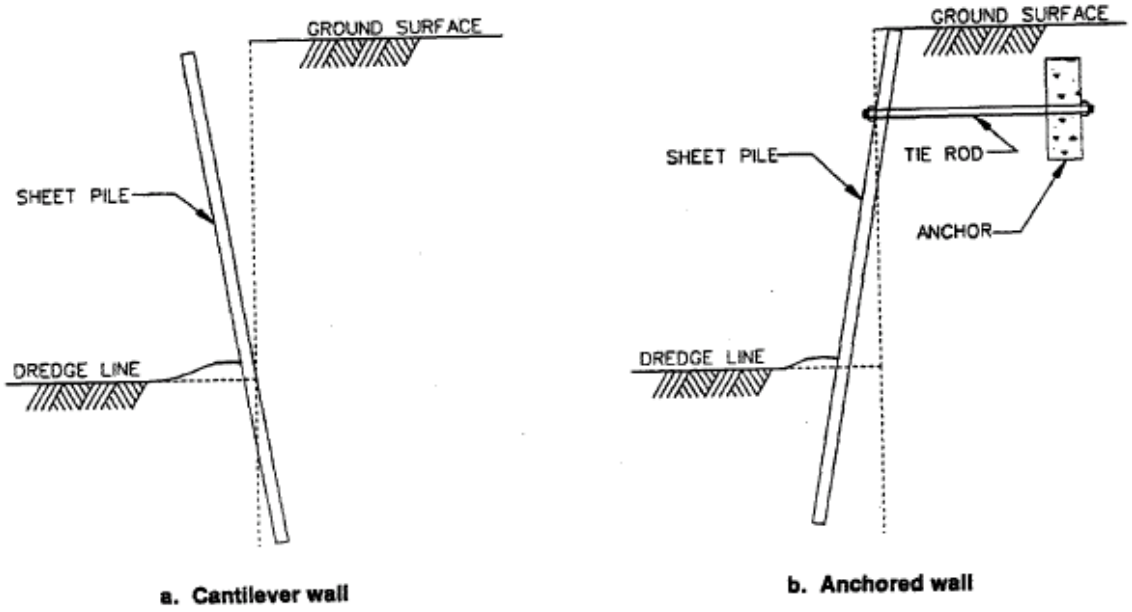

Figure 2.65 Rotational failure modes due to inadequate penetration (website of Hercules Machinery Corporation)

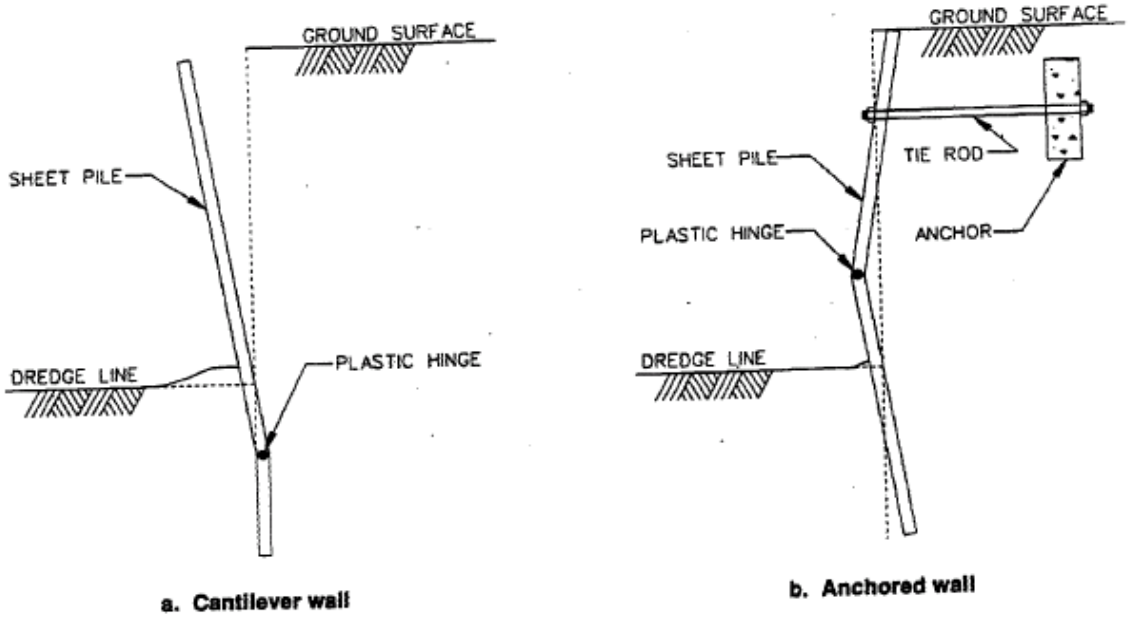

Figure 2.66 Flexural failure of a sheet pile wall (website of Hercules Machinery Corporation)

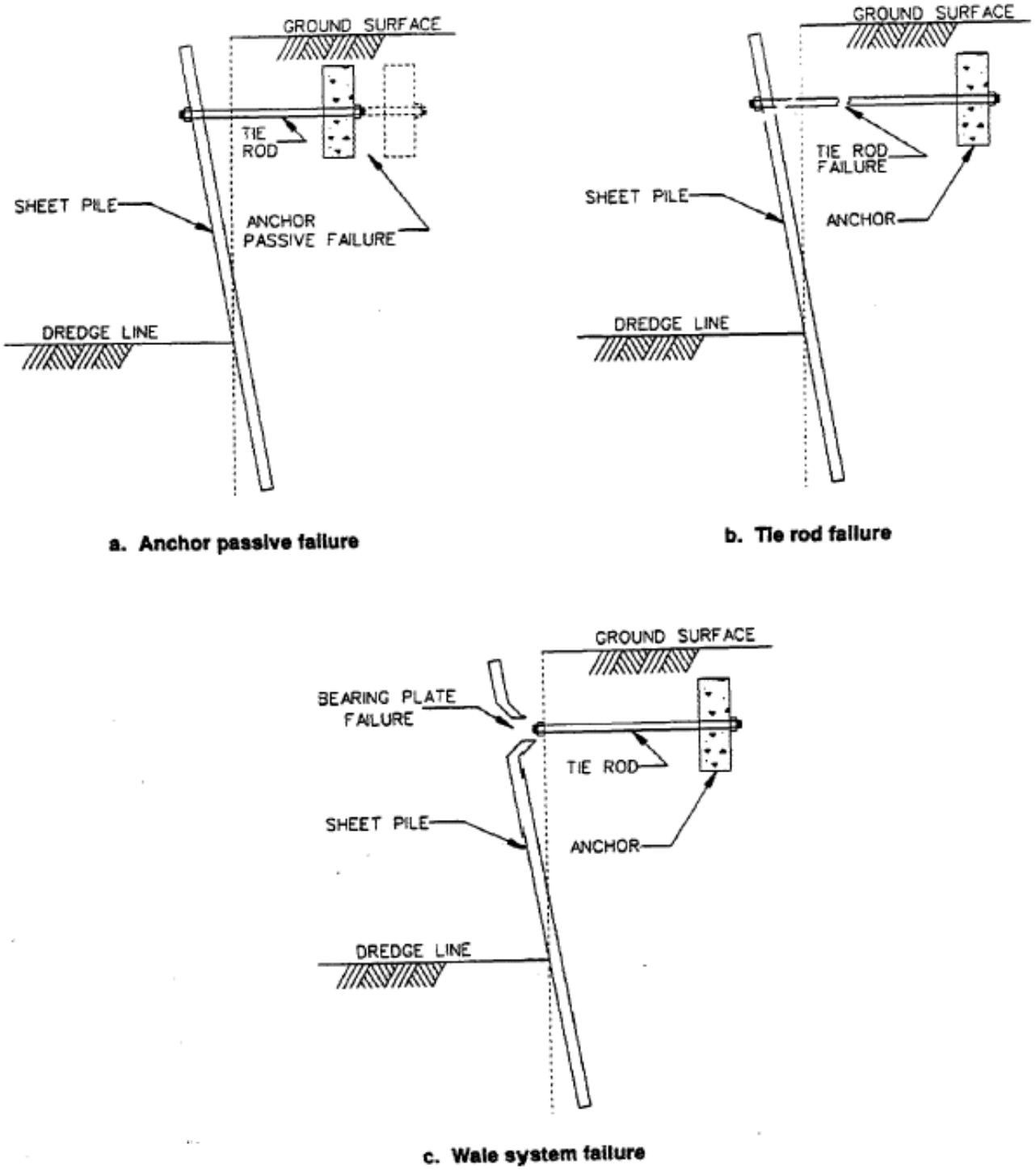

Figure 2.67 Anchorage failure of sheet pile wall (website of Hercules Machinery Corporation)

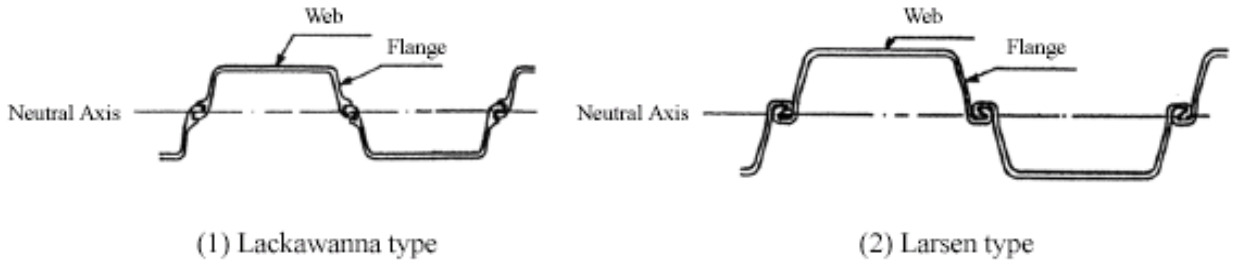

Figure 2.68 Typical configuration of U-shaped steel sheet pile sections (website of Atlantic Sheet Pile, Inc.)

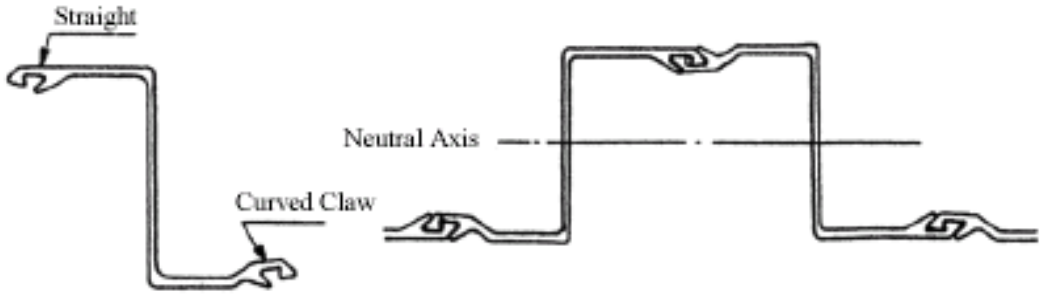

Figure 2.69 Typical configuration of Z-shaped steel sheet pile sections (website of Atlantic Sheet Pile, Inc.)

Figure 2.70 Typical configuration of straight or flat shaped steel sheet pile sections (website of Atlantic Sheet Pile, Inc.)

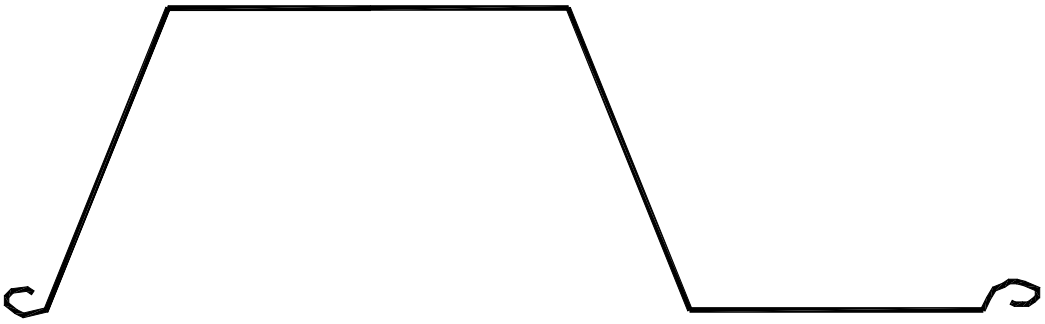

Figure 2.71 Typical section configuration of arch shaped and lightweight gauge steel sheet pile (website of Atlantic Sheet Pile, Inc.)

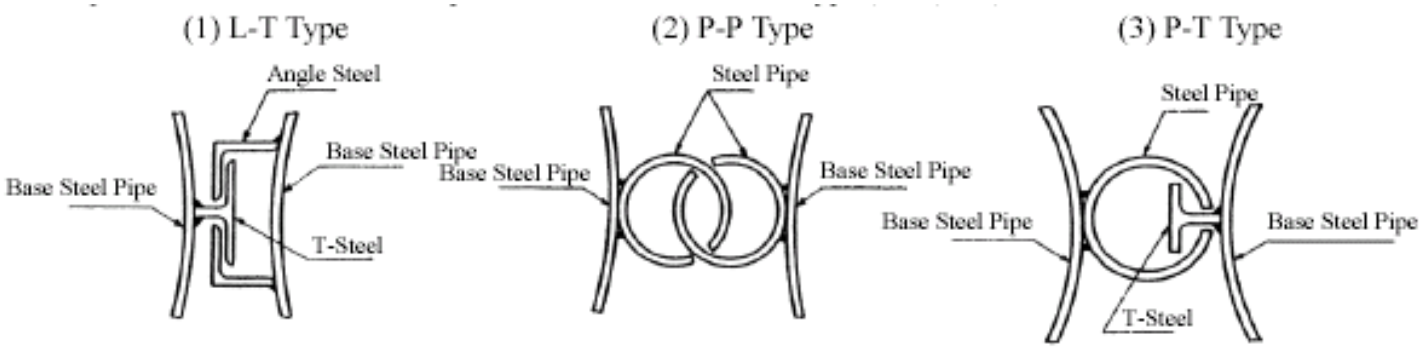

Figure 2.72 Typical cross-section configurations of steel pipe sheet pile (website of Atlantic Sheet Pile, Inc.)

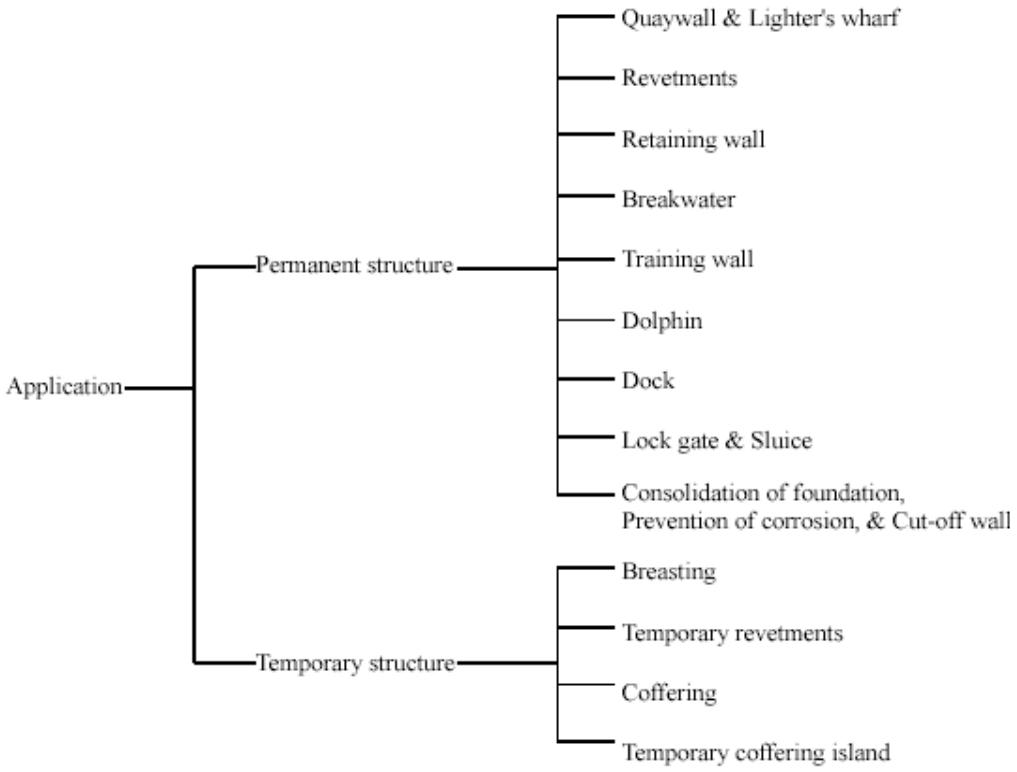

Figure 2.73 Classification of steel sheet pile according to application ((website of Atlantic Sheet Pile, Inc.)

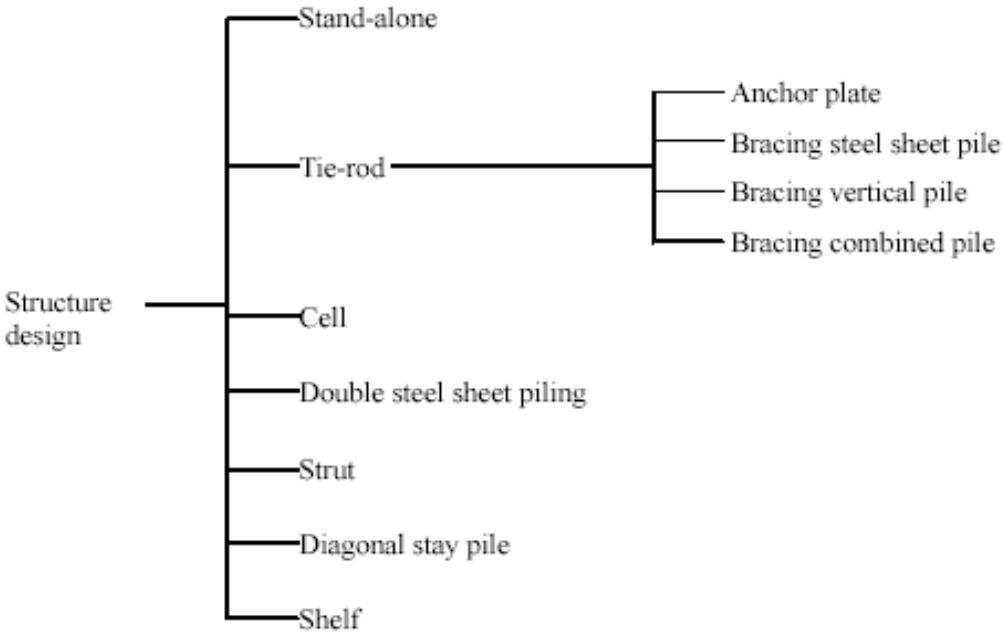

Figure 2.74 Classification of steel sheet pile press fit according to structure design (website of Atlantic Sheet Pile, Inc.)

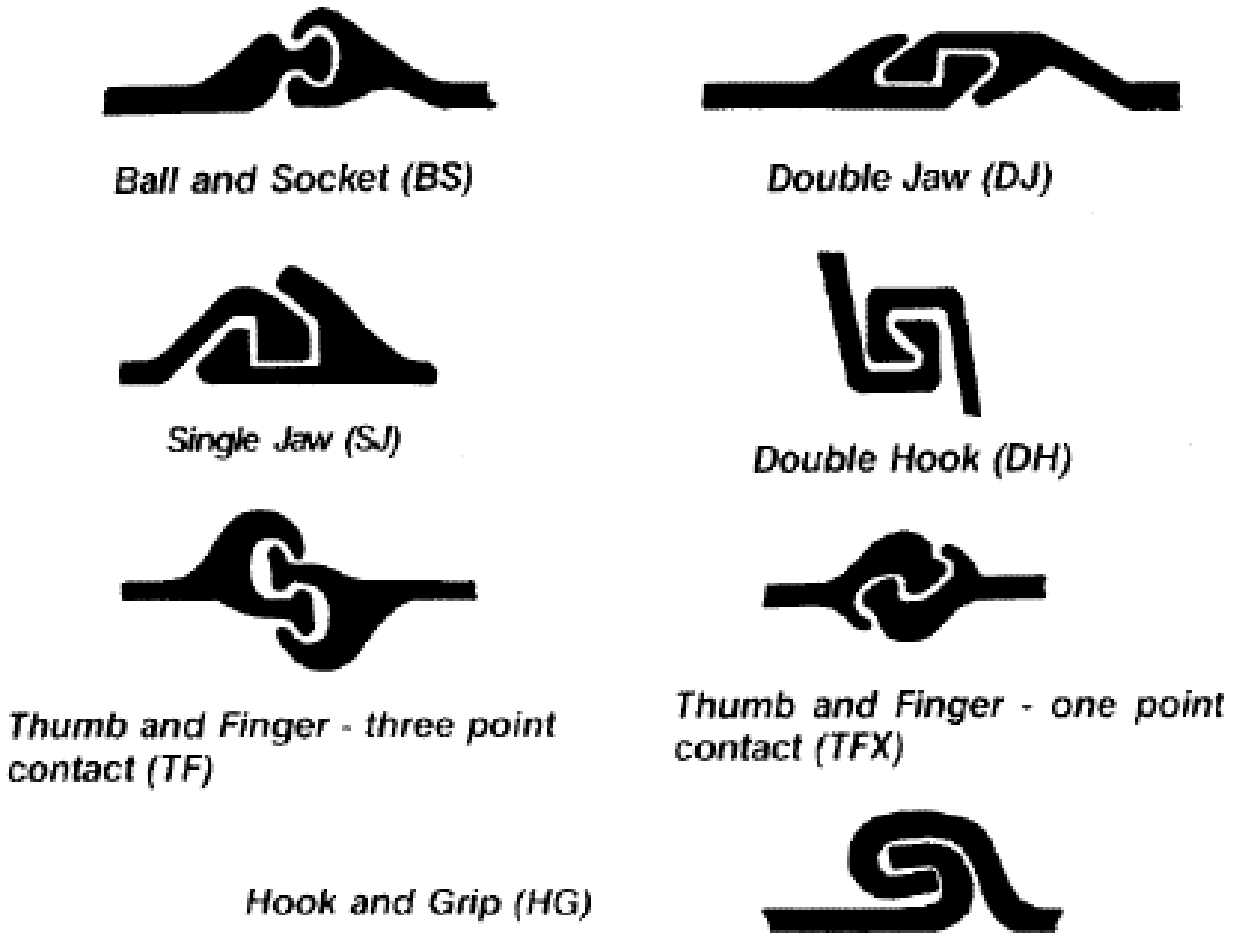

Figure 2.75 Typical configuration of steel sheet pile interlocks (website of Atlantic Sheet Pile, Inc.)

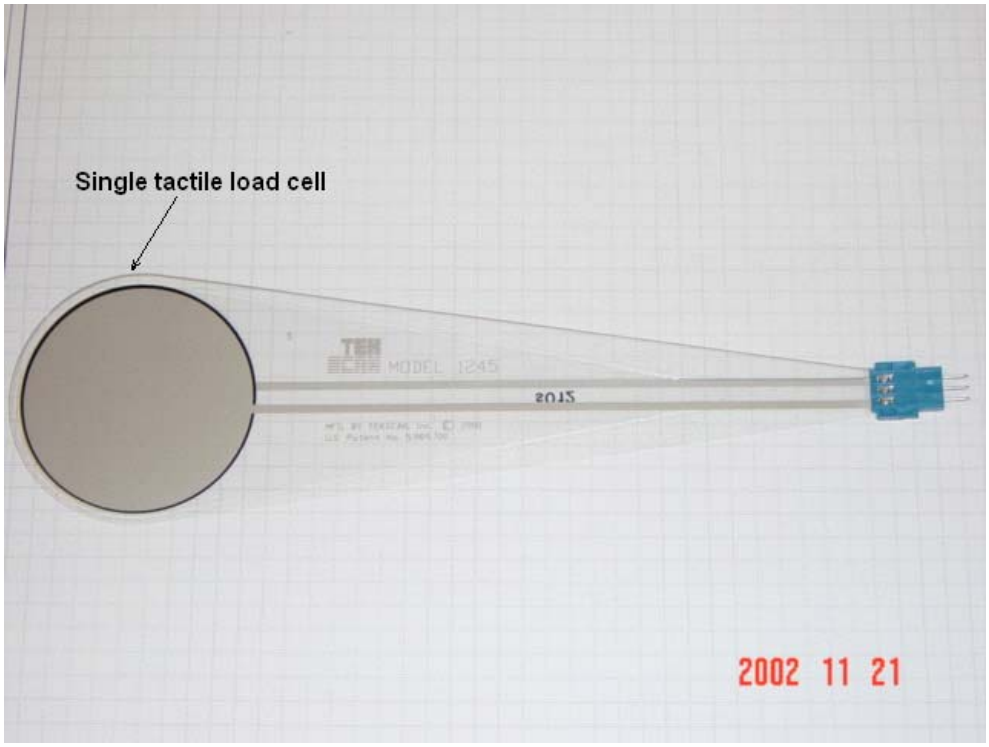

Figure 2.76 The view of single tactile load cell

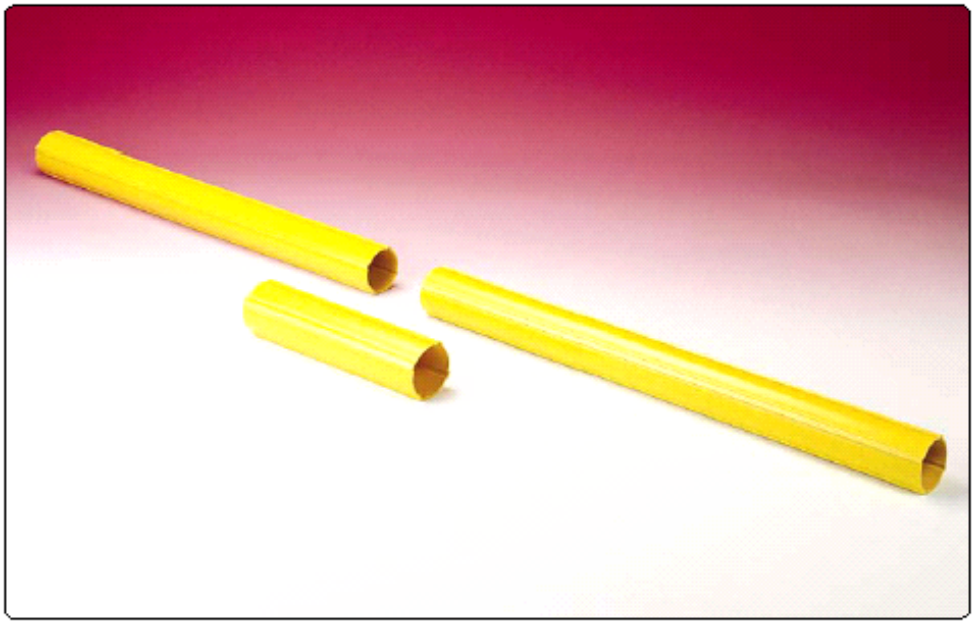

Figure 2.77 Sections of inclinometer casing (website of Geokon, Inc.)

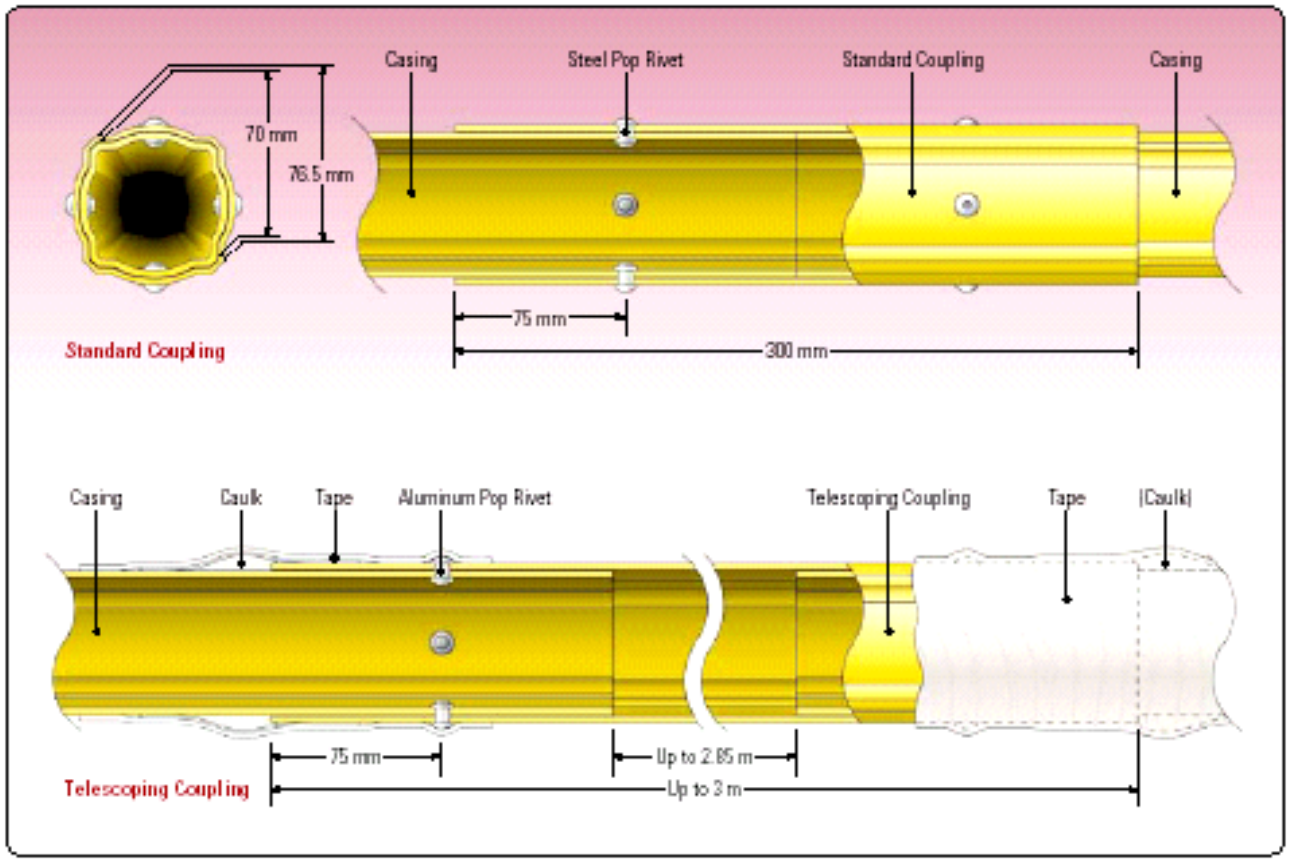

Figure 2.78 The configuration of inclinometer casing and telescoping couplings (website of Geokon, Inc.)

Figure 2.79 The inclinometer system (website of Geokon, Inc.)

Figure 2.80 Inclinometer probe and cable (website of Geokon, Inc.)

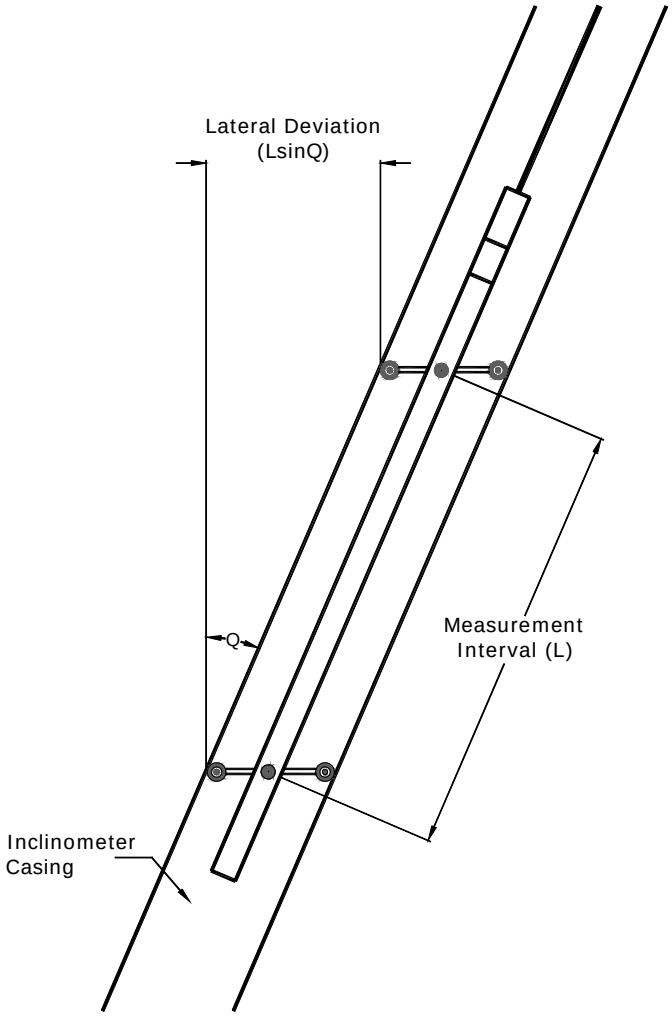

Figure 2.81 Inclinometer probe in casing

Figure 2.82 Model GK-603 vibrating wire readout box (website of Geokon, Inc.)

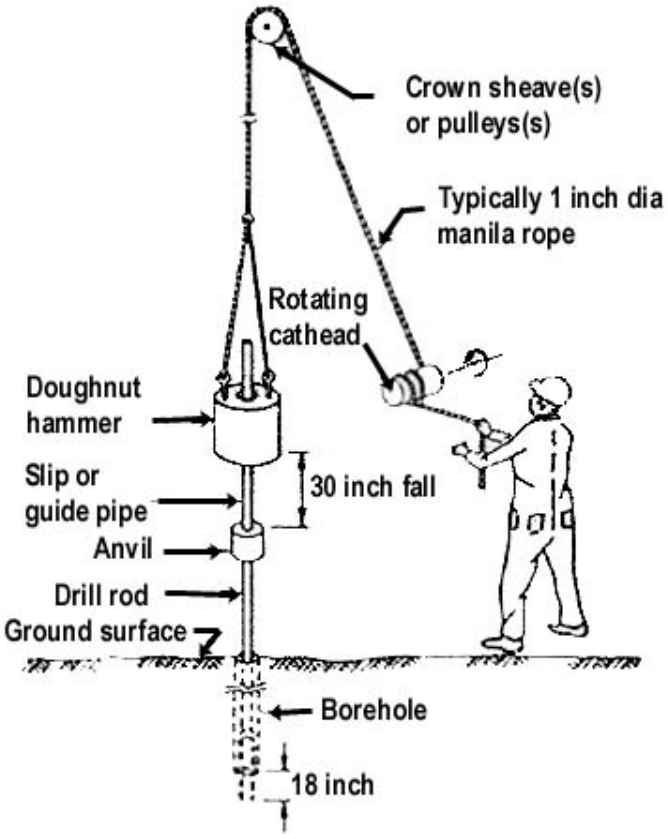

Figure 2.83 Elements of standard penetration test (SPT)
(website of Golden Associate, Inc.)

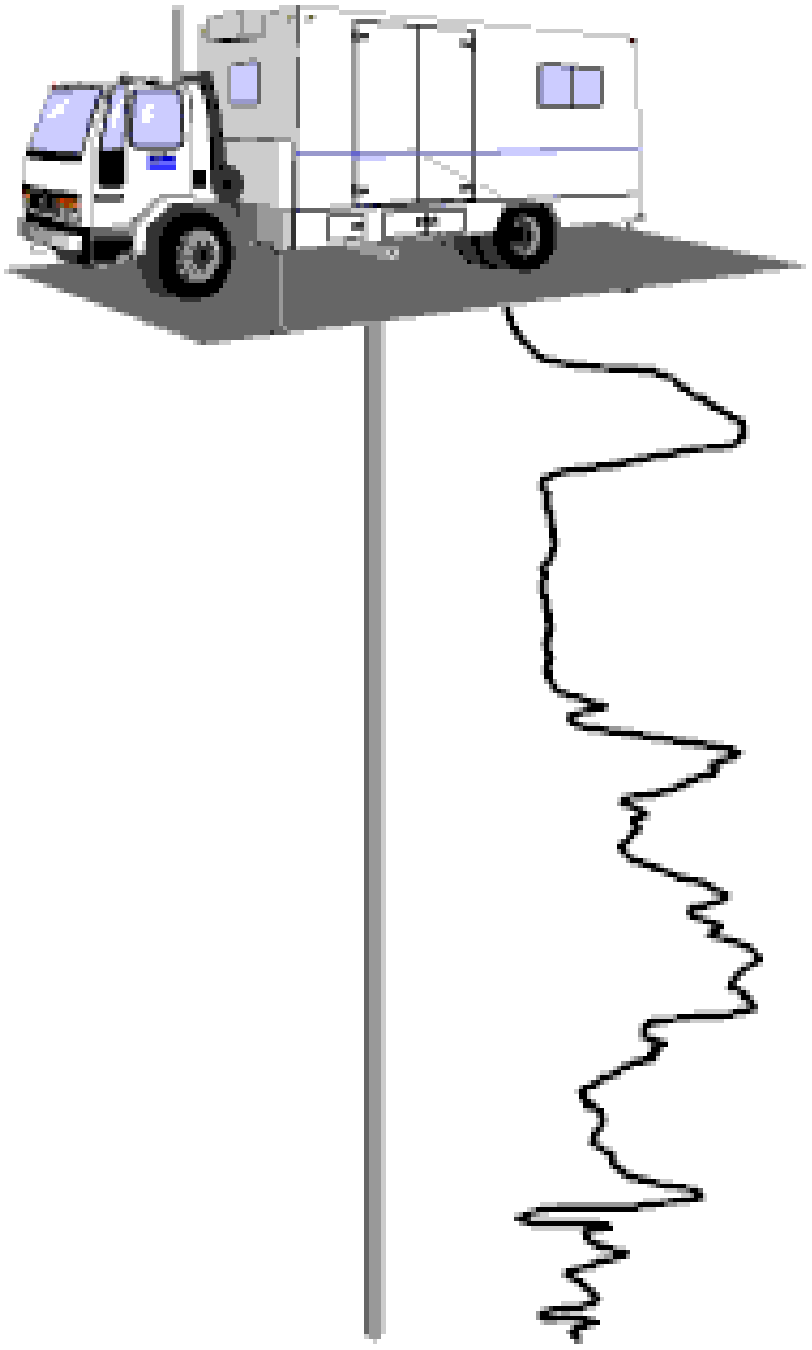

Figure 2.84 Elements of cone penetration test (CPT) (website of Frugo, Inc.)

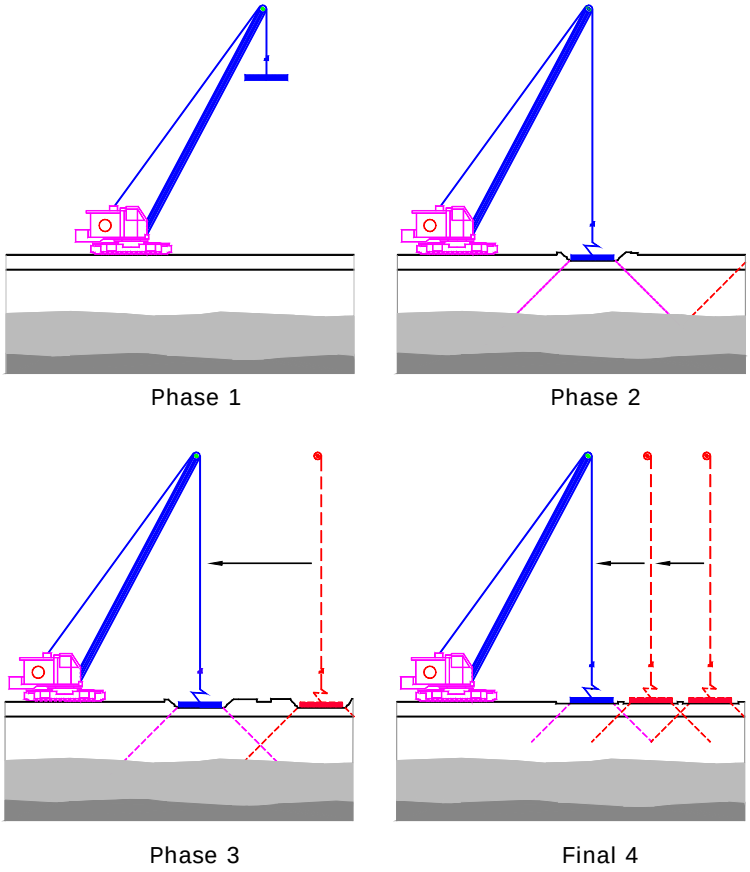

Figure 2.85 Phases in dynamic compaction phases (DDC)

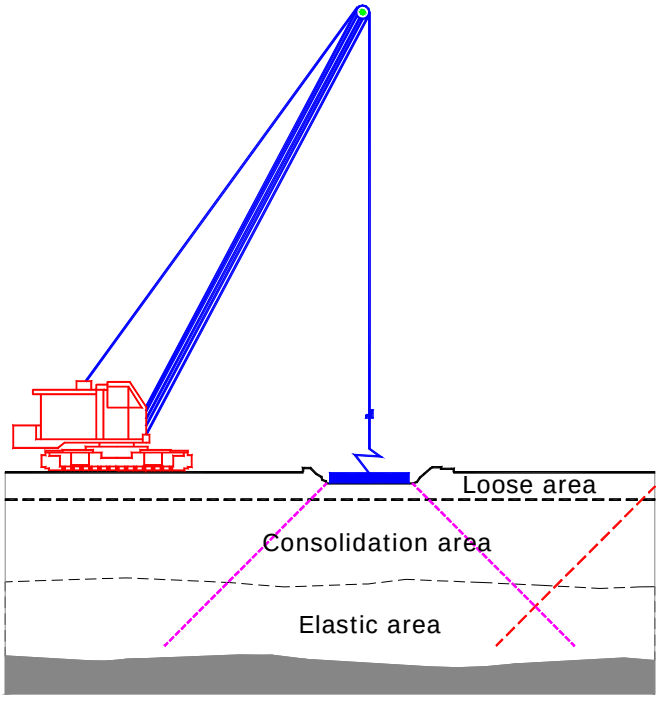

Figure 2.86 Different areas in soils caused by deep dynamic compaction (DDC)

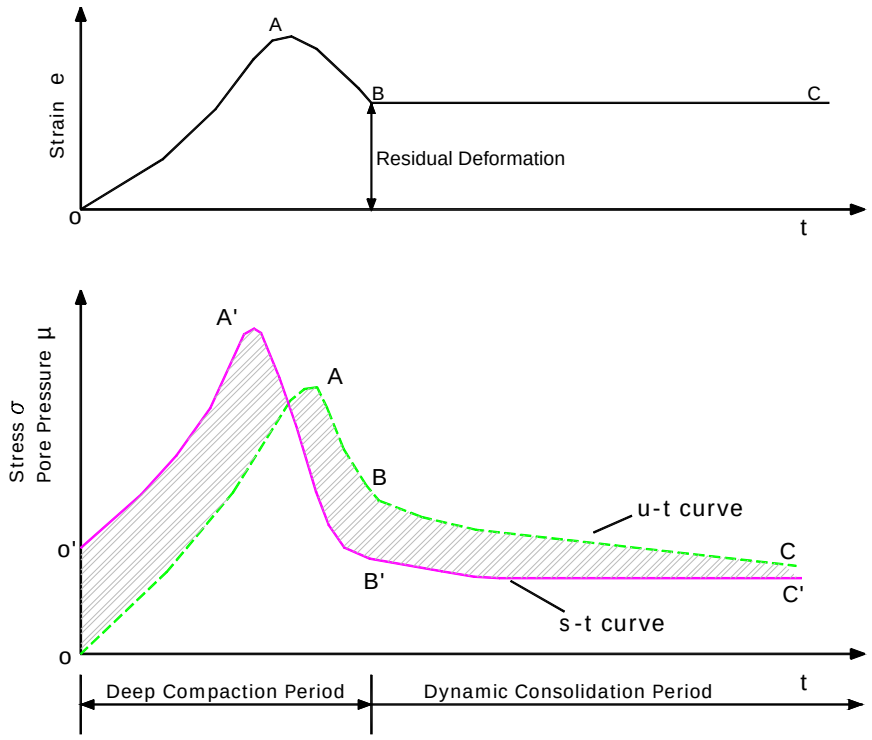

Figure 2.87 The influence of shock wave in soils (redrawn after Ye et al., 1992)

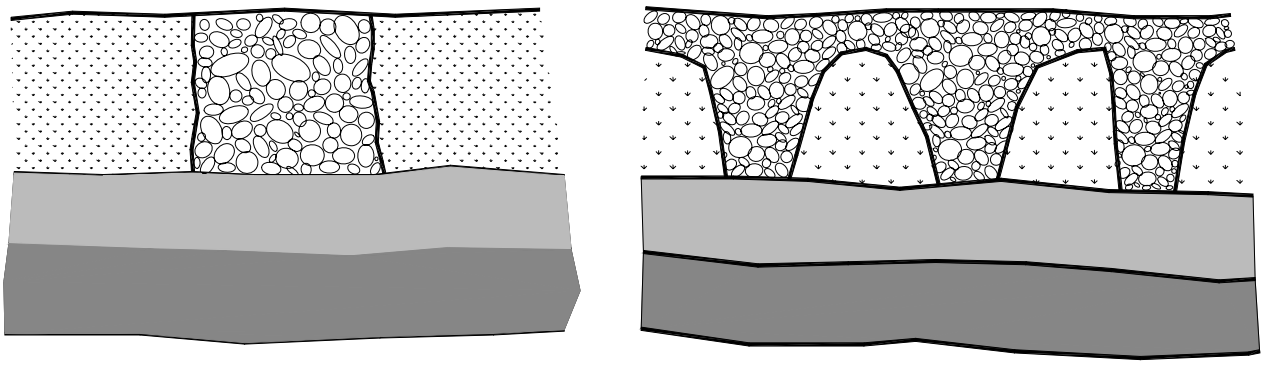

(a) Interal replacement (b) Pile type replacemnet

Figure 2.88 Types of dynamic replacement

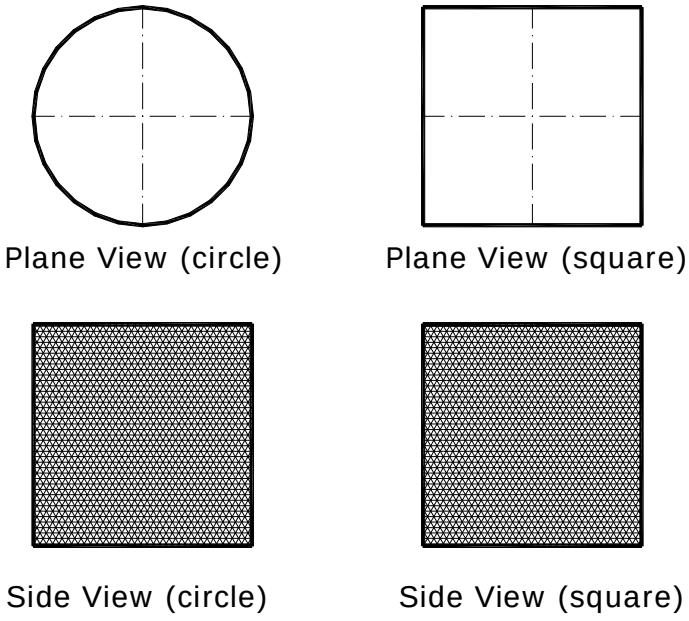

Figure 2.89 Tamper shape (sealed)

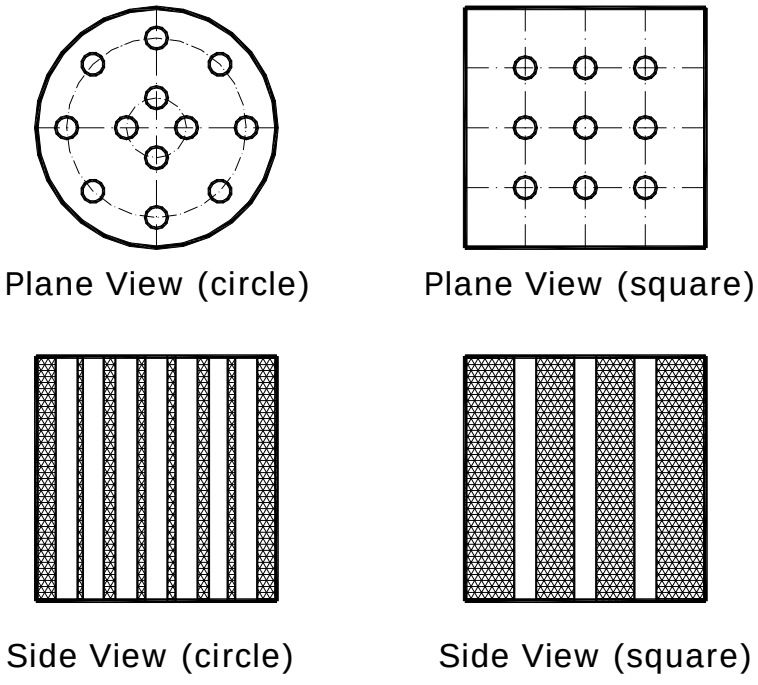

Figure 2.90 Tamper shape (air-void)

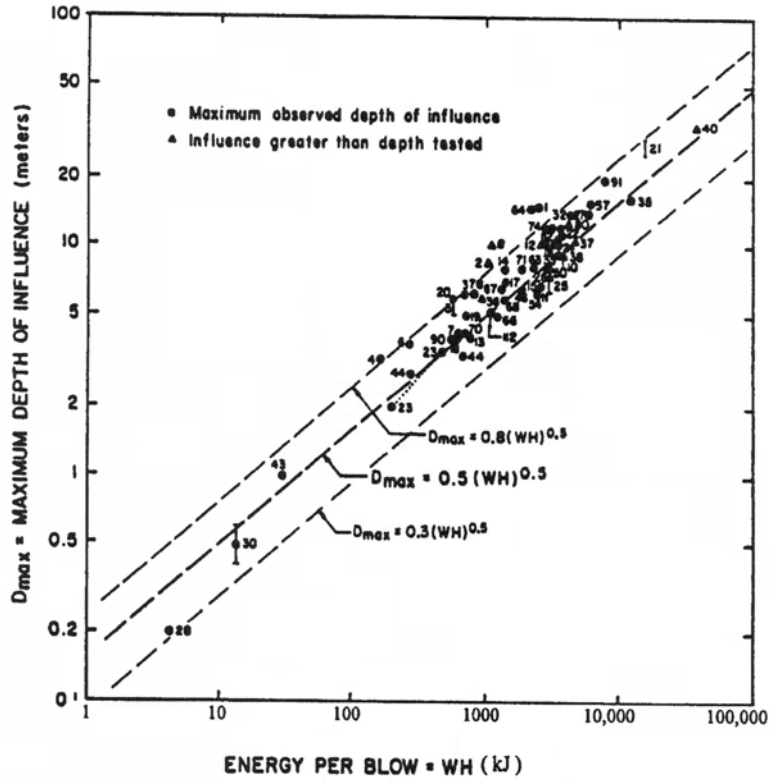

Figure 2.91 Trend between apparent maximum depth of influence and energy per blow (Mayne et al., 1984)

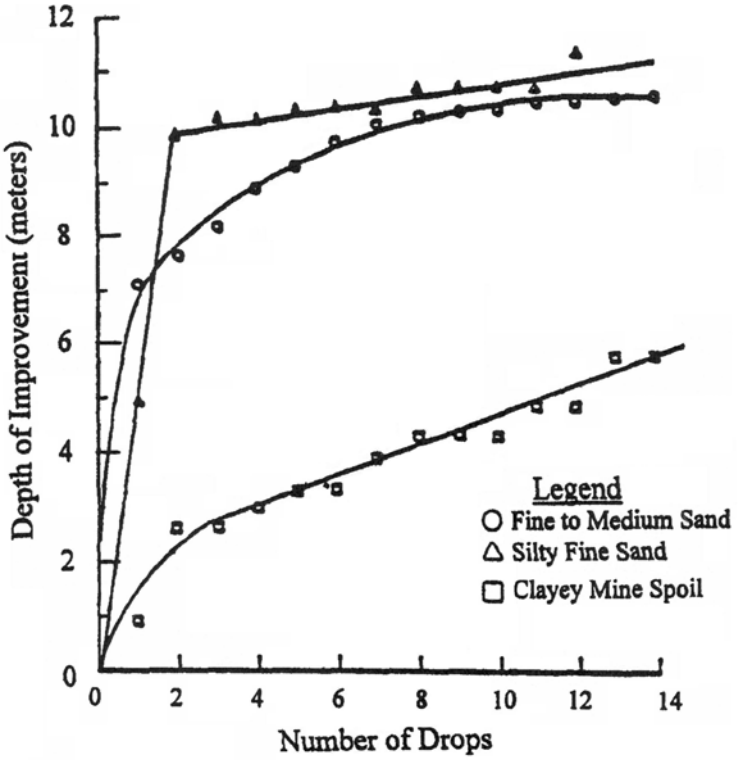

Figure 2.92 Depth of improvements as measured by lateral deflection obtained at inclinometer located 3.0 m from center of drop point (Lukas and Schexnayder, 1986)

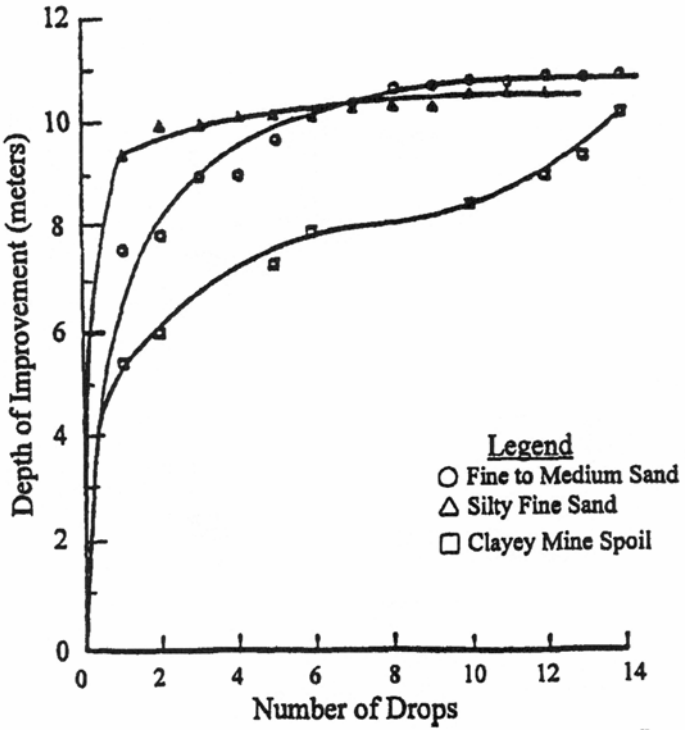

Figure 2.93 Depth of improvements as measured by lateral deflection obtained at inclinometer located 3.0 m from center of drop point (Lukas and Schexnayder, 1986)

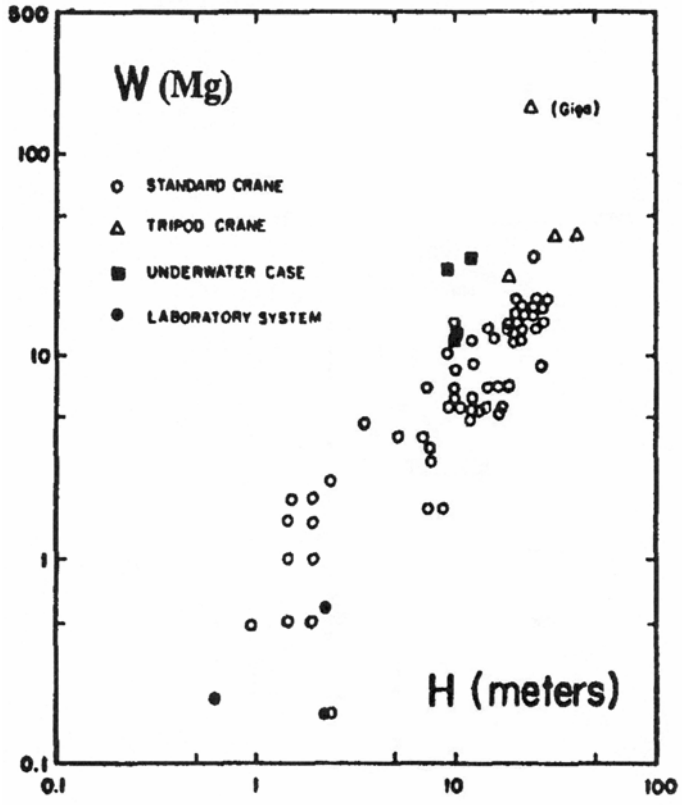

Figure 2.94 Relationship between size of tamper and drop height (Mayne et al., 1984)

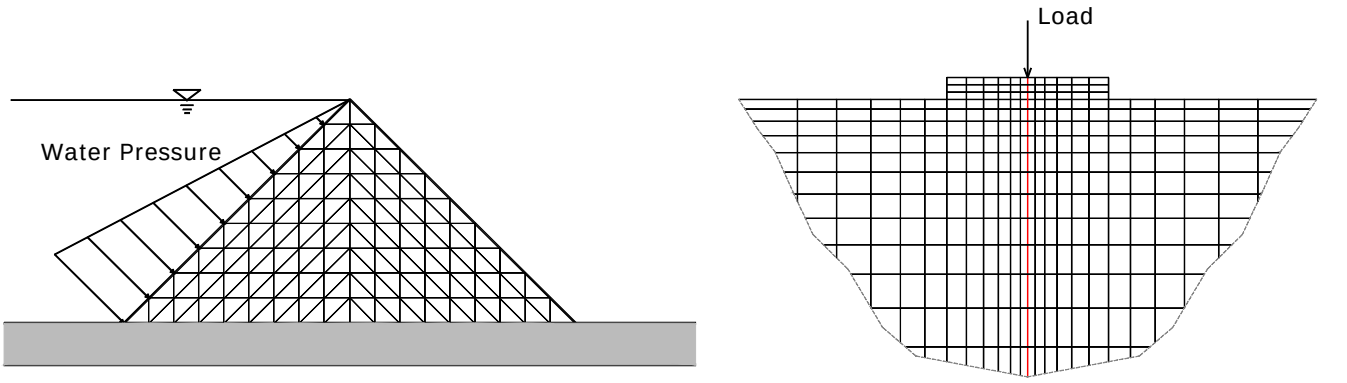

(a) dam subjected to water load and triangular elements (b) footing on soil or rock, rectangular elements

Figure 2.95 Finite element meshes

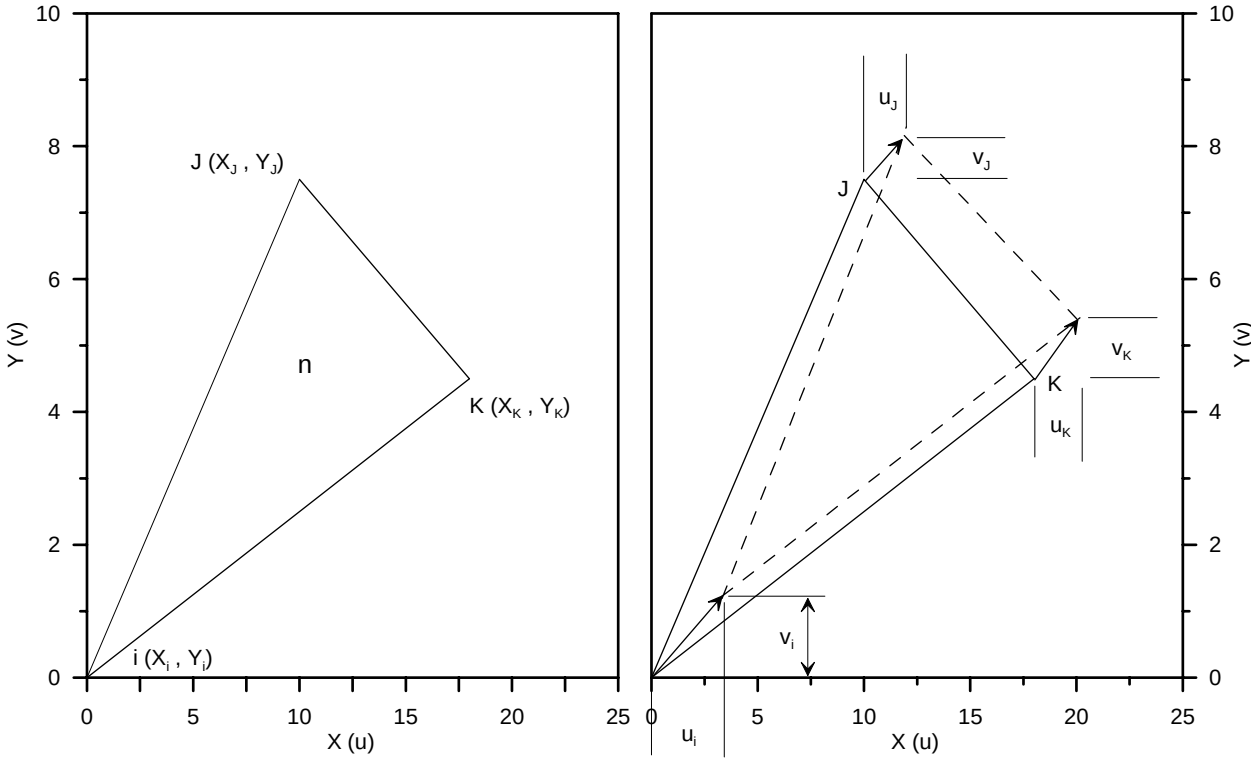

(a) coordinate scheme (b) displacement element

Figure 2.96 Displacement of triangular finite element